Universidade do Vale do Paraíba

Instituto de Pesquisa e Desenvolvimento - IP&D

Programa de Pós Graduação em Física e Astronomia

Mark Armah

DOUBLY IONIZED NEON IONIC ABUNDANCE OF SEYFERT 2 NUCLEI BASED ON INFRARED AND OPTICAL EMISSION LINES

São José dos Campos, SP

2020

Universidade do Vale do Paraíba

Instituto de Pesquisa e Desenvolvimento - IP&D

Programa de Pós Graduação em Física e Astronomia

Mark Armah

DOUBLY IONIZED NEON IONIC ABUNDANCE OF SEYFERT 2 NUCLEI BASED ON INFRARED AND OPTICAL EMISSION LINES

Thesis submitted in partial fulfillment of the requirements for the degree of Master of Science to the Graduate Program in Physics and Astronomy of the Universidade do Vale do Paraíba – Univap.

Advisor: Prof. Dr. Oli Luiz Dors Junior

São José dos Campos, SP

2020

Fundação Valeparaibana de Ensino

BIBLIOTECA

TERMO DE AUTORIZAÇÃO DE DIVULGAÇÃO DA OBRA

Ficha catalográfica

Armah, Mark
Doubly ionized neon ionic abundance of seyfert 2 nuclei based on infrared and optical emission lines / Mark Armah; orientador, Prof. Dr. Oli Luiz Dors Junior. - São José dos Campos, SP, 2020.
1 CD-ROM, 124 p.

Dissertação (Mestrado Acadêmico) - Universidade do Vale do Paraíba, São José dos Campos, Programa de Pós-Graduação em Física e Astronomia.

Inclui referências

1. Física e Astronomia. 2. Galáxias. 3. Seyfert (Galáxias). I. Dors Junior, Prof. Dr. Oli Luiz, orient. II. Universidade do Vale do Paraíba. Programa de Pós-Graduação em Física e Astronomia. III. Título.

Eu, Mark Armah, autor(a) da obra acima referenciada:

Autorizo a divulgação total ou parcial da obra impressa, digital ou fixada em outro tipo de mídia, bem como, a sua reprodução total ou parcial, devendo o usuário da reprodução atribuir os créditos ao autor da obra, citando a fonte.

Declaro, para todos os fins e efeitos de direito, que o Trabalho foi elaborado respeitando os princípios da moral e da ética e não violou qualquer direito de propriedade intelectual sob pena de responder civil, criminal, ética e profissionalmente por meus atos.

I, Mark Armah, author of the aforementioned work, authorize the total or partial dissemination of the work in printed, digital or in any other media, as well as its total or partial reproduction, the user of the reproduction being obligated to attribute credit to the author of the work.

I hereby declare, with legal intent, that this work was elaborated respecting moral and ethical principles and it did not violate any ownership laws of intellectual property, under the penalty of civil, criminal, ethical and professional sanctions.

São José dos Campos, 11 de janeiro de 2021.

Autor(a) da Obra

Data da defesa: 19 de outubro de 2020.

DECLARATION

I hereby declare that no part of this thesis has been previously submitted to this or any other University as part of the requirement for a higher degree. The work described here was conducted mainly by the undersigned. Contributions from others are acknowledged in the text.

Mark Armah

São José dos Campos, SP

2020

Universidade do Vale do Paraíba

Instituto de Pesquisa e Desenvolvimento

MARK ARMAH

"NEON TOICE IONIZED IONIC ABUNDANCE OF SEYFERT 2 NUCLEI BASED ON INFRARED AND OPTICAL EMISSION."

Dissertação aprovada como requisito parcial à obtenção do grau de Mestre, do Programa de Pós-Graduação em Física e Astronomia, do Instituto de Pesquisa e Desenvolvimento da Universidade do Vale do Paraíba, São José dos Campos, SP, pela seguinte banca examinadora:

PROF.ª DR.ª ANGELA CRISTINA KRABBE _____

PROF. DR. OLI LUIZ DORS JUNIOR _____

PROF. DR. GUILLERMO FEDERICO HAGELLE - UNLP _____

PROF. ª DR.ª ANNA FELTRE – INAF-OAS _____

Prof.ª Dr.ª Lúcia vieira

Diretora do IP&D – Univap

São José dos Campos, 19 de outubro de 2020.

Acknowledgements

I would like to express my deepest gratitude to Prof. Dr. Oli Luiz Dors Junior of IP&D at Universidade do Vale do Paraíba (UNIVAP), my research advisor, for his patient guidance, enthusiastic encouragement and useful critiques of this research work. Prof. Oli always advised and gave valuable tips, without which the path would have been much more arduous. The door to Prof. Oli's office was always open whenever I ran into a trouble spot or had a question about my research. He consistently allowed this work to be my own work, but steered me in the right direction whenever he thought I needed it.

I would also like to thank the experts who were involved in the validation evaluation for this research project without any order of preference: Profs.Drs., Ana Feltre, Ângela Cristina Krabbe, Guillermo Federico Hägele, and João Evangelista Steiner. Without their passionate participation and input, the validation evaluation could not have been successfully conducted.

I thank *Coordenação de Aperfeiçoamento de Pessoal de Nível Superior (CAPES)* for the scholarship, without which none of this would be possible. I take this opportunity to extend my thanks and gratitude to all UNIVAP students and employees who helped me directly or indirectly throughout this research work.

Last but not least, I wish to thank my family and friends especially Stephen Kwasi Armah, Adamu Issifu, Adriana Ribeiro Da Silva, Ebenezer Agyei Yeboah, and Vera Yesutor Tsali Brown for their support and encouragement throughout my studies.

ABUNDÂNCIA IÔNICA DO NEÔNIO EM SEYFERT 2 BASEADAS EM LINHAS DE EMISSÃO NO INFRAVERMELHO E NO ÓPTICO

RESUMO

O método mais confiável para determinar abundâncias químicas de elementos pesados em nebulas gasosas é o método $T_{\rm e}$, que é baseado em medidas de linhas de emissão aurorais (e.g. [O III]λ4363). No entanto, este método gera abundâncias subsolares e irreais para regiões de linhas estreitas (NLRs) de AGNs Seyfert 2. Este problema é chamado "problema de temperatura" e sua origem é uma questão em aberto na astrofísica nebular. A comparação entre abundâncias baseadas em linhas de emissão obsevadas no óptico e infravermelho podem ser usadas para obter o nível de flutuações de temperatura eletrônica em AGNs, geralmente atribuídos à origem do problema de temperatura. Neste trabalho, utilizamos intensidades de linhas de emissão estreitas 36 núcleos de galáxias Seyfert 2 observadas na faixa espectral do óptico e infravermelho compiladas da literatura e utilizadas para calcular a abundância iônica do neônio duas vezes ionizado em relação a do hidrogênio (Ne^{2+}/H^{+}). Esta metodologia torna possível obter o nível de flutuação de temperatura eletrônica necessária para conciliar valores de abundância derivadas a partir de linhas observadas no óptico e no infravermelho. Nós investigamos o uso do decremento Balmer $3 \rightarrow 2$ (Hα λ6563 Å) and $4 \rightarrow 2$ (Hβ λ4861 Å) para corrigir a extinção em Seyfert 2 e encontramos que $I(\mathrm{H}\alpha/\mathrm{H}\beta) = 2,85$ produz valores de temperatura electrônia 700 ± 30 K maiores que quando $I(\mathrm{H}\alpha/\mathrm{H}\beta) = 3,10$ é considerado. Nossos resultados mostram diferenças (D) entre valores de abundância via linhas no ótico e no infravermelho variando de $0,1334 \pm 0,0219$ a $2,0636 \pm 0,0151$ dex, com um valor médio de $0,6931 \pm 0,0052$ dex. Este valor médio é um fator $\sim 0,01 \pm 0,01$ dex mais alto do que o derivado em regiões II. Nenhuma correlação entre a diferença de abundância iônica do neônio (D) e o parâmetro de ionização (U) foi encontrada para a amostra de objetos. Nós estimamos o nível de flutuação de temperatura em termos do parâmetro t^2 no intervalo de 0,0006 a $0,4365 \pm 0,0053$ com um valor médio de $0,1859 \pm 0,0011$. Concluímos que, se flutuações de temperatura eletrônica estão presentes em AGNs, esta é mais predominante do que as em H II regiões.

Palavras-chave: Galáxias: Abundâncias - Galáxias: Ativas - Galáxias: ISM: Abundâncias - Galáxias: Nuclei - Galaxias: Seyfert.

ABSTRACT

One of the most reliable method to determine the chemical abundance of heavy elements in gaseous nebulae is the T_e-method, which is based on the measurements of auroral emission lines (e.g., [O III]λ4363 Å). However, this method yields unreal and subsolar abundances in AGNs. This phenomenon is customarily referred to as "temperature problem", and its origin is an open question in nebular astrophysics. Comparison between optical and infrared abundances can be used to obtain the level of electron temperature fluctuations in AGNs, generally attributed to the origin of the temperature problem. In this work, optical and infrared emission-line intensities of neon from a sample of 36 Seyfert 2 nuclei compiled from the literature and used to calculate the ionic abundance of the neon twice ionized in relation to the hydrogen one ion (Ne^{2+}/H^{+}). This methodology makes it possible to obtain the level of electron temperature fluctuation necessary to conciliate the optical and infrared abundance values. We investigated the use of the Balmer decrement observed ratio of intensities of the $3 \rightarrow 2$ (Hα λ6563 Å) and $4 \rightarrow 2$ (Hβ λ4861 Å) transitions of the hydrogen atom compared to their intrinsic intensity ratio so as to yield a relative extinction in the Narrow Line Region (NLR) of Seyfert 2 nuclei and find that the use of $I(\mathrm{H}\alpha/\mathrm{H}\beta) = 2.85$ gives T_e values of 700 ± 30 K higher than the T_e values derived from $I(\mathrm{H}\alpha/\mathrm{H}\beta) = 3.10$. Our analysis show that, differences (D) between abundance values from optical and infrared lines range from 0.1334 ± 0.0219 to 2.0636 ± 0.0151 dex, with an averaged value of 0.6931 ± 0.0052 dex. This averaged value is approximately $\sim 0.01 \pm 0.01$ dex higher than the one derived in H II regions studies. We did not find any relation between the ionic abundance difference (D) and the ionization parameter (U), which implies D is independent from U. We estimated the level of temperature fluctuation in terms of the t^2 parameter in the range from 0.0006 to 0.4365 ± 0.0053 with an average value of 0.1859 ± 0.0011. We conclude that, if electron temperature fluctuations are present in AGNs, they are somewhat more significant than in H II regions.

Keywords: Galaxies: Abundances – Galaxies: Active – Galaxies: ISM: Abundances – Galaxies: Nuclei – Galaxies: Seyfert.

List of Figures

Figure 1 – A diagnostic or BPT diagram for emission-line ratio of [N II]λ6583 Å/Hα versus [O III]λ5007 Å/Hβ distinguishing AGNs 20
Figure 2 – Seyfert galaxy nucleus with black hole and accretion disk at its centre. 22
Figure 3 – Candidate of a "true" Type II Seyfert galaxy 25
Figure 4 – Optical spectra of three Seyfert galaxies transition from Sy 1 to Sy 2 . 29
Figure 5 – The unified model of Active Galactic Nuclei 33
Figure 6 – Histogram of Seyfert 2 nuclei based on the T_e, semi-empirical calibration, and extrapolation methods 35
Figure 7 – Oxygen abundance values for the NLR from two proposed calibrations. 37
Figure 8 – Comparison between 12 + log (O/H) from two distinct methods. . . . 38
Figure 9 – Comparison between t_3 values from T_e-method and photoionization predictions. 41

Figure 10 – Reddening-corrected diagnostic diagrams for [O III]λ5007 Å/Hβ versus [N II]λ6584 Å/Hα and [S II]($\lambda\lambda$6716, 6731 Å)/Hα. 69

Figure 11 – Diagnostic diagrams containing observational data from SDSS DR7. . . 72
Figure 12 – Histogram containing the distribution of the spectral index α_{ox} derived by Miller et al. (2011) for about 700 radio-intermediate and radio-loud quasars. 73
Figure 13 – Spectrum of the region No.2 in NGC 2541. 77
Figure 14 – STIS G430L spectrum of the central NLR knot in Mrk 573. 78
Figure 15 – Infrared spectrum of Mrk 573 showing Paγ and other emission lines. . . 81

Figure 16 – Comparison between ionic abundance of the Ne^{2+}/H^+ derived using Visible−lines and IR−lines methods. 88
Figure 17 – Comparison between ionic abundance of the Ne^{2+}/H^+ derived via IR−lines methods separating the Paschen and Brackett Series. 89
Figure 18 – Logarithm of the ionization parameter U versus the Ne^{2+}/H^+ abundance difference (D). 90
Figure 19 – Comparison between electron temperature (T_e) and the average temperature (T_0). 93

List of Tables

Table 1 – Classification of Active Galactic Nuclei 18

Table 2 – Neon Mid-infrared fine structure lines and near to mid-infrared Paschen and Brackett series observational fluxes for selected Seyfert 2 nuclei in units of 10^{-14} erg cm^{-2} s^{-1}. 59

Table 3 – Observed reddening-uncorrected optical emission-line intensities of Seyfert 2 nuclei compiled from the literature. 61

Table 4 – Reddening-corrected optical emission-line intensities of Seyfert 2 nuclei relative to Hβ = 1.00 compiled from the literature. 70

Table 5 – H I emissivity ratio values (Case B). 81

Table 6 – 12+log(Ne^{2+}/H^{+}) abundances derived by using the IR−method. 85

Table 7 – Doubly ionized neon chemical abundances (Ne^{2+}/H^{+}) values from T_e and IR−lines methods, the differences between the optical and infrared ionic abundance estimations, T_e, T_0, and t^2 values. 86

List of abbreviations and acronyms

AGNs	*Active Galactic Nuclei*
BLR	*Broad Line Region*
ENLR	*Extended Narrow Line Region*
ESO	*European Southern Observatory*
FIR	*Far Infrared*
FWHM	*Full Width at Half Maximum*
HST	*Hubble Space Telescope*
IC	*Index Catalogue*
IR	*Infrared*
IRAF	*Image Reduction and Analysis Facility*
IRAS	*Infrared Astronomical Satellite*
ISM	*Interstellar Medium*
LINER	*Low Ionization Nuclear Emission Region*
MIR	*Mid Infrared*
MPG/ESO	*Max Planck Gesellschaft/European Southern Observatory*
MCG	*Morphological Catalog of Galaxies*
MRK	*Markarian*
NGC	*New General Catalogue*
NIR	*Near Infrared*
NLR	*Narrow Line Region*
OVV	*Optically Violent Variable*
PNe	*Planetary Nebulae*
PBLR	*Polarized Broad Line Region*

QSO	*Quasi-Stellar Object*
QSO2	*Quasi-stellar Object 2, High Power Sy2*
QUASAR	*Quasi-Stellar Radio Source*
S/N	*Signal-to-Noise Ratio*
SMBH	*Supermassive Black Hole*
SNe	*Supernovae*
Sy1	*Seyfert 1, FWHM* $\gtrsim$ *1 000 km* s^{-1}
Sy2	*Seyfert 2, FWHM* $\lesssim$ *1 000 km* s^{-1}
Type 1	*Sy1 and QUASARs*
Type 2	*Sy2 and QSO2*
VLA	*Very Large Array*
WHT	*William Herschel Telescope*
3C	*Third Cambridge Catalog*
3CR	*Third Cambridge Revised Catalog*

Table of Contents

1 Introduction . . . 15
- 1.1 Active Galactic Nuclei . . . 15
- 1.2 Classification of Active Galactic Nuclei . . . 17
  - 1.2.1 Seyfert Galaxies . . . 21
  - 1.2.2 Unification Scheme of AGNs . . . 30
- 1.3 Oxygen abundance discrepancy in AGNs . . . 34
- 1.4 Motivation . . . 39
- 1.5 Objectives . . . 42

2 Data . . . 43
- 2.1 Observational data . . . 43
- 2.2 The hydrogen emission lines . . . 58
- 2.3 Reddening correction . . . 62

3 Methodology . . . 71
- 3.1 Determination of neon ionic abundances . . . 75
  - 3.1.1 $T_{\rm e}-$method . . . 75
  - 3.1.2 Infrared – lines method . . . 79
  - 3.1.3 Temperature fluctuations measure (t^2) . . . 83

4 Results and discussions . . . 84

5 Conclusions . . . 94
- 5.1 Summary . . . 94
- 5.2 Future work . . . 95

Bibliography . . . 96

1 Introduction

1.1 Active Galactic Nuclei

According to available literature, Edward Arthur Fath is the first person known to have observed an Active Galactic Nucleus (AGN). He detected strong emission lines from the nuclei of NGC 1068 and Messier 81 while studying galaxy spectra for his PhD dissertation (Fath, 1909). Further discoveries of the jet in Messier 87 by Curtis (1918) and spectroscopic studies which led to the observations of the presence of unusual emission lines in some galaxy nuclei (Slipher 1917, Humason 1932; Mayall 1934, 1939). Notably, the NGC 1068, NGC 4051 and NGC 4151 objects were considered to be planetary nebulae by Hubble (1926). Seyfert (1943), made a systematic study of galaxies with emission lines, and focused on those with high excitation nuclear emission lines (NGC 1068, NGC 1275, NGC 3516, NGC 4051, NGC 4151, and NGC 7469). The work by Jansky (1932) on sources of static affecting trans-Atlantic radio communications brought to bare that: static from local thunderstorms, static from distant thunderstorms, and a steady hiss type static of unknown origin which latter seemed to be associated with the sun (Jansky, 1933). Jansky later implied that the radiation was coming from the center of the Milky Way galaxy. Finally, Jansky (1935) concluded that the radiation came from the entire disk of the Milky Way, being strongest in the direction of the Galactic center. Jansky's work became a motivating factor for Reber (1940a, 1940b) in building a 31 foot reflector and publishing a map of the radio sky at 160 MHz showing several local maxima, including one in the constellation Cygnus that proved important for AGN studies by Reber (1944). Detections at 160 MHz of Cygnus-A (the 2nd brightest source in the sky) with interferometry double radio structure was confirmed by Bolton & Stanley (1948) as a discrete source. Some earliest detected radio sources in the development of radio astronomy are, in fact, nearby active elliptical galaxies such as Messier 87 and Centaurus A (Bolton, Stanley & Slee, 1949) as well as Cygnus A (Hey, Parsons & Phillips, 1946; Baade & Minkowski, 1954). Double radio structure became apparent with the introduction of interferometry (e.g. Hanbury Brown; Jennison; Gupta, McCready; Pawsey; Payne-Scott). Schmidt (1951) obtained accurate position for Cyg-A, optically identified by Baade & Minkowski (1954). To advance the frontiers of knowledge in astronomy led to the publications of the Third Cambridge (3C) Catalog of Radio Sources survey at 159 MHz and its revision, the 3CR Catalog survey at 178 MHz by Edge et al. (1959) and Bennett (1962), respectively, with detected sources down to a limiting flux of 9 Jy[1], together with the Parkes Radio Tele-

[1] A jansky (Jy), named after the pioneering radio astronomer Karl Jansky, is a unit of specific flux, simply called a "flux unit", defined as 1 Jy = 10^{-26} watts m^{-2} Hz^{-1} = 10^{-23} erg s^{-1} cm^{-2} Hz^{-1}.

scope (Bolton, Gardner & Mackey, 1964) teams, originally at 408 MHz (detection limit 4 Jy) and later at 1410 MHz (to 1 Jy) and 2650 MHz (to 0.3 Jy) (Ekers, 1969). The Fourth Cambridge (4C) survey was a more sensitive version (limiting flux 2 Jy) of the 3C, which was also undertaken at 178 MHz (Pilkington & Scott, 1965; Gower, Scott & Wills, 1967). The radio source was rapidly associated with an optical counterpart, an unresolved stellar object of 13th magnitude. Because of their star-like appearances, these strong sources of radio came to be called quasi-stellar radio objects, shortened as "quasar". Schmidt (1963) was able to obtain the quasar 3C 273 optical spectrum from a lunar occultation accurate position (Hazard, Mackey & Shimmins, 1963), thereafter, 3C 48 was observed by Greenstein & Matthews (1963) and Greenstein (1963).

Sandage (1965) found that most quasars are radio-quiet (blue-colour selected). First extensive Seyfert galaxy searches through compactness was carried out by Zwicky (1964) and Zwicky (1966) and through UV excess by Markarian (1969a) (but see also Markarian, 1969b, 1969c, Markarian & Lipovetsky, 1971, 1972, 1973, 1974, 1976a, 1976b, Markarian, Lipovetskii & Stepanian, 1977a, 1977b, 1979, 1980, 1981). Victor Amazaspovich Ambartsumian was the first to introduce "active nucleus" to astronomy in his famous report at the Solvay Conference on Physics, Brussels 1958. In Ambartsumian's view, the "activity" of the galaxy nuclei manifests mainly in the forms as described (see, Ambartsumian, 1956; Ambartsumian, 1958; Ambartsumian, 1962). AGN was first used in a paper and PhD dissertation titled "nuclei that contain extensive star formation or luminous non-thermal sources" Weedman (1974) and "Cosmic Ray Acceleration of Gas in Active Galactic Nuclei" by Eilek (1975) at the University of British Columbia, respectively. "Activity" was usually taken to mean "radio source", although sometimes also meant "starburst", which came to be used to encompass "Seyfert galaxies"and "quasars" stated as "...energetic phenomena in the nuclei, or central regions, of galaxies which cannot be attributed clearly and directly to stars" in "An Introduction to Active Galactic Nuclei" by Peterson (1997).

AGNs are currently known as a dense region at the center of a galaxy (compact nucleus) that has a higher luminosity than the one in normal or peculiar galaxy considering the smallest portion of the electromagnetic spectrum (huge amount of energy up to 10^4 times more than a normal galaxy emitted from a tiny region with radius < 1 pc) which shows that the luminosity produced is non-stellar. The non-stellar nuclear bolometric luminosity ranges from $\sim 10^{40}$ erg s^{-1} (1 erg = 0.1 μJ) in nearby galaxies to $\sim 10^{47}$ erg s^{-1} for distant quasars. Since an AGN energy output is too strong to be related to stellar activity and, being ∼10 times more efficient than nuclear fusion at converting rest mass into radiation (e.g. Frank; King; Raine, 1992), gas accretion onto a super-massive ($M \gtrsim 10^6$ M$_\odot$) black hole (SMBH) is generally proposed as the source producing the observed power within a sufficiently small volume (Salpeter, 1964; Zel'dovich & Novikov,

1964; Begelman, Blandford & Rees, 1984; Rees, 1984). The observation of this non-stellar emission has been undertaken in all the seven known wavebands (Padovani, 2017). Any galaxy serving as a host to an AGN is popularly known as active galaxy. The most luminous sources of electromagnetic radiation in the Universe are active galactic nuclei and, as such can be used as a way of detecting distant objects, their evolution as a result of cosmic time often places limitations on cosmological models. An AGN's observed characteristics depend on several properties such as the mass of the central black hole, the rate of gas accretion on the black hole, the accretion disk orientation, the degree of dust obscuration of the nucleus, and the presence or absence of jets. Based on their observed characteristics, several AGN sub-classes have been defined, such as Seyfert, Quasars, Blazars, etc..

1.2 Classification of Active Galactic Nuclei

The classification for a single object can change with time due to AGN variability, therefore, general overview of different types of AGNs and some ideas on their unification have been discussed to somewhat details in succeeding subsections. Typically, AGNs are divided into two categories, which are referred to as "radio-quiet" and "radio-loud" nuclei. Optically selected AGNs are historically divided as being radio-loud or radio-quiet depending on the value of the radio loudness parameter R, defined as the ratio between the monochromatic luminosities at radio and optical frequencies (i.e., $R = L_{5GHz}/L_B$), where, radio-quiet objects show values of R concentrated between 0.1 to 1.0, whereas in radio-loud sources the R values range from 10 to 100 (Kellermann et al., 1989), so that the boundary between the two classes is normally defined at R= 10 (Visnovsky et al., 1992; Kellermann et al., 1994). The radio-loud category corresponds to AGNs that have radio emissions produced by both the accretion disk and the jets, thus, Quasi Stellar Radiosource (QSR). Radio-quiet AGNs are simpler because any emission from jet is negligible, hence, Quasi-Stellar Object (QSO). Radio-quiet AGNs are further subdivided into Seyfert type 1 and type 2 galaxies named after Carl Keenan Seyfert who discovered the first class of AGN (Khachikyan & Weedman, 1974).

In Table 1, a summarized description of each sub-class of AGN is presented. AGNs with the broad permitted lines emerging from hot, high-velocity gas that is near the black hole are Type 1 AGNs. In the radio-quiet group, these include the Seyfert 1 galaxies and the higher-luminosity radio-quiet quasars. The radio-loud Type 1 AGN are the Broad-Line Radio Galaxies (BLRG) at low luminosities and radio-loud quasars at high luminosities. AGNs with only narrow emission lines are Type 2 AGNs. They have a weak continuum and only narrow emission lines. That means either they do not have any high-velocity gas or the line of sight to such gas is obscured by a thick torus. Radio-quiet Type 2 AGN include Seyfert 2 galaxies at low luminosities, as well as the narrow-emission-line X-ray galaxies. Likely candidates for their high-luminosity are the infrared-luminous IRAS AGN

(Sanders et al., 1988; Wills et al., 1993). Radio-loud Type 2 AGNs are the Narrow-Line Radio Galaxies (NLRG). Type 3 AGNs are the lower luminosity AGNs, which consist of the Low-Ionization Nuclear Emission-line Regions (LINERs) in the radio-quiet version while the radio-loud counterparts are the Weak-Line Radio Galaxies (WLRGs). Those AGNs showing rapid variability at optical wavelengths are labelled as Type 0 AGNs. They include Blazars and OVVs.

Table 1 – The main classification labels used for active galactic nuclei. AGNs with broad permitted lines detected at optical wavelengths are generally known as Type 1 AGNs, while those with only narrow emission lines are known as Type 2 AGNs. Lower luminosity AGNs are sometimes referred to as Type 3 AGNs, while those showing rapidly variability at optical wavelengths are sometimes labelled Type 0 AGNs.

Radio-quiet	**Radio-loud**
Radio-quiet quasars (RQQ)	**Radio-loud quasars (RLQ)**
Broad absorption-line (BAL)	Steep radio spectrum (SSRLQ)
	Flat radio spectrum (FSRLQ)
Type 1	
Seyfert 1 (Sy1)	**Broad line radio galaxy (BLRG)**
Sy 1.0.....1.9	
Narrow line Sy1 (NLSy1)	
Seyfert 2 (Sy2)	**Narrow line radio galaxy (NLRG)**
NLX-ray galaxy (NLXG)	
Type 2	
LINERs	**Weak line radio galaxy (WLRG)**
Type 3	
	Blazar: BL Lac/OVV
Type 0	
	Fanaroff Riley class I (FRI)
	Fanaroff Riley class II (FRII)

Face-on	**Edge-on**
Seyfert 1	**FR-I**
QSO	**NLRG**
	FR-II
Edge-on	**Face-on**
Seyfert 2	**BL Lac**
FIR Qalaxy	**BLRG**
	Quasar

Source: Reconstructed from Tadhunter (2008)

Baldwin, Phillips & Terlevich (BPT) diagrams show how to differentiate LINERs from regular H II regions and normal AGNs (Seyferts and QSOs) on the basis of their [O III] λ5007 Å/Hβ, [N II] λ6584 Å/Hα, [S II] ($\lambda\lambda$6716, 6731 Å)/Hα, and [O I] λ6300 Å/Hα flux ratios (Baldwin, Phillips & Terlevich, 1981; Veilleux & Osterbrock, 1987).

Figure 1 shows the emission line intensity ratio diagnostic diagram of [O III] λ5007 Å/Hβ versus [N II] λ6583 Å/Hα for various excitation mechanism (AGN, Starburst, shock-heated, and planetary nebulae) of galaxies as indicated in different colours. The various points (dotted and plus shapes) represent emission in different regions located at the nuclei of each object. The curves represent the division between star-forming galaxies (H II-like objects) and AGN-like objects proposed by Kauffmann et al. (2003) and Kewley et al. (2001). Below the pure star forming curve proposed by Kauffmann et al. (2003) are located the Starbursts represented by the blue plus coloured indicators while green plus coloured indicators are located in the composite zone. Above the maximum starburst curve proposed by Kewley et al. (2001) the AGNs are located (red plus and yellow points). Between these two curves are located the composite objects. The solid line, proposed by Schawinski et al. (2007), separates AGNs between Seyferts and LINERs. LINERs are distinguished from H II regions by higher values of [N II] λ6583 Å/Hα, and from Seyfert galaxies by lower values of [O III] λ5007 Å/Hβ. Transition galaxies located between empirical **(Kauffmann line)** and theoretical **(Kewley line)** demarcation lines are found to be systematically associated with narrower line widths and weaker [O III] λ5007 Å broad wings, as well as younger stellar populations than Seyfert galaxies (Kewley et al., 2006), which implies that the kinematics of the emission-line gas is different in the two kinds of objects (Wang, Mao & Wei, 2011).

Figure 1 – A diagnostic or BPT diagram for emission-line ratio of [N II] λ6583 Å/Hα (horizontal axis) versus [O III] λ5007 Å/Hβ (vertical axis) distinguishing AGNs, composite objects (COMP) and star-forming galaxies . The solid curves are boundaries proposed by Kauffmann et al. (2003) and Kewley et al. (2001) for the empirical and theoretical division between the two classes of objects indicated (i.e., to distinguish between hard and soft radiation, respectively). The solid line represents the division between Seyfert galaxies and LINERs by Schawinski et al. (2007).

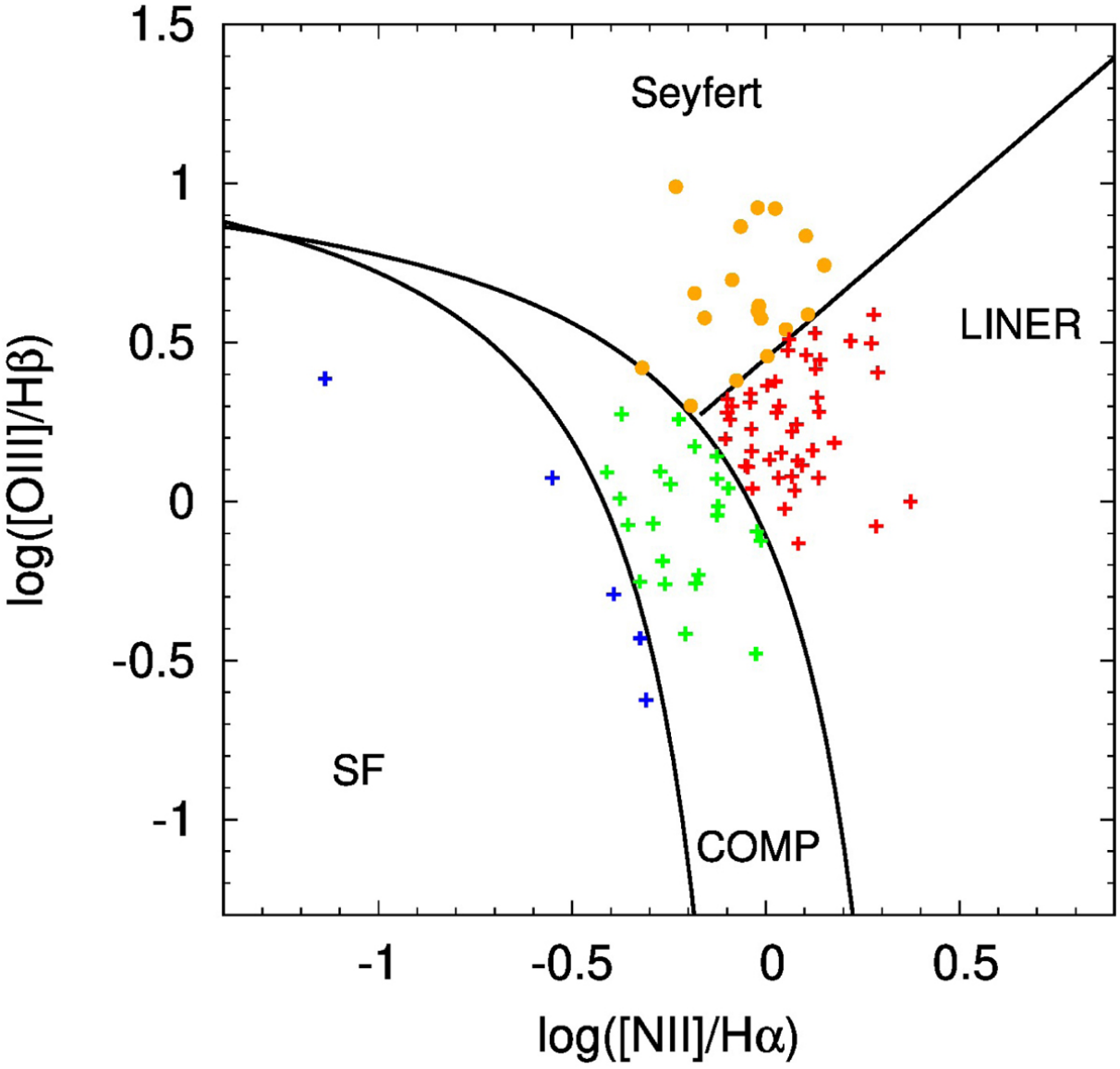

Source: Zajaček et al. (2019)

1.2.1 Seyfert Galaxies

Until 1955, when NGC 1068 and NGC 1275 were observed as radio sources, Seyfert galaxies received no further study. Afterwards, Woltjer (1959) made the first attempt to understand the physics of Seyfert galaxies and noted the following:

- The nuclei are unresolved (size of the nucleus $<$ 100 pc).
- The nuclear emission must last more than 10^8 years, because Seyfert galaxies constitute about 1 in 100 spiral galaxies. This is a simple argument. One extreme scenario is that galaxies which are Seyferts are always Seyferts, in which case their lifetime is the age of the Universe (10^{10} years). The opposite extreme is one where all spirals pass through a Seyfert phase (or phases) - since 1 spiral in 100 is currently in the Seyfert phase, it must last of order $10^{10}/100 = 10^8$ years.
- If the material in the nucleus is gravitationally bound, the mass of the nucleus must be very high. This is a simple virial argument, i.e., $M \approx v^2\, r/\mathrm{G}$. The velocity dispersion is obtained from the widths of the emission lines and is of the order of 10^3 km s^{-1}. We have an upper limit to the size of the nucleus ($r \lesssim 100$ pc) from the fact that it is spatially unresolved. The emission lines are characteristic of a low-density gas, which effectively provides a lower limit $r \gtrsim 1$ pc. Thus the mass of the nucleus can be inferred to be in the range $M \approx 10^{9\pm1}\,\mathrm{M}_\odot$.

The last point tells us that something very extraordinary is occurring at the center of Seyfert galaxies. If a large value of r is assumed, then it must be concluded that something like 10% of the mass of the galaxy is contained in a volume ~ 100 pc across. On the other hand, if r is much smaller than the upper limit set by ground-based spatial resolution, then the problem to be faced is how to generate an extraordinary amount of energy in a tiny volume. Figure 2 is the representation of the nucleus of a Seyfert galaxy where the central black hole is surrounded by a luminous accretion disk. The waved lines indicate roughly from which directions the emission is observed in the case of type 1 and type 2 Seyfert nuclei. Broad emission lines are produced by the disk itself and perhaps in clouds orbiting above the disk. A dense dusty torus obscures the broad-line region from the transverse lines of sight; some continuum and broad-line emission can be scattered through the warm electrons pervading the field into those lines of sight. In the production of the hard X-ray continuum, a hot corona above the accretion disk can also play a role. Narrow lines are produced farther from the central source in clouds. Seyfert galaxies account for $\sim 10\,\%$ of all galaxies (Maiolino & Rieke, 1995; Ho, Filippenko & Sargent, 1997). In particular, Maiolino & Rieke (1995) found that to every type 1 there are around four type 2 nuclei according to their sub-classification scheme (Osterbrock, 1981; Meurs & Wilson, 1984; Edelson, 1987; Osterbrock & Shaw, 1988; Schmitt & Kinney, 1996; Schmitt et al., 1997).

Figure 2 – Illustration showing the nucleus of a Seyfert galaxy depicting the black hole and accretion disk at the centre. Material approaching us appears bluer, while receding gas appears redder.

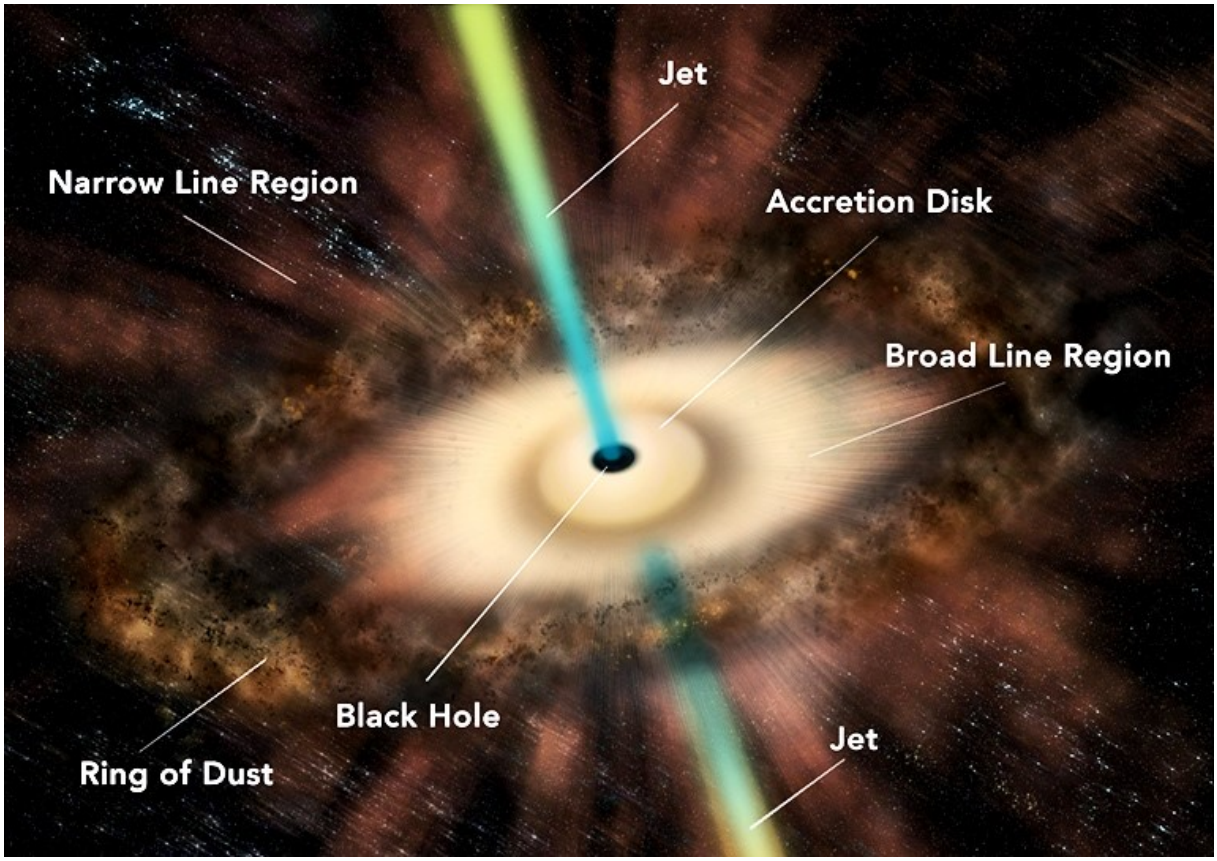

Source: Tasoff (2019)

Type 1 Seyfert galaxies have both narrow and broad optical emission lines, which imply the existence of clouds of high-density gas ($N_e \gtrsim 10^9$ cm^{-3}), as well as gas velocities between 1 000 $-$ 5 000 km s^{-1} near the nucleus. Osterbrock (1977, 1981) further classified Type 1 Seyfert galaxies into the Type 1.0, 1.2, 1.5, 1.8, and 1.9 categories based on the appearance of the Balmer lines. The subclasses were based on the spectrum's optical structure, with the numerically larger subclasses having poorer broad-line components compared to the narrow lines. Type 1.9, for instance, shows only a broad component in the Hα line, not in higher Balmer line series, in type 1.8, it is possible to detect very weak broad lines in both Hγ and Hβ lines, even though they are very weak compared to Hα, whereas the strength of the Hα and Hβ lines is comparable in type 1.5, Seyfert Type 1.2 have strong broad Hβ component (Osterbrock, 1981), last but not least, Seyfert 1.0s are typical class members as defined by Khachikyan & Weedman (1971, 1974). Another very important subset are the narrow line Type I galaxies (NLSy1) characterized by the full width at half maximum (FWHM) of the Hβ broad emission line lower than 2 000 km s^{-1} and the flux ratio of ([O III] λ5007 Å/Hβ) < 3, which in recent years have undergone

extensive research (Osterbrock & Pogge, 1985). They have much narrower lines than the broad lines from classic Type I galaxies, steep hard and soft X-ray spectra and strong Fe II emission with high Eddington ratio that place them in the extreme upper right corner of the R_{4570} - ξ_{Edd} diagram (Boller, Brandt & Fink, 1996; Rakshit et al., 2018), where R_{4570} is the Fe II strength representing the ratio of Fe II line flux in the wavelength range 4434 - 4684 Å to Hβ flux greater than 0.01 and the Eddington ratio (ξ_{Edd}) defined as the ration of bolometric luminosities to Eddington ratios ($\xi_{Edd} = L_{bol}/L_{Edd}$, where $L_{Edd} = 1.3 \times 10^{38} M_{BH}/M_\odot$ erg s^{-1}). Their properties suggest that NLSy1 galaxies are young AGNs with high accretion rates, suggesting a relatively small but growing central black hole mass (Mathur & Grupe, 2005). There are theories suggesting that NLSy1s are galaxies in an early stage of evolution, and links between them and ultraluminous infrared galaxies or Type II galaxies have been proposed (Komossa, 2008). Seyfert type 1 has been reclassified by Winkler (1992) on the basis of quantitative standards as follows:

- Sy1.0 $5.0 < I_\lambda$
- Sy1.2 $2.0 < I_\lambda < 5.0$
- Sy1.5 $0.33 < I_\lambda < 2.0$
- Sy1.8 $I_\lambda < 0.33$ broad component visible in Hα and Hβ
- Sy1.9 broad component visible in Hα but not in Hβ

where I_λ is the intensity of the ratio Hβ/[O III] λ5007 Å.

Type 2 Seyferts, in contrast, have narrow (forbidden and permitted) emission lines. These narrow lines are emitted in low density gas clouds ($100 \lesssim N_e \lesssim 3\,000$ cm^{-3}, see Dors et al., 2012) that are at greater distances from the nucleus than BLRs, and indicate more-modest gas velocities of about 500 to 1 000 km s^{-1}. Seyfert 2 galaxies usually have a high ratio of [O III] λ5007 Å/Hβ; the empirical criterion for Seyfert 2 is [O III] λ5007 Å/H$\beta \gtrsim 3$ (Shuder & Osterbrock, 1981; Veilleux & Osterbrock, 1987). Baldwin, Phillips & Terlevich (1981) introduced the method popularly called BPT diagram, to divide star-forming galaxies and Seyfert 2 galaxies depending on the ratios of emission lines. Currently, the BPT diagrams with different dividing lines derived from theoretical and empirical methods are widely used in galaxy classification (e.g., Veilleux & Osterbrock, 1987; Véron-Cetty, Véron & Gonçalves, 2001; Kewley & Dopita 2002; Kauffmann et al., 2003; Kewley et al., 2006; Schawinski et al., 2007).

Véron-Cetty & Véron (2010) pointed to several objects which have been found to show extreme spectral variability, changing from Seyfert 1.8 or 1.9 to Seyfert 1.0 as a result of reddening towards the BLR or changes in ionizing flux. In some Seyfert 2

nuclei, a broad Paβ line has been detected, indicating a highly reddened broad line region and several Seyfert 2s have the spectra of Seyfert 1s in polarized light, these objects are called S1i and S1h respectively (Véron-Cetty & Véron, 2010). Typical full widths at half-maximum of the Balmer lines in Seyfert 1s lie in the range $2\,000 - 6\,000\,\mathrm{km\,s^{-1}}$; however, there is a group of active galactic nuclei with all the properties of Seyfert 1s, but with unusually Balmer lines narrower than $2\,000\,\mathrm{km\,s^{-1}}$ FWHM, which are called narrow Seyfert 1 (S1n) (Véron-Cetty & Véron, 2010). NGC 3147 ($z = 0.009346$: Epinat et al., 2008) is one of the three 'true' Type 2 Seyfert galaxies (NGC 3147, NGC 4698, and 1ES 1927+654) confirmed by simultaneous optical and X-ray observations (Bianchi et al., 2008; Panessa et al., 2009; Shi et al., 2010; Tran, Lyke & Mader, 2011; Bianchi et al., 2012). NGC 3147 is about 130 million light years away in the northern circumpolar constellation Draco the Dragon, in good agreement with redshift-independent distance estimates of 100 to 180 million light years. Given that and its apparent size of about 3.6 by 3.0 arcmin, it is 135 to 140 thousand light years across. In Figure 3, an image of NGC 3147 is shown, which contains a Seyfert type 2 nuclei and is considered the best candidate to be a "true" Type II Seyfert galaxy, which has neither a dust ring nor the broad emission lines (Tran, 2001; Tran, 2003; Bianchi et al., 2008; Shi et al., 2010; Tran, Lyke & Mader, 2011; Matt et al., 2012; Bianchi et al., 2017), however, recent findings by Bianchi et al. (2019) questions the very existence of true type 2 AGNs. In Figure 4, typical optical spectra of Seyfert 1 and 2 BLR and NLR emission lines are shown.

In general, the magnitude of Hα luminosities in Seyfert 1 nuclei is higher than in Seyfert 2 nuclei (Gu et al., 1997). From a study of the statistical differences between Seyfert 1 and Seyfert 2 nuclei, Keel (1980), Maiolino & Rieke (1995), and Curran (2000) found that intermediate Seyferts of type 1, 1.2 and 1.5 will occur in face-to-face galaxies while those of type 1.8 and 1.9 will occur in edge-on cases. Altogether, these findings provide strong support for a unified model in which Seyfert 2 nuclei contain a dusty torus seen more edge-on than the torus in Seyfert 1 nuclei (Schmitt et al., 2001).

Figure 3 – NGC 3147 (PGC 30019 with *redshift*, z = 0.009346 : Epinat et al., 2008) discovered (April 3, 1785) by William Herschel and also observed (November 4, 1831) by John Herschel. A magnitude 10.6 spiral galaxy (type SA(rs)bc) in Draco (RA 10 16 53.6, Dec +73 24 03). Historical Identification: Per Dreyer, NGC 3147 (= GC 2024 = JH 674 = WH I 79, 1860 RA 10 04 48, NPD 15 54.4). Based on a recessional velocity of 2 800 km s^{-1} and Hubble constant, $H_0 = 70$ km s^{-1} Mpc^{-1}. NGC 3147 is a Seyfert galaxy type 2 (Sy2).

Source: Hubble Space Telescope (ESA/Hubble & NASA, A. Riess et al.)

Since quantum mechanics had opened the door to quantitative spectral analyses of the sun and stars, there are selection rules for many electron atoms which include the total spin quantities L, S, and J. These are: (i) parity, defined as $\sum_i l_i$, must change, (ii) the change in total angular momentum must be $\Delta L = 0, \pm 1$, (iii) the change in total angular plus spin momentum must be $\Delta J = 0, \pm 1$, but $J = 0 \rightarrow 0$ is forbidden, (iv) only one single electron wavefunction nl changes, with $\Delta l = \pm 1$, and (v) total spin cannot change: $\Delta S = 0$. Allowed transitions are those that obey all of these selection rules. Forbidden transitions are those which violate any of the first four rules. Semi-forbidden transitions are those that follow the first four rules, but break the last spin rule. The allowed transitions have the largest transition probabilities and the lifetime of excited states that decay through this process is of order 10^{-8} s. Forbidden transitions have decay time-scales of the order of 1 s, whereas semi-forbidden transitions have time-scales intermediate those of allowed and forbidden transitions. The distinction between forbidden and semi-forbidden transitions is accomplished by denoting the former with double square brackets (e.g., [O III] $\lambda\lambda$4959, 5007 Å) while the latter is presented with a single square bracket (e.g., Si IV/O IV] λ1400 Å, N IV] λ1486 Å, O III] λ1663 Å, N III] λ1750 Å Si III] λ1892 Å, C III] λ1909 Å, and O II/C II] λ2323 Å).

The origin of the differences between type 1 and type 2 Seyferts is either not known or certainly controversial. The main difference between Seyfert 1 and Seyfert 2 galaxies originates from the optical and UV spectroscopy, where type 1s have broad permitted lines, thus, hydrogen recombination lines including the Balmer lines (Hβ, Hγ, Hδ), He II λ4686 Å and He I λ5876 Å as well as Fe II $\lambda\lambda$4570, 5250 Å, in the optical, intercombination lines – e.g., C IV λ1459 Å, Mg II λ2798 Å – and semi-forbidden lines, e.g., C III] λ1909 Å in the near UV, lines with FWHM FWHM $\sim$ 1 000 $-$ 10 000 km s^{-1} and the full widths at nearly zero intensity (FW0I or FWZI) of these same lines defined in the range from 5 000 to 30 000 km s^{-1} (Osterbrock & Shuder, 1982). However, both type 1 and type 2 have narrow permitted (e.g., H I, He I, He II, Fe II, Mg II, C IV) and forbidden (e.g., [Ne III] λ3869 Å, [O I] $\lambda\lambda$6300, 6364 Å, [O II] $\lambda\lambda$3726, 3729 Å, [O III] $\lambda\lambda$4959, 5007 Å, [S II] $\lambda\lambda$6717, 6731 Å, [N II] $\lambda\lambda$6548, 6583 Å, [Fe VII] λ6087 Å, [Fe X] λ6375 Å, etc.) lines with widths FWHM $\sim$ 500 $-$ 1 000 km s^{-1}.

The Balmer line strengths in Seyferts and quasars were found in the early 1980s to form a single tight correlation with the non-stellar continuum strength, confirming a basic link between the two: continuum emission photoionizes the broad-line region gas which then produces line radiation. An estimate of the gas density in the broad-line region comes from the absence of any broad components on the forbidden lines. These forbidden emission lines cannot occur via the fast electric dipole mode. With only slower modes of transition available (e.g. magnetic dipole), the ions are vulnerable to collisional de-excitation in a high density gas where the mean time between collisions is small. The

critical density above which collisional de-excitation becomes important varies widely for different lines, so one can bracket the gas density in the broad-line region by noting which lines have broad components and which do not. For example, while the [O III] λ4363 line with critical density $\sim 3 \times 10^7\,\mathrm{cm}^{-3}$ has no broad component, the semi-forbidden C III] λ1909 line with critical density $\sim 3 \times 10^{10}\,\mathrm{cm}^{-3}$ has broad component, implying a gas density in the BLR somewhere in the range $10^8 - 10^{11}\,\mathrm{cm}^{-3}$. In contrast to the forbidden lines, the so-called 'permitted' lines arise from fast ($\sim 10^{-8}$ s) electric dipole transitions with correspondingly high critical densities $\sim 3 \times 10^{17}\,\mathrm{cm}^{-3}$. Therefore, permitted and recombination lines are easily produced in the broad-line region gas. The broad-line region electron density is estimated to be $\sim 10^9\,\mathrm{cm}^{-3}$, and since there is practically no direct information on the temperature in the broad-line region, a good approximation of the temperature is $\sim 10^4$ K because the observed Fe II emission shows T $< 35\,000$ K and would collisionally ionized to Fe III at a higher temperature (Osterbrock & Ferland, 2006).

In the spectra of Seyferts, the narrow forbidden and permitted emission lines come from the Narrow Line Region (NLR), a region well outside the Broad Line Region (BLR), spanning a few tens of pc to about 1 kpc. The mere presence of forbidden lines in the NLR indicates that gas densities are lower than in the BLR. At these lower densities the physics of line production is simpler and line ratios may be used to estimate or characterize physical properties of the ionized gas, such as the nature and strength of the interstellar radiation fields, chemical abundance, local temperature and gas density. For instance, the two typical line-ratios are [O III](λ4959 Å + λ5007 Å)/λ4363 Å and [S II] λ6717 Å/λ6731 Å which yield electron temperatures in the range of $\sim 1 - 2 \times 10^4$ K and electron densities from the observational estimations varying from 10 to 1 300 cm^{-3} or from the theoretical with models input of $N_e = 100, 500, 1500, 3000\,\mathrm{cm}^{-3}$, respectively (see Dors et al., 2020b). Such simple estimates must be viewed with caution, however, because they represent weighted averages over a wide range of conditions, for instance, gas densities may probably rise in the inner regions from $\sim 10^2\,\mathrm{cm}^{-3}$ on kpc scales to $\sim 10^{6-8}\,\mathrm{cm}^{-3}$. The critical densities from the optical spectrum which shows narrow permitted and forbidden lines are $\sim 10^{14}\,\mathrm{cm}^{-3}$ and $\sim 10^4\,\mathrm{cm}^{-3}$, respectively (Osterbrock & Ferland, 2006).

There are a few clear examples where galaxies have been identified as type 2 Seyferts because the broad components of the lines have proven to be very difficult to detect, whereas there have been cases where the broad lines in Seyfert 1 galaxies have nearly completely disappeared (e.g., NGC 4151 see Antonucci & Cohen, 1983; Penston & Perez, 1984 and NGC 1566 Alloin et al., 1986). Again, NGC 7582 was a prototype Sy2, that fit all criteria to be a hidden Sy1 seen edge on until it became a true Sy1 (Halpern, Kay & Leighly, 1998; Aretxaga et al., 1999). Apart from the temporal disappearance of broad lines experienced by NGC 4151 and NGC 7582, three other classical Seyfert 2 nuclei Mrk 6, Mrk 993, and Mrk 1018 developed broad lines (broad emission-line variability of

Seyfert galaxies) in the past, which were reported by Khachikian & Weedman (1971), Tran, Osterbrock & Martel (1992), and Cohen et al. (1986), respectively. One group of scientists holds an entrenched position that all Seyfert 2s are intrinsically Seyfert 1s where broad spectra peaks is unable to be seen from a particular vantage point. Antonucci (1993, 2012) proposed that the spectral types of Seyfert differ solely due to inclination of the axis with respect to the line of sight. It is not clear, however, that this scenario can explain all of the observed differences between the two sub-classes. Since Seyfert classifications depend on the resolution of the spectra used and the noise in the spectra (Goodrich, 1989; Grupe, Thomas & Leighly, 1999), further sub-classification of Seyfert 1 class into Seyfert $1.5-1.9$ present a new challenge. The galaxy NGC 3147 at the center of the Seyfert debate seems to have been settled by Bianchi et al. (2019), thus, the two types of Seyfert galaxies are, in fact, one class of objects. However, the sub-classifications of the Seyfert galaxies will remain until similar discoveries of all the other type 2 Seyfert have uncovered their broad emission lines.

In Figure 4, optical spectra of three Seyfert galaxies of different types (Seyferts 1, 1.5, 2) from the Lick Observatory are shown in the three panels where the classification focuses on the relative strength of the broad hydrogen lines, compared to the narrow forbidden oxygen lines. The type I Seyfert galaxy spectrum in the top panel has both broad and narrow components in the permitted lines, whereas the forbidden lines like [O III] have only the narrow component. For the type 1.5 Seyfert galaxy in the middle panel the narrow lines are seen to grow stronger while the broad lines become weaker and vanish completely in the spectra of the type II Seyfert galaxy in the bottom panel. In fact, Seyfert types 1 and 2 are not as clear cut as they first seemed, since weak broad lines have now been found in Seyferts previously classified as type 2. Types 1 and 2 are better understood as extreme ends of a range of intermediate Seyfert types classified according to the relative strengths of their broad and narrow lines. For instance, in a Seyfert 1.5, there are broad and narrow lines but the broad lines are not as strong as those found in type 1 Seyferts.

Figure 4 – Optical spectra of three Seyfert galaxies that illustrate the transition from Seyfert 1 (top) to Seyfert 2 (bottom). The classification focuses on the relative strength of the broad hydrogen lines, compared to the narrow forbidden oxygen lines. Note that the broad hydrogen lines (especially Hβ) visible in Seyfert 1 appear narrower in Seyfert 2.

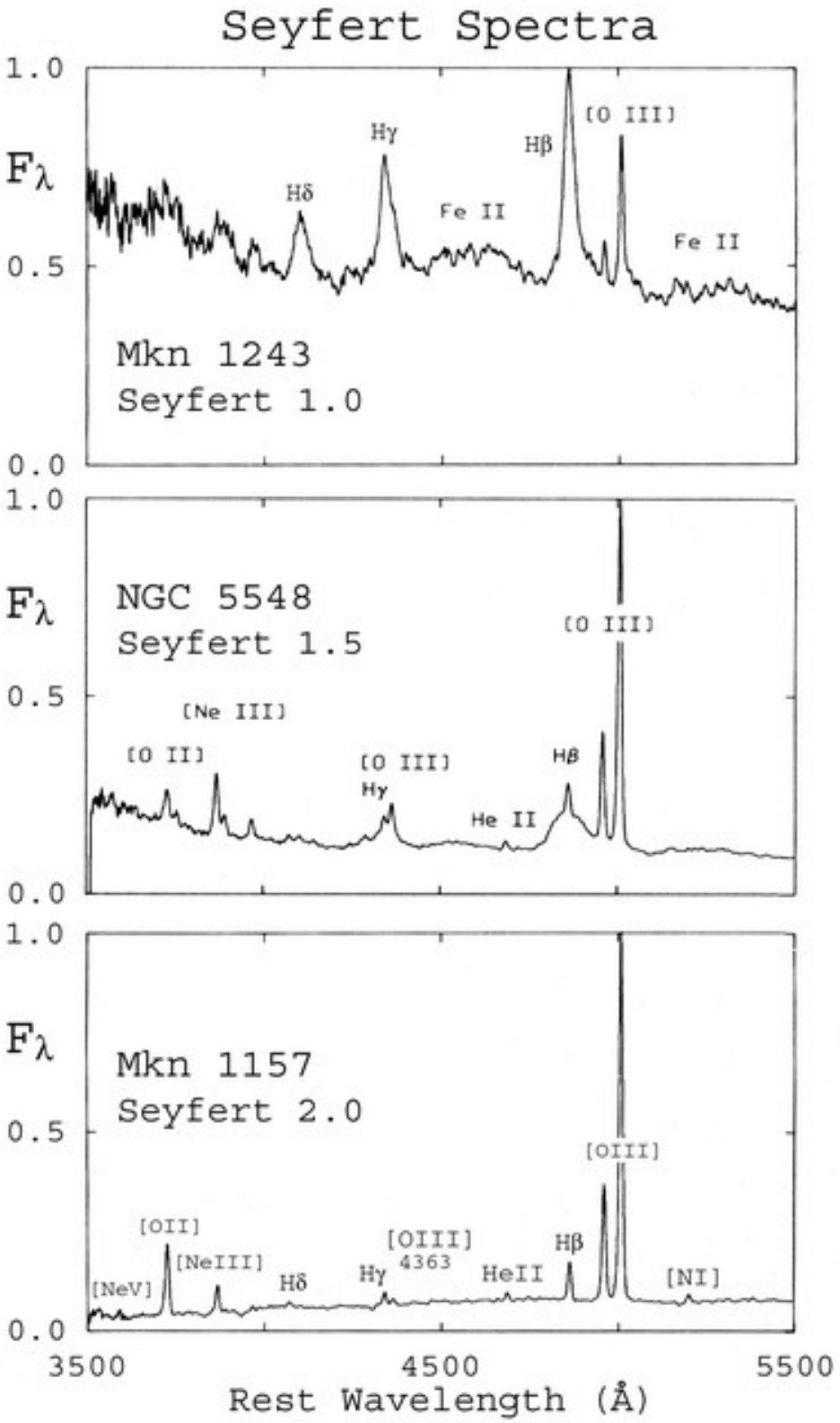

Source: Osterbrock (1984)

1.2.2 Unification Scheme of AGNs

The unification scheme of AGNs dates back to, at least, near the end of 70 decade in both optical and radio wavebands studies by Rowan-Robinson (1977) and Cohen et al. (1977), respectively, and became popular by subsequent reviews in the mid-80s and 90s (Lawrence, 1987; Antonucci, 1993; Urry & Padovani, 1995; Urry & Padovani, 1996; Goodrich, 2001). To answer the question how to bring all the underlying physical principle such as orientation, time evolution, black hole mass, black hole spin, availability of fuel, interaction ambient medium, etc., to relate the classes of AGNs into a single framework led to the postulate for a standard model for the structure of AGNs. According to the unification scheme, all AGNs (quasars, QSOs, Seyferts, etc.) are fundamentally the same type of objects (Rowan-Robinson, 1977; Antonucci, 1993; Urry & Padovani, 1995), but viewed from different angles. Toroidal obscuring region (torus) equals the optically and geometrically thick at optical. Type 1 with broad line region and Type 2 without broad line region depending on the viewing angle. In effect the unification model depicts that different types of AGNs are caused by different viewing angles (Osterbrock, 1978; Antonucci & Miller, 1985; Miller & Goodrich, 1987; Antonucci, 1993; 2012). For example, Seyfert 1 galaxies are viewed face-on relative to the accretion disk and torus with its associated broad line region in full view whereas Seyfert 2 galaxies are viewed edge-on with only the more extended narrow line clouds observed directly (Antonucci, 1993). The observed broad line radiation is polarised ($\gtrsim 15\,\%$), suggesting that it has been scattered, and is therefore a reflection of the central source (Antonucci & Miller, 1985; Krolik & Begelman, 1986; Miller & Goodrich, 1990; Heisler, Lumsden & Bailey, 1997). Traditional optical spectral observations led to the detection of the polarized broad line region (PBLR) spectroscopic observations in type 2 Seyfert AGNs, e.g., NGC 1068: (Antonucci, 1993; Antonucci & Miller, 1985) and detection of the broad line radiation through IR spectroscopy (Nagar et al., 2002; Reunanen, Kotilainen & Prieto, 2003). This result strongly supports the unification model of Seyfert 1 and Seyfert 2 galaxies. Therefore, the origin of the Active Galactic Nuclei (AGNs) unification model was the observation of broad hydrogen recombination lines of the Seyfert 2 galaxy of NGC 1068 in an optically polarized spectrum. Since then, a search for the hidden broad-line region (HBLR) of nearby Sy2s started, but polarized broad lines have only been detected in $\sim 30-50\,\%$ of the nearby Sy2s observed to date (Moran et al., 2001; Tran, 2001; Tran, 2003; Ramos Almeida et al., 2016). Some studies show that the non-detection of a PBLR is due to the genuine lack of a broad line region (Elitzur & Ho, 2009; Tran, Lyke & Mader, 2011). Complex effects of obscuration are demonstrated in the work by Gu, Maiolino & Dultzin-Hacyan (2001), who found that AGNs with PBLR have slightly lower column density ($N_{\rm H}$) than those without PBLR. Similarly, Lumsden, Alexander & Hough (2004) and Shu et al. (2007) showed that the detection rate of PBLRs decreases as a function of $N_{\rm H}$, suggesting that the absorption effect by dusty torus could play a role in the detectability of PBLRs in AGNs. Seyfert 2

nuclei have the largest absorption columns, many of which imply the medium is Compton thick, so that X-rays are suppressed below 10 keV (Mushotzky, 1982; Risaliti et al., 1999; Bassani et al., 1999; Trippe et al., 2010). Seyfert 2 nuclei also have colder IR colours than Seyfert 1 nuclei, as inferred from a sample of 10 Seyfert galaxies with ISO colours (Perez Garcia, Rodriguez Espinosa & Santolaya Rey, 1998), where T_{Sy2}=112 – 136 K and $T_{Sy1} \approx 150$ K, which can be explained if the torus is partially thick at MIR wavelengths. The host galaxies of Seyfert 1 and Seyfert 2 nuclei are dominated by large bulge fractions, and Seyfert 2 galaxies are more likely to be located in disk galaxies, whereas most Seyfert 1 galaxies are located in bulge-dominant galaxies. These results indicate that the types of AGNs are related to their host galaxies and cannot be explained by the conventional Seyfert galaxy unification model (Chen & Hwang, 2017).

A number of Seyfert 2 nuclei show clear anisotropy in the highly ionized emission lines (e.g., [O III] λ5007) which, often, resemble a radiation cone (Pogge, 1988). The ionization cone is "collimated" by the obscuring torus and one can readily assess that the radiation field is anisotropic (Neugebauer et al., 1980; Wilson, Ward & Haniff, 1988; Storchi-Bergmann, Wilson & Baldwin, 1992; Pogge & De Robertis, 1993). A comparison between the number of ionizing photons $N_{H\beta}$ to produce Hβ, and the number of ionizing photons, N_i, inferred by extrapolation of the directly observed continuum, which yielded $(N_i/N_{H\beta}) < 1$, suggesting that the ionization cone sees a more luminous continuum than we do (Wilson, Ward & Haniff, 1988). There are searches for broad-recombination lines in the NIR spectrum of Seyfert 2 nuclei, where the extinction less affects the emitted spectrum. On the bases of a conservative estimation for the intrinsic broad-line strength, Goodrich, Veilleux & Hill (1994) suggested that the broad emission lines will be detectable if $A_V \lesssim 11$ mag for Paβ, $A_V \lesssim 21$ mag for Paα, $A_V \lesssim 26$ mag for Brγ and $A_V \lesssim 68$ mag for Brα. These searches have had moderate success of about 25% of Seyfert 2 galaxies showing some broad component in the infrared (Veilleux, Goodrich & Hill, 1997).

The orientation-based unification models has been criticized from the beginning of its proposal up-to-date. There are problems regarding the polarization levels as in the most of the Seyfert 2 nuclei, the continuum is seen in direct light while the broad lines are just seen in polarized light which can not be explained clearly with Unification Models. Also, the continuum is polarized at a lower level compared to the broad lines (Miller & Goodrich, 1990; Tran, 1995a). Few Seyfert nuclei change type in a very short timescale, which is too fast to be explained by a cloud moving into our line of sight. Such events encouraged the proposal of considering Seyfert 2 nuclei as switched-off Seyfert 1 nuclei (Penston & Perez, 1984). It is not common to have a scattered BLR in the Seyfert 2 nuclei (Cid Fernandes & Terlevich, 1995). But going by the unification model one expects more frequent detection of the polarized scattered light from BLRs of Seyfert 2 nuclei. While we see many Seyfert 2 nuclei, it is not that easy to find a narrow line QSO. This curious

absence of radio-loud counterpart of Seyfert 2 nuclei can be explained by a modified unification scheme of a Receeding Torus Model (Hill, Goodrich & Depoy, 1996). In the Unification Model Scenario, we can not fit in the Weak Line Radio Galaxies (WLRGs) with either anisotropy or beaming effect (Tadhunter, 2008). Moreover, the status of Broad Line Radio Galaxies (BLRGs) which are the radio-loud version of Seyfert 1s and Narrow Line Radio Galaxies (NLRGs) which are like Seyfert 2s with no broad emission lines spectra but having a strong radio emission are not clear under this unification scheme. Moreover, we assume that the obscuration in AGNs is by a compact torus made of gas and dust and the distribution of Interstellar Medium (ISM) remains fixed over the complete lifetime of an AGN. But the high resolution observation reveals much extended ISM distribution in the form of dust lanes. Moreover, making these assumptions questionable, we have found direct kinematic evidence for outflows in few AGNs (Nesvadba et al., 2008).

In summary, it is a strong possibility that the gas in Seyferts 2 is on all scales intimately connected to somewhat, as far as the molecular ring (Maiolino; Rieke, 1995; Schmitt et al., 1997; Curran, 2000; Schmitt et al., 2001), thus being in accordance with evolutionary models of AGNs. The theory of an evolutionary difference (e.g. see Spinoglio & Fernández-Ontiveros, 2019) is in line with Blandford (1990) and Dopita (1999), who suggested that for AGNs in general, a critical look at the accretion rate as well as the mass and angular momentum of the central black hole may also have to be taken into consideration in order to provide a satisfactory scheme of unification. Alonso-Herrero, Shastri & Singh (2008) and Singh, Shastri & Risaliti (2011) found a statistical correlation among the X-ray luminosities ($L^{c}_{2.0-10\ keV}$), the bolometric luminosities (L_{Bol}), the black hole masses (M_{BH}), and the Eddington ratios (λ) for types 1 and 2 Seyferts consistent with the orientation and obscuration based on the Seyfert unification scheme. In Figure 5, a representation of the unified model depicting the different AGN types could be the same objects observed with different orientation is shown.

Extensive literature review of critical critique of the unification scheme by Antonucci (2012) led to the conclusion that uncertainties and erroneous assumptions are made by these unification model critique proponents, and almost all their findings are weak or erroneous. Nevertheless, the unification scheme can successfully explain many AGN characteristics and properties even though some questions still remain unanswered since it is still too simplified but it is the best explanation we have for developing a common model for an AGN.

Figure 5 – The unified model of Active Galactic Nuclei (Radio-loud & - quiet AGNs, Seyfert I & II Galaxies).

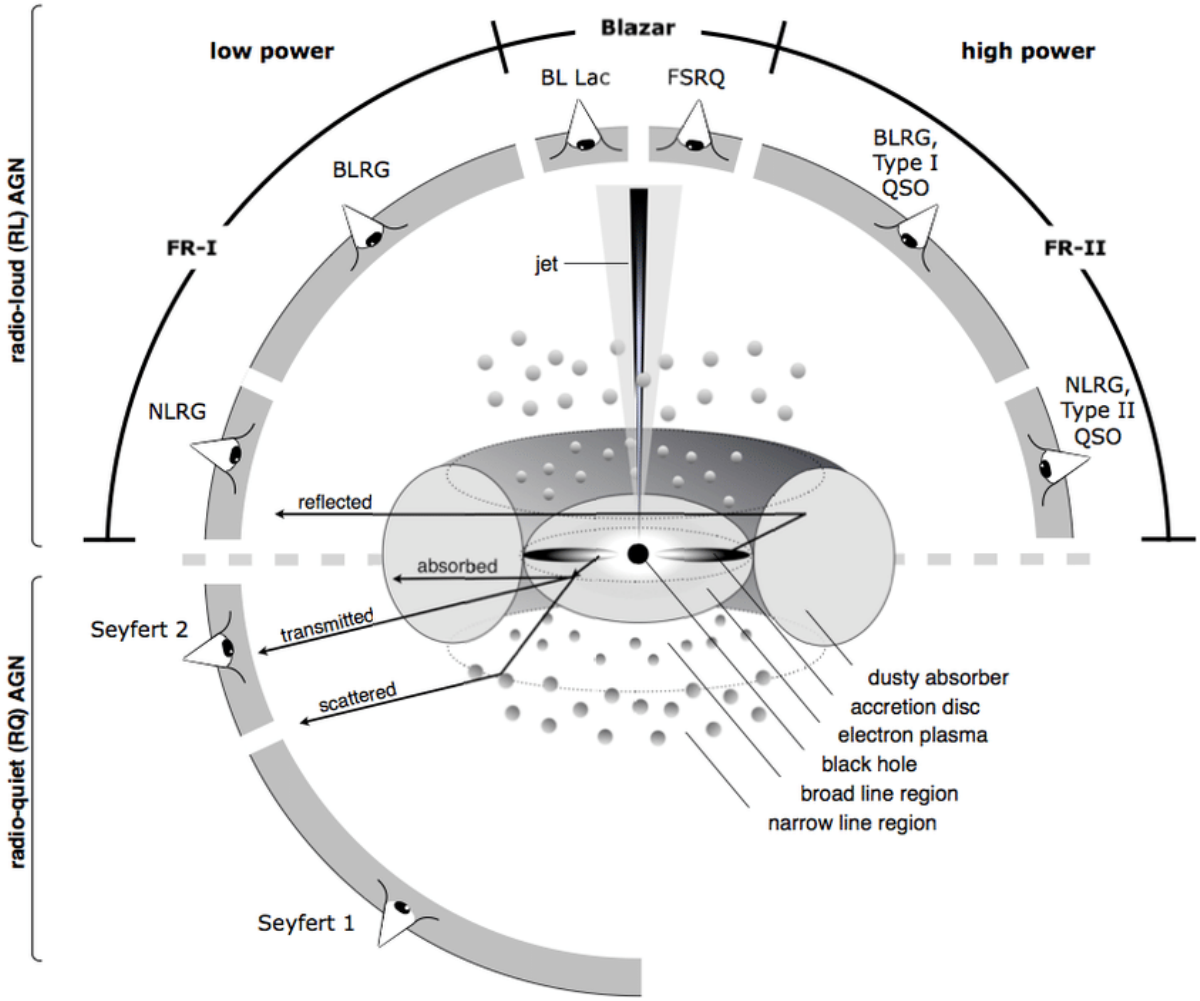

Source: Beckmann & Shrader (2012)

1.3 Oxygen abundance discrepancy in AGNs

Active Galactic Nuclei (AGNs) and Star-Forming regions (SFs) present in their spectra prominent emission-lines whose relative intensities can be used to estimate the metallicity and chemical abundances of heavy elements (O, N, Ne, S, etc.) in the gas-phase of these objects at a wide redshift range. The metallcity Z is defined by the sum of the abundance (in number of atoms) of all heavy elements in relation to the hydrogen abundance:

$$Z = \frac{N(\mathrm{O})}{N(\mathrm{H})} + \frac{N(\mathrm{N})}{N(\mathrm{H})} + \frac{N(\mathrm{Ne})}{N(\mathrm{H})} + \ldots \ . \tag{1.1}$$

Since it is impossible to estimate the abundance of all elements, it is usual to define an element as Z tracer. The relative abundance of oxygen to hydrogen (O/H) is usually used as a tracer of the total metallicity (Z) in galaxies hence the prominent emission-lines from their main ionic stages are generally detected with high signal to noise ratio (S/N, higher than 10) in the optical spectra in both SFs and AGNs. In fact, the most abundant oxygen ions are O^+ and O^{2+} which emit the strong optical forbidden emission lines [O II] $\lambda\lambda$3726, 3729 Å and [O III] $\lambda\lambda$4959, 5007 Å, respectively. As a good approximation the total oxygen abundance relative to hydrogen can be obtained by,

$$\frac{N(\mathrm{O})}{N(\mathrm{H})} = \frac{N(\mathrm{O}^+)}{N(\mathrm{H}^+)} + \frac{N(\mathrm{O}^{2+})}{N(\mathrm{H}^+)}. \tag{1.2}$$

Recently, Dors et al. (2020b) and Flury & Moran (2020) showed that the presence of O^{3+} ion in the NLR of AGNs leads to a correction in the total O/H abundance of up to only 20 %. Thus, in principle, Equation 1.2 produces a good estimation of the O/H abundance. For example, in the solar atmosphere, the solar oxygen abundance is $\left(\frac{N(\mathrm{O})}{N(\mathrm{H})}\right)_{\odot} = 10^{-3.31}$. The metallicity is usually defined by,

$$Z \equiv 12 + \log(\mathrm{O/H}), \tag{1.3}$$

where the value 12 has been added so that any element, even the rarest, has a positive solar value from the expression.

In Figure 6, a histogram containing the oxygen abundance distributions of a sample of Seyfert 2 nuclei taken from Dors et al. (2020a) is shown. These authors considered a sample of 463 galaxies obtained from the Sloan Digital Sky Survey and derived the O/H abundance, for each object, through the T_e-method and by using the semi-empirical calibration between the metallicity and the $N2O2 = \log([\mathrm{N\,II}]\ \lambda6584\ \text{Å}/[\mathrm{O\,II}]\ \lambda3727\ \text{Å})$ proposed by Castro et al. (2017). Also, represented in Figure 6 is the O/H distribution obtained from extrapolation of the O/H abundance gradients in a sample of spirals. It is worthy to note that, the distribution based on O/H values from the T_e-method developed for SFs (see e.g., Hägele et al., 2008 and references therein) indicates that the AGNs have lower values in comparison with the O/H values obtained via the other two methods.

Since the extrapolation estimation is an independent method, this method does not use the lines emitted by the AGNs. Dors et al. (2015) and Dors et al. (2020a) concluded that the T_e−method underestimates the O/H abundance, in other words, the T_e−method does not seem to work for AGNs.

Figure 6 – Histogram containing the oxygen abundance distributions for a sample of Seyfert 2 nuclei based on the T_e−method, semi-empirical calibration using photoionization models, and extrapolation of the abundance gradient, as indicated.

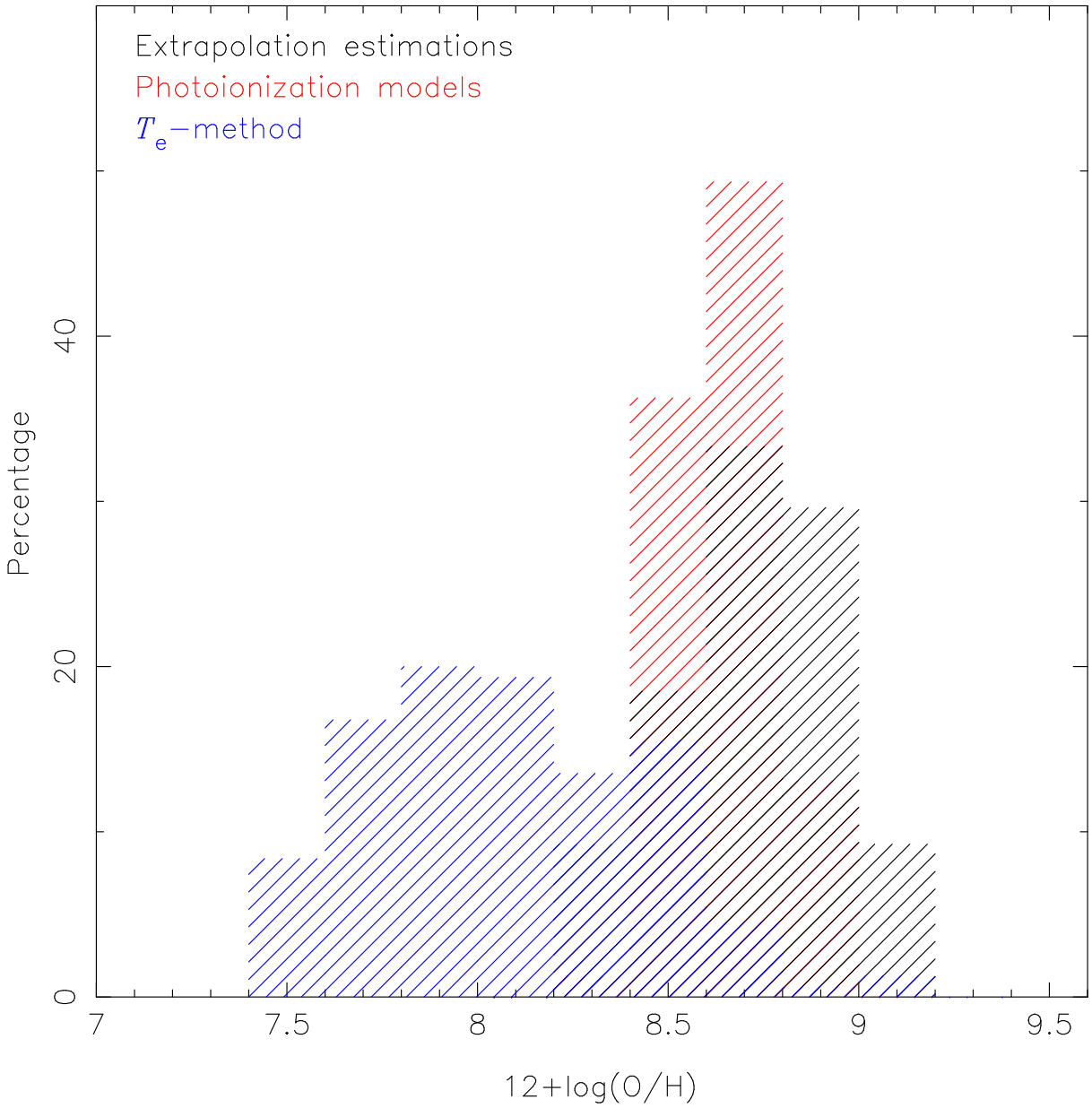

Source: Adapted from Dors et al. (2020a)

One would assume that since the T_e-method[2] is one of the most reliable method for star-forming regions, O/H estimations for AGNs based on it are correct and those obtained via photoionization models as well as inference from extrapolation method are implicitly in error. Enumerated below are the reasons in support of the assertion that T_e-method is not good for AGNs O/H abundance estimations:

1. Storchi-Bergmann et al. (1998) compared O/H abundances obtained by their theoretical calibrations for a sample of seven Seyfert 2 with values from O/H abundance extrapolations. These authors found a good agreement between the estimations via both methods (see Figure 7 taken from the work by Storchi-Bergmann et al., 1998).

2. Dors et al. (2015) confirmed the Storchi-Bergmann et al. (1998) result considering a larger sample of Seyfert 2 (12 objects) and star-forming nuclei (33 objects; see Figure 8 taken from the work by Dors et al., 2015).

3. Chemical evolution models (e.g. Mollá & Díaz, 2005) predict for central part of spiral and elliptical galaxies in the Local Universe solar or over-solar metallicities. Otherwise, O/H values based on the T_e-method for AGNs are, in most part, sub-solar values ($12 + \log(\mathrm{O/H}) < 8.3$).

Recently, Dors et al. (2020b) have investigated the origin of the O/H abundance discrepancy which in principle can be attributed to three origins underscored as:

1. The standard formalism usually considered for SFs cannot be applied to AGNs in the sense that a new relation between temperatures for the O^+ and O^{2+} must be considered.

2. There is a second heating or ionization source in AGNs beyond gas accretion.

3. There is a large electron temperature fluctuation in AGNs.

The diagonal line in the bottom panel of Figure 8 is the one-to-one relation and the upper panel shows the differences between the spectral and central intersect abundances.

[2] T_e-method: Generally, it is based on the collisional excited emission lines, and if the results derived using recombination lines (only available to H II regions, see Peimbert, Storey & Torres-Peimbert, 1993; Esteban et al., 2005; Peimbert, Peimbert & Delgado-Inglada, 2017, and references therein) are taken into account, significant differences are realised. The cause of this discrepancy has been attributed to the presence of temperature fluctuation in the gas. In principle, since the estimations through the recombination lines are less dependent on the derived electron temperatures, the most reliable method is the use of recombination lines. The principal downside, however, is that the metal recombination lines are extremely weak, hence, triggering indirect methods (extrapolation and strong-line methods) when no estimation of the temperature can be derived where strong-line methods are consistent with the direct method if they are empirically calibrated.

The hatched area indicates a band of 0.15 dex adopted for the oxygen abundance uncertainty, while solid line shows the linear regression D = 12 $\times(-0.25 \pm 0.06)$ + $\log(O/H)_0$ + 2.10 ($\pm$0.59) taking into account all the data considered by Dors et al. (2015).

Figure 7 – Oxygen abundance values 12 + log (O/H) for the NLR, obtained from the two proposed calibrations, plotted against the values obtained from the H II regions. Filled symbols represent the Seyfert 2 galaxies, and open symbols and triangles represent the LINERs. Bottom, first calibration, involving the line ratios [N II]/Hα and [O III]/Hβ; top, second calibration, involving log ([N II]/Hα) and log ([O II]/[O III]).

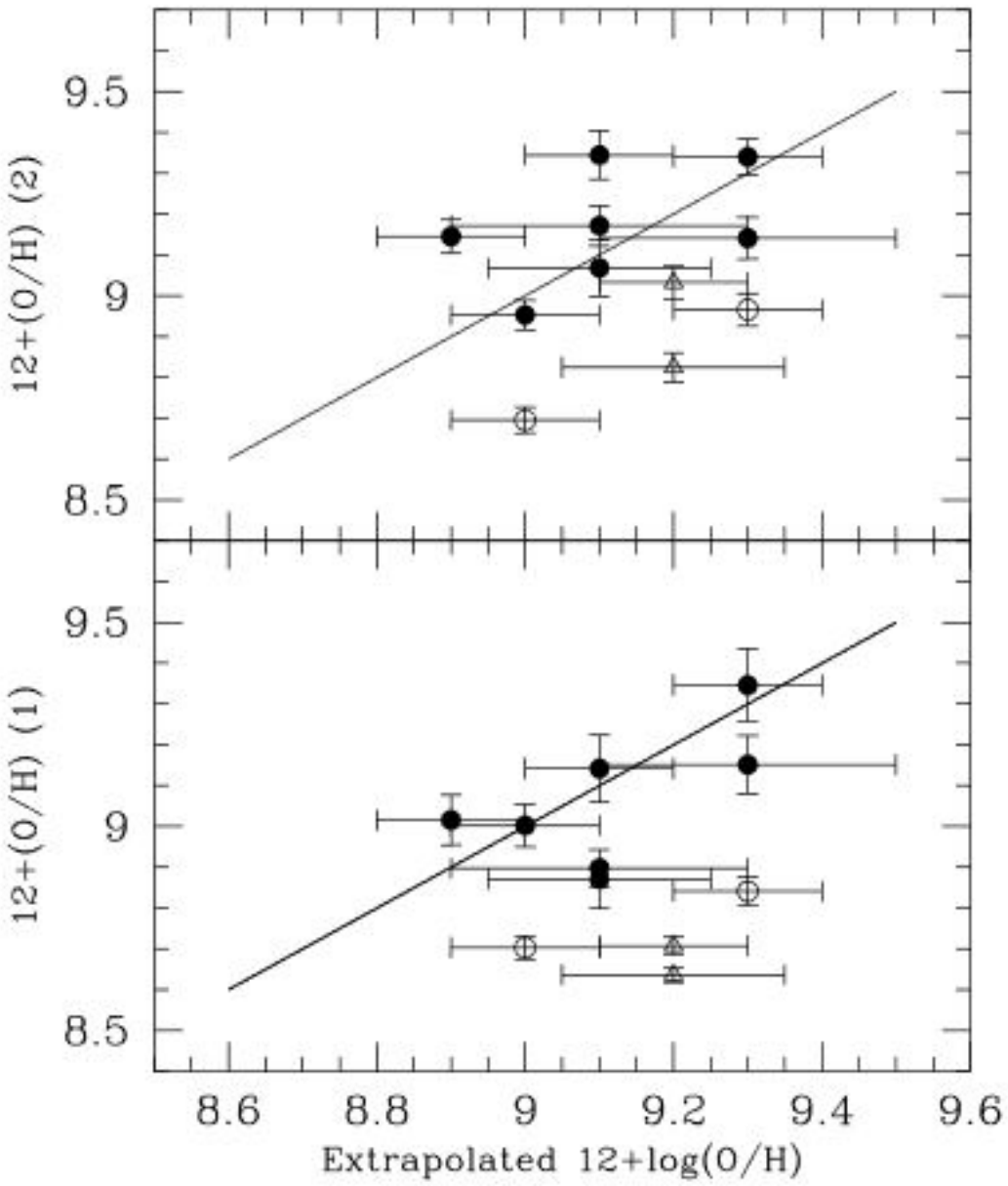

Source: Storchi-Bergmann et al. (1998)

Figure 8 – Comparison between central intersect oxygen abundances derived from the radial abundance gradients $(O/H)_0$ and the central abundances determined from the spectra of the central regions from Ho, Filippenko & Sargent (1997) through the Storchi-Bergmann et al. (1998) first calibration for the AGNs (filled squares) and through the modified counterpart method (C_{NS} method) by Pilyugin et al. (2013) for the H II-like regions (open circles).

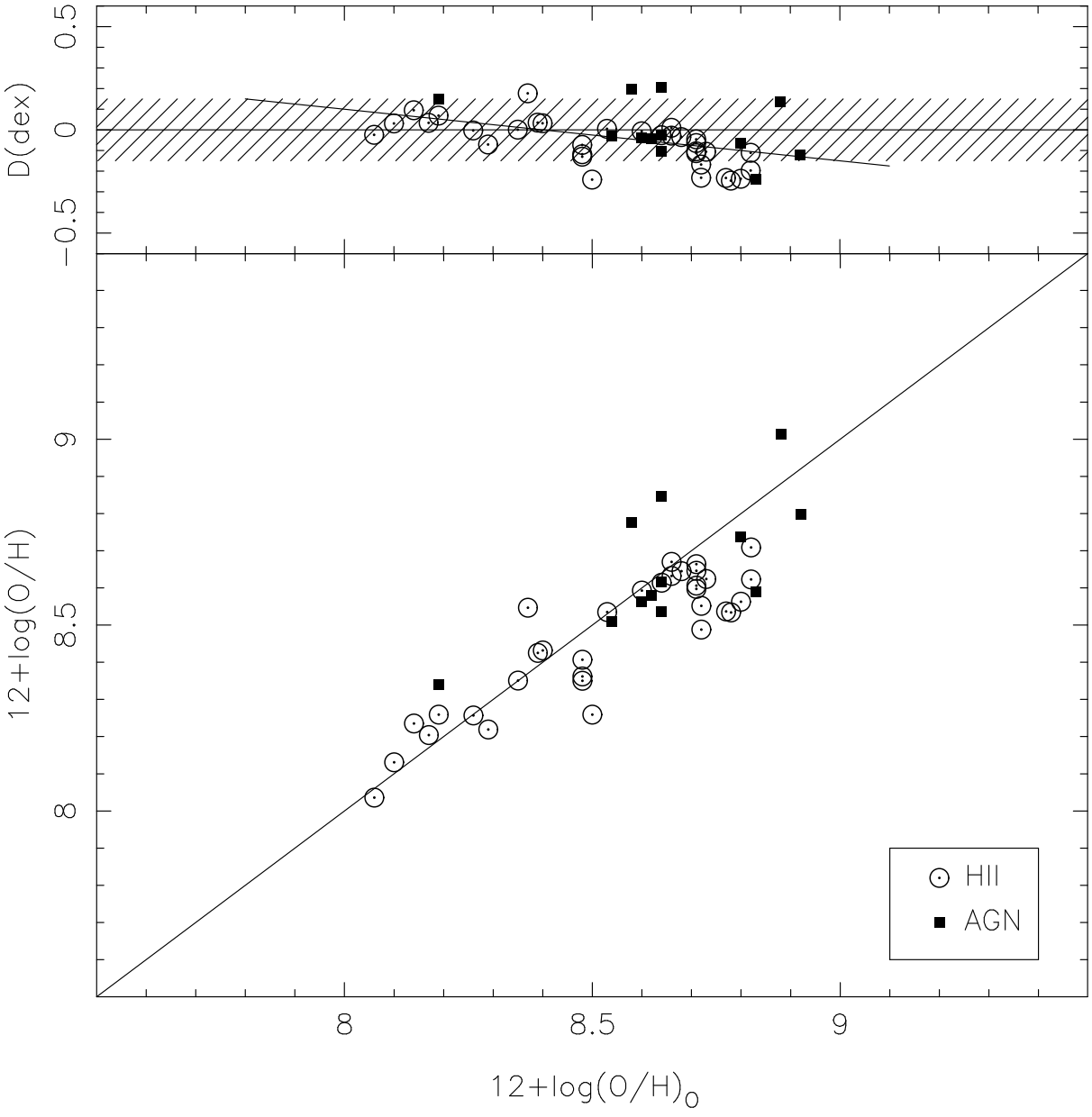

Source: Dors et al. (2015)

1.4 Motivation

Dors et al. (2020b) suggested a new formalism for the T_e-method, which reduces the difference in the O/H abundance derived with this method and photoionization models, however some issues still remain unresolved in chemical abundance determinations of AGNs, such as the presence of a second heating/ionization source and/or electron temperature fluctuations. Moreover, the applicability of the T_e-method has some limitations to AGNs studies. For instance, electron temperature can be calculated from $R_{O3} = ([O\,III](\lambda4959 + \lambda5007)/\lambda4363)$ line ratio in the range of $700 \gtrsim R_{O3} \gtrsim 30$ which corresponds to $7000 \lesssim T_e(K) \lesssim 23\,000$ (Hägele et al., 2008). However, R_{O3} values lower than 30 are derived in some Seyfert 2 nuclei (see Dors et al., 2020b and references therein), indicating $T_e > 23\,000$ K and a limited use of the T_e-method for this class of objects.

In Figure 9, bottom panel, the temperature of the electrons (in units of 10^4 K) that are exciting the O^{2+} ions, defined by t_3, derived by Dors et al. (2020b) for a sample of Seyfert 2 by using detailed photoionization models is compared to those obtained by the use direct estimation of the observational ratio $R_{O3} = [O\,III](\lambda4059$ Å $+ \lambda5007$ Å$)/\lambda4363$ Å, i.e. using the T_e-method. It can be seen that the electron temperature derived by using the T_e-method is higher than the model predictions, with differences ranging from ~ 0 to $\sim 10\,000$ K. The high electron temperature values derived from the observational ratio R_{O3} translate in deriving a low oxygen abundance via the T_e-method, as shown in Figure 6. The presence of gas shock in the NLR of Seyfert 2 has an important contribution to the heating and/or ionization, or high level of electron temperature fluctuations could be the sources of the discrepancy shown in Figure 9.

In light of the above considerations, the main motivations why it is important to estimate abundance for AGNs and to understand the physical conditions of the ionized gas in AGNs, specifically to this work are are highlighted in the following:

1. Direct abundance estimations (values derived from the T_e-method, a reliable method for star-forming regions) for Seyfert 2 are clearly underestimated in comparison with the ones obtained from several other methods and are clearly unreal values.

2. There is limited understanding of the difference in the electron temperature of Seyfert 2 nuclei values found when the values of this parameter derived from observational line ratios is compared to theoretical photoionization model predictions.

3. There are published infrared emission line fluxes of Seyfert 2 nuclei in the literature which can yield more reliable abundance estimations than those derived via optical emission lines and photoionization models.

4. Neon abundance comparison between values based on infrared emission-lines and on the $T_{\rm e}-$method could give important insights about the temperature problem in AGNs.

5. Observations carried out with future infrared satellites, for instance, Origin Space Telescope (OST) Concepts 1 and 2 with design specifications of (i) a mid-infrared imager/spectrograph/coronagraph instrument that could operate from 5 to 38 µm, with resolving powers, $R \sim 300$, $1\,000 - 3\,000$, and $20\,000 - 30\,000$, (ii) a far-infrared, medium-spectral resolution, direct detection spectrometer, optimized for multi-object spectroscopy and large area mapping, spanning 30 to 600 µm, with $R \sim 500$ and 40 000, (iii) a far-infrared, high-spectral resolution, direct detection spectrometer, spanning 20 to 300 µm, with $R \sim 1 \times 10^6$, (iv) a far-infrared imager/polarimeter operating from 35 to 500 µm, and (v) a heterodyne spectrometer operating from 500 to 4 750 GHz with $R < 1 \times 10^7$ will make it possible to access the far infrared AGN spectra, which present strong metal emission lines.

6. Dors et al. (2013) carried out a comparison between neon abundance derived from infrared and optical lines emitted in H II regions. Such analysis can easily be extended to AGN studies.

7. The level of electron temperature fluctuation in AGNs has not been established in the literature reviewed so far, therefore, if it is found to be different from the canonical values in gaseous nebulae of H II regions and PNe, it may reveal major insights in nebular astrophysics.

8. Neon abundance determinations in AGNs based on infrared lines are little dependent on the electron temperature and could be more reliable than those obtained by $T_{\rm e}-$method or photoionization models (mainly dependent on the input parameters).

Figure 9 – Bottom panel: t_3 values predicted by detailed photoionization models [$(t_3)_{\rm mod.}$] versus those calculated through the T_e-method [$(t_3)_{\rm meas.}$] Top panel: Difference between $(t_3)_{\rm meas.}$ and $(t_3)_{\rm mod.}$. Temperature values are in units of 10^4 K.

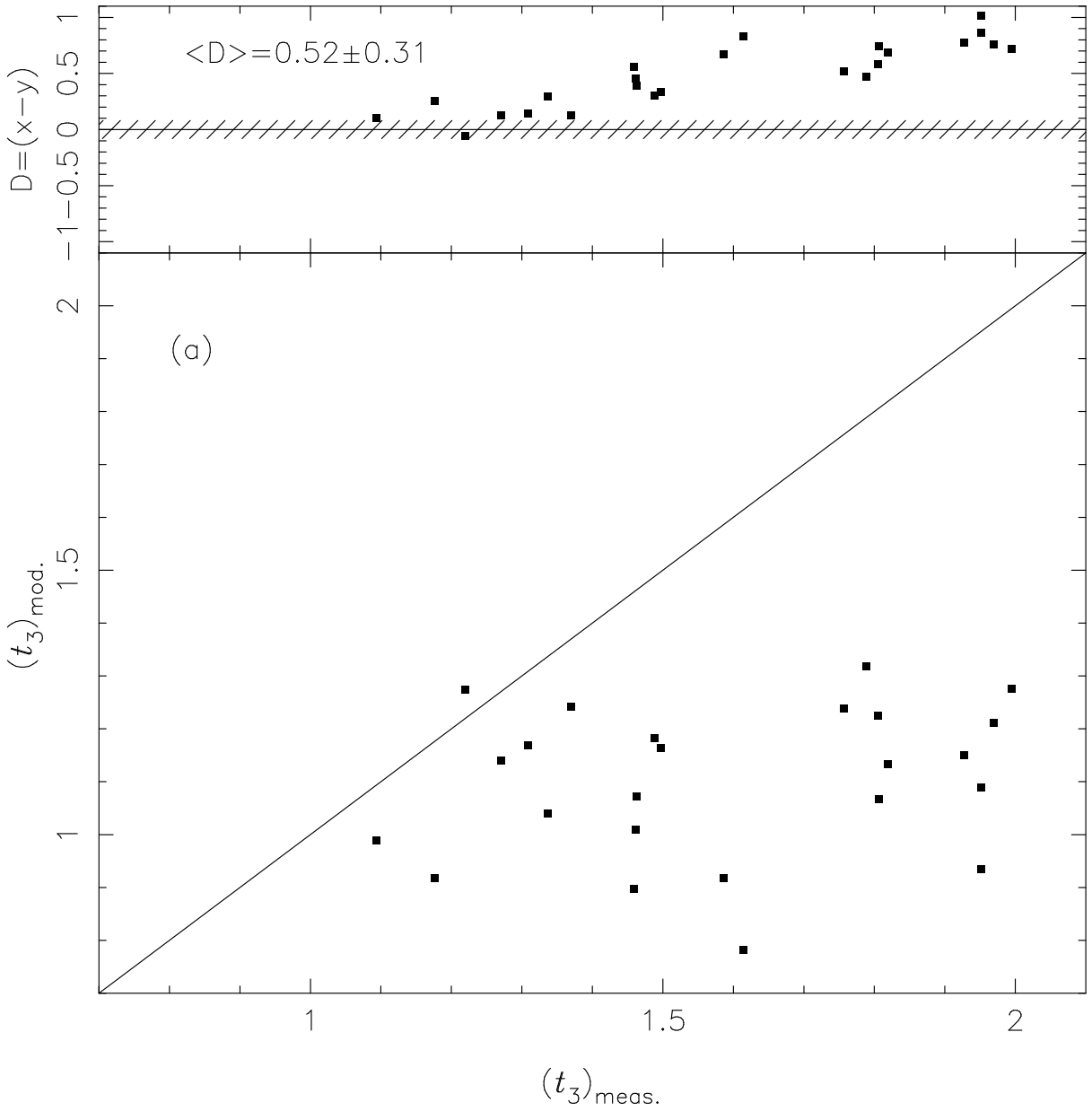

Source: Dors et al. (2020b)

1.5 Objectives

1. Understanding the low (unrealistic) metallicity values derived when the T_e-method is applied to Seyfert 2 studies.

2. To investigate the possible presence of electron temperature fluctuations in Seyfert 2 nuclei.

3. To investigate the reliability of chemical abundance determinations based on infrared emission lines of Seyfert 2 AGNs.

4. To develop a methodology to determine metallicity or chemical abundance based on infrared emission lines of Seyfert 2 AGNs.

The aforementioned motivations and objectives make this research possible contemporaneously with the advent of IR space observations such as *Spitzer* (Werner et al., 2004) and *Herschel* (Pilbratt et al., 2010), the prospect of new major spectroscopic IR surveys with the next generation satellites like the OST Concepts, and the possibility of observing the rest-frame FIR wavelength range in distant galaxies with groung based millimeter/sub-millimeter observatories such as Atacama Millimeter/Submillimeter Array (ALMA) and NOrthern Extended Millimeter Array (NOEMA) in conjunction with Institute for Radio Astronomy in the Millimeter Range (IRAM), have fostered the investigation of MIR/FIR transitions as metallicity tracers.

This work is structured as follows: Chapter 2 presents the data set compiled from the literature, as well as a brief description of the objects of study in this work. Chapter 3 gives an outline of the methodology use to derive elemental or ionic abundances with a particular emphasis on the advantages and disadvantages of the present methods and the preferable method for determining the ionic abundance of neon available in the literature. In Chapter 4, discussions and summary of the results of this work are presented; finally, Chapter 5 presents the conclusions and recommendations for future work.

2 Data

2.1 Observational data

We compiled from the literature optical and infrared emission-line fluxes of Seyfert 2 nuclei. The infrared sample consists of near infrared (NIR) to mid – infrared (MIR) spectroscopic observations of 36 Seyfert 2 nuclei:

(i) performed with the Physics and Astronomy Classification Scheme (PACS) instrument on board the European Space Agency (ESA) Herschel Space Ship in the short cross-dispersed mode (R $\sim$ 360) covering the *JHK*-bands, together with an ancillary data from

(ii) *Spitzer*-Infrared Spectrometer (IRS) spectroscopic survey consisting of the short wavelengths ranging from 9.9 to 19.6 µm covered by the Short-High (SH) module in the high spectral resolution mode ($R \sim 600$) and from 8 to 2.4 µm;

(iii) The cooled grating spectrometer 4 (CGS4) on United Kingdom Infrared Telescope (UKIRT), IRSPEC (Infrared Spectrometer) infrared array spectrometer ($R \sim 1\,500$) at the ESO 3.6 m telescope;

(iv) Medium resolution ($R \sim 1\,500$) of Infrared Space Observatory Short Wavelength Spectrometer (ISO-SWS) $2.4 - 45$ µm spectra, both high-resolution ($R = 1\,260$) and low-resolution ($R = 345$ and 425) $JHK-$band spectra of 4 µm spectroscopy with ISAAC at the European Southern Observatory Very Large Telescope array (ESO VLT);

(v) Infrared Spectrometer And Array Camera Long Wavelength (ISAAC-LW) medium resolution spectroscopy mode covering a range from 3.93 to 4.17 µm at spectral resolving power $\sim$ 2500;

and

(vi) NIR integral field spectroscopy of moderate resolution ($R \sim 1\,000$ and $R \sim 2\,000$) $HK-$bands spectra, etc.

The optical data taken within the spectral range $4000 < \lambda$ (Å) < 8000 comprise of:

(i) low-dispersion spectra using telescopes at Las Campanas, Anglo-Australian, Lick, and European Southern observatories

and

(ii) Faint Object Spectrograph spectroscopy (FOS) aboard Hubble Space Telescope (HST) at a wavelength of $4000 < \lambda$ (Å) < 7000.

A summarized description of each galaxy of the sample is presented below.

NGC 3081 (IC 2529): NGC 3081 ($z = 0.00795$, (R_1R_2')SAB(r, nr)0/a) is a nearby Seyfert 2 galaxy with four rings comprising of the normal ring features of the outer (R_1), inner (r), nuclear (nr) types with the outer ring arms forming part of a classical double ring/pseudoring R_1R_2' morphology component, and R_2' which forms the two spiral arms that break from the R_1 component (Buta & Purcell, 1998). The $J-$band spectrum of NGC 3081 showed faint narrow Paβ and [Fe II] λ 1.2567 µm emission lying on top of a strong stellar continuum (Goodrich, Veilleux & Hill, 1994). No attempt was made to observe NGC 3081 in the $K-$band because detection of a broad component to Paβ is difficult unless the stellar continuum is very carefully removed from the data. The $H-$ and $K-$band spectra of NGC 3081 by Reunanen, Kotilainen & Prieto (2003) showed the detection of narrow Brγ and a weak [Fe II] 1.644 µm with the Brγ extended by ~ 2 arcsec. It has a near-IR bar aligned at P.A. $= 123°$ (Mulchaey, Regan & Kundu, 1997). The detection of broad Hα in polarised light with a width of $\sim 7\,000$ km s^{-1} from the nucleus has been reported by Moran et al. (2000).

NGC 4388 (UGC 7520/MCG 2-32-41): Infrared spectroscopy study by Blanco, Ward & Wright (1990) and Goodrich, Veilleux & Hill (1994) showed no evidence for broad Paβ emission in NGC 4388, which was confirmed by Ruiz, Rieke & Schmidt (1994). Veilleux, Goodrich & Hill (1997) attempted to detect a broad line in Brγ and Brα but no obvious sign of a broad component to any of these lines from the spectra were detected despite the off-nuclear broad Hα in NGC 4388 presented by Shields & Filippenko (1988). Since both the line-to-continuum contrast and S/N of the new data are slightly lower than in the $J-$band data presented by Goodrich, Veilleux & Hill (1994), the constraints on broad Brγ and broad Brα are relatively weaker than that on broad Paβ (Veilleux, Goodrich & Hill, 1997). There was a general tendency for the amount of reddening derived from the narrow lines in NGC 4388 to increase toward longer wavelengths, but for the color excess derived from Brγ_n/Hα_n, which suggests the presence of an obscured source of narrow-line emission only visible at infrared wavelengths (Veilleux, Goodrich & Hill, 1997).

NGC 4507: It has a NIR bar aligned at P.A. $= 53°$ (Mulchaey, Regan & Kundu, 1997). Schmitt et al. (2003) presented [O III] image of this Seyfert 2 galaxy where the emission is elongated along P.A. $= -35°$ in the inner $2''$ region, becoming more circular in the outer regions and the major extent of the emission is $3''.5$ (800 pc). The bulk of the emission is related to the nucleus and a blob located at 100 to the NW. A strong and asymmetric broad Hα in polarised flux with a width of $\sim 10\,000$ km s^{-1} (Moran et al., 2000).

NGC 5135 (ESO 444 G32/MCG -5 - 32- 13): NGC 5135 (SABb, $z = 0.00135$) belongs

to a group of seven galaxies (Kollatschny & Fricke, 1989) and its nucleus shows high-excitation lines thereby being classified as a Seyfert 2 nucleus (Phillips, Charles & Baldwin, 1983). It has a near-IR bar aligned at P.A. = 123° (Mulchaey, Regan & Kundu, 1997). The projected spectrum size of 2.7×5.4 kpc through the International Ultraviolet Explorer (IUE) aperture depicted mix Seyfert and starburst characteristics (Thuan, 1984; Kinney et al., 1993). The radio continuum map at 6 and 20 cm shows an asymmetric structure with faint emission extended to the northeast (P.A.= 30°) of the bright core source (González Delgado et al., 1998). The overall linear extent is about 9″. The Hα narrowband image shows extended emission aligned with the radio emission (Haniff, Wilson & Ward, 1988; García-Barreto et al., 1996). The high-excitation gas mapped through the [O III] λ5007 emission line, is aligned north-south on a 2″ scale.

NGC 5643 (ESO 272-G016): The NGC 5643 (z = 0.003999, Sturm et al., 2002) cross-dispersed (XD) grating spectrum obtained by Winge et al. (2000) along the axis of the optical ionization cone, which showed [S III], He I 1.083 µm, Paβ, and the tip of the Paα emission line where only the Paβ profile was marginally resolved spatially in the central regions, but both the Paβ line and [S III] λ9532 show a second emission feature $\sim$ 3 arcsec east of the nucleus. Schmitt, Storchi-Bergmann & Baldwin (1994) confirmed a biconical morphology for the high-excitation gas and indicated that the cone axis is slightly tilted relative to the bar and speculate that the active nucleus is hidden and located at $\sim$ 3″ from the peak of the continuum.

NGC 5728 (MCG-03-37-5): This is one of the Seyfert 2 galaxies (SAB, z = 0.00935) that displays prominent co-linear biconical emission line cones, separated by a dark band (Wilson et al., 1993). X-ray observations with the Burst Alert Telescope onboard the Swift space observatory by Cusumano et al. (2010) indicated a flux at 15-150 keV of $7.40 \pm 0.54 \times 10^{-11}$ erg cm^{-2} s^{-1} for this object. In the NIR, the K-band spectroscopy has been published by Veilleux, Goodrich & Hill (1997) and Sosa-Brito et al. (2001). They both show a spectrum dominated by molecular H_2 and weak Brγ emission. The composite JHK spectroscopy by Riffel, Rodríguez-Ardila & Pastoriza (2006) reveals a poor emission line spectrum, dominated by unresolved [S III] 9532 Å and He I 1.083 µm. Also, these authors reported the first detection of [Si VI] 19630 Å, in the K-band, implying the existence of high-ionized gas. Moreover, [Si VI] is the only line spectroscopically resolved, with a FWHM of $\approx$ 430 km s^{-1}. The continuum emission is steep and almost featureless. The only absorption lines detected are the CO bandheads at 2.3 µm and Na 2.207 µm in K. Based on a J-band spectrum, NGC 5728 was classified by Goodrich, Veilleux & Hill (1994) as a possible candidate for an obscured Seyfert 1 galaxy.

IC 5063 (ESO 187- G023/PKS 2048-57): The Seyfert 2 galaxy IC 5063 (z = 0.011348, Sturm et al., 2002) ground-based [O III] image shows emission extended over a region larger than $\sim$ 30″, along P.A.= −65° (Morganti, Oosterloo & Tsvetanov, 1998; Morganti

et al., 1999). The line emission is aligned with the radio emission and the host galaxy major axis. This galaxy is also known to have polarized broad emission lines (Inglis et al., 1993). [O III] image by Schmitt et al. (2003) confirms the ground-based results but shows only a much smaller portion of the extended emission, owing to the field of view of the Linear Ramp Filter. This emission can be represented by a bicone centered at the nucleus, with opening angle of 60°, extending by 12″ (2640 pc) along P.A.= −65° and ∼ 3″ (660 pc) along the perpendicular direction. At distances larger than 3″ north of the nucleus the emission seems to split on the two sides of the host galaxy major axis, giving it the appearance of an X-shaped NLR.

IC 5135 (NGC 7130): IC 5135 was originally identified as a Seyfert 2 galaxy by Phillips, Charles & Baldwin (1983). The spectrum size of 3.1 × 6.2 kpc through the IUE aperture showed a mix characteristics of Seyfert and starburst emission lines (Thuan, 1993, Kinney et al., 1993, see also near-IR wavelength study by Goldader et al., 1997). Shields & Filippenko (1990) also confirmed the presence of a circumnuclear starburst through detail study of the optical emission-line spectrum in this object while the line intensity ratios in the nucleus are typical of Seyfert 2 galaxies. No spectrum was obtained in the $J-$band and the line emission from Brγ and H_2 2.121 µm dominates the $K-$band spectrum by Veilleux, Goodrich & Hill (1997). Both lines have similar widths, and neither shows any obvious broad wings at low intensity levels. Any broad (FWHM ≈ 2600 km s^{-1}) emission at Brγ must be weaker than about 3×10^{-15} erg cm^{-2} s^{-1}. A number of other features may be identified in the spectrum. The line at 2.094 µm is redshifted He I λ2.058, while the weaker features at 2.26 µm and 2.110 µm probably correspond to H_2 λ2.223 and H_2 λ2.073, respectively.

MRK 3 (UGC 3426/MCG 12-6-19): BLR in Markarian 3 ($z = 0.013509$, Sturm et al., 2002) has been detected using spectropolarimetry (Miller & Goodrich, 1990; Tran, 1995b), but low-resolution $J-$band spectra do not reveal any obvious BLR at Paβ (Goodrich, Veilleux & Hill, 1994). Veilleux, Goodrich & Hill (1997) could not obtain high-resolution UKIRT data of Mrk 3 because of the high declination. The strong emission lines of [Ne V] indicate ionization of the narrow-line region by the AGN (Weedman et al., 2005).

MRK 273 (IRAS F13428+5608/A1342+56/UGC 8696/MCG +9-23-4/I Zw 71/VV 851): Markarian 273 ($z = 0.0372$, Mazzarella & Balzano, 1986) galaxy was classified by Goldader et al. (1995) as a super luminous LINER ($12.07 \lesssim \log(L_{\rm IR}/L_\odot) \lesssim 12.14$). It has been characterized as a double nucleus (Wehinger & Wyckoff, 1977) or a triple-nucleus system (Korovyakovskii et al., 1981). Mrk 273 has a strongly distorted disk which is actually composed of an extremely bright Seyfert nucleus, generally assumed to be the original nucleus of Mrk 273, and two lesser blobs which are most likely major clumps of star formation, while the northern companion has a strong H II region-like emission-line spectrum (Sanders et al., 1988). Adams (1977) first noted there may be an extension of the envelope to the east

of the northern part of Mrk 273. The optical spectroscopy study by Koski (1978), Sanders et al. (1988) and the $K-$band spectrum by Veilleux, Sanders & Kim (1999), as well as ISO observations by Genzel et al. (1998) indicated an AGN contribution to the excitation of the nuclear region of Mrk 273. The $K-$band spectrum presented by Goldader et al. (1995) demonstrated the starburst nature of the nucleus, though this spectrum does extend beyond the red nuclear region to the bluer disk (Scoville et al., 2000). Conversely, $K-$band spectra extracted over the central $4''$ by Sosa-Brito et al. (2001) are much redder with apparently weaker stellar features and are consistent with the spectrum presented by Veilleux, Sanders & Kim (1999) over a similar region. Iwasawa (1999) found that Mrk 273 contains a Seyfert nucleus at moderate luminosity through ASCA observations. Colina, Arribas & Borne (1999) concluded that the northeastern region coincided with the optical nucleus of the galaxy and displayed the spectral characteristics of low-luminosity LINER, while [O III] emission dominated the southwestern region and was classified as a Seyfert 2 nucleus. Observations of the nuclear region at higher spatial resolution in the NIR (Knapen et al., 1997, Scoville et al., 2000, U et al., 2013) and in the radio (Knapen et al., 1997; Carilli & Taylor, 2000; Bondi et al., 2005) collectively showed the nucleus to be composed of three separate sources, representing northern (N), southeastern (SE), and southwestern (SW). From the two bright NIR sources (N and SW), only N was detected in the radio. The SE nuclear source seen in the HST NICMOS image at $0''.22$ resolution (Scoville et al., 2000) was not detected by Knapen et al. (1997). Knapen et al. (1997), Scoville et al. (2000), Carilli & Taylor (2000), U et al. (2013), Bondi et al. (2005), and U et al. (2013) all opined on the nature of the three sources, and came at odds conclusions. Scoville et al. (2000), Carilli & Taylor (2000), and Bondi et al. (2005) asserted that the northern source was a starburst, whereas Knapen et al. (1997) gave an opposing view to the N source as being an AGN. Carilli & Taylor (2000) further detailed the H I absorption line data from the northern nucleus as indicative of a gaseous disk in rotation, with the inferred enclosed mass of 2×10^9 $M_\odot$, which is in a complete agreement with the molecular gas observed by Downes & Solomon (1998). Scoville et al. (2000) and U et al. (2013) posited that the AGN is the SW nucleus.

Using Chandra X-ray image together with the optical and NIR images from HST, Iwasawa et al. (2011) identified the absorbed, hard X-ray source of the Seyfert 2 nucleus in Mrk 273 with the SW nucleus, which revises the previous identification to the N or northeastern (NE) nucleus. U et al. (2013), Iwasawa et al. (2018), and Liu et al. (2019) claimed Mrk 273 to be double AGN on the basis of putative strongly absorbed X-ray source ($\sim 2-10$ keV) in N but still maintained the SW to be a Seyfert nucleus. It is very clear hitherto that the SW of Mrk 237 is a Seyfert 2 nucleus.

MRK 348 (NGC 262/UGC 499): Markarian 348 ($z = 0.0151$, Mazzarella & Balzano, 1986) is a CfA galaxy hosting a Seyfert 2 nucleus with strong emission lines and un-

derlying featureless continuum in the optical (Koski, 1978). The host galaxy is an early-type spiral galaxy which is oriented nearly face-on and has a nearby companion galaxy, NGC 266 (Heckman et al., 1982; Simkin et al., 1987). A broad Hα component has been found in polarized light with a FWHM of 8400 km s^{-1} (Miller & Goodrich, 1990). Veilleux, Goodrich & Hill (1997) did not find broad Brγ in their IR spectrum but found a Brγ profile broader than $H_2\,1-0\,S(1)$. $K-$band spectrum from Sosa-Brito et al. (2001) agrees with Veilleux, Goodrich & Hill (1997), although the lower S/N of their spectrum does not permit more conclusive comparisons. A hard X-ray detection (Awaki et al., 1991) gives $N_{\rm H} = 1.1 \pm 0.2 \times 10^{23}$ cm^{-2} and supports the idea that Mrk 348 harbors an obscured Seyfert 1 nucleus. Neff & de Bruyn (1983) report that its nuclear radio source consists of a compact core plus two knots aligned along position angle 168°, with a total size of about 0″.15. They also report variation at 6 and 21 cm on timescales of months. A high resolution HST image published by Capetti et al. (1996) showed a linear structure of narrowband [O III] λ5007 emission extended 0″.45 at a position angle $\sim$ 55°.

MRK 573 (UGC 01214/UM 363/MCG-0- 05-33): The Seyfert 2 galaxy Mrk 573 (Huchra & Burg, 1992) is a SAB with redshift $z = 0.017259$ (Sturm et al., 2002). X-ray observations with the ROSAT satellite by Tajer et al. (2005) indicated a flux at 0.1-2 keV of $6.70 \pm 0.34 \times 10^{-13}$ erg cm^{-2} s^{-1} for this object. It is a well-studied AGN with two ionization cones seen in [O III] maps (i.e.; extended [O III] emission, see Haniff, Wilson & Ward, 1988; Pogge & De Robertis, 1993, 1995; Falcke, Wilson & Simpson, 1998) in alignment with the observation of a radio triple source (Ulvestad & Wilson, 1984a). It is also known for the bright high-ionization emission lines displayed in its optical nuclear spectrum (Durret, 1994). The NIR spectrum of Mrk 573 presented by Riffel, Rodríguez-Ardila & Pastoriza (2006) shows strong emission lines of [S III], He I, and H I dominates the J-band. Also, strong high-ionization lines were detected, including those of [S IX] 12520 Å, [Si X] 14300 Å, and [Ca VIII] 23218 Å. The line profiles are narrow, with a typical FWHM of 400 km s^{-1}.

NGC 1068 (M 77/Arp 37): NGC 1068 ($z = 0.003829$, Sturm et al., 2002) is the nearest Seyfert 2 galaxy and has been very extensively studied. NGC 1068 has a polarized optical spectrum similar to that directly observed in Seyfert 1 nuclei, with FWZI$\approx$ 7500 km s^{-1} for the Balmer lines (Antonucci & Miller, 1985). A compact stellar cluster has been found by Thatte et al. (1997), and they show that its contribution to the total bolometric nuclear (within a radius 2″.5) luminosity is at least 7 %. They also observe that 94% of the light in the K band in the central 1″ originates from a compact source which they interpreted as hot dust emission. The [O III] line emission morphology has a conical shape which extends 7″.5 at P.A. $\sim$ 35° with opening angle $\sim$ 45° (Evans et al., 1991). A ring of star formation (of outer diameter 36″) apparently powers half of the mid-/far-IR luminosity, while the other half comes from the Seyfert nucleus (Pogge & De Robertis,

1993). Significant amounts of hot dense molecular gas is shown by the $H_2\ 1-0\ S(1)$ line emission extending over a region of 350 pc around the nucleus (Rotaciuc et al., 1991; Blietz et al., 1994) and thought to be excited in the gas heated by UV radiation or by X-ray photons from a central source (Rotaciuc et al., 1991). Weak $H_2\ 1-0\ S(1)$ line emission, possibly due to shock excitation, also extends for 10″ along the stellar bar (Davies, Sugai & Ward, 1998, Scoville et al., 1988). The [Fe II] λ1.644 µm forbidden line has been mapped (Blietz et al., 1994) and compared to the structure of the radio elongated emission (Wilson & Ulvestad, 1983). The [Fe II] λ1.644 µm and radio emission line are colinear, with the lobes of the radio emission "faring out" at the end of the significant [Fe II] λ1.644 µm emission. A forbidden [Si VI] λ1.962 µm line has been detected (Oliva & Moorwood, 1990) in this object, however, in our spectrum this spectral region is not covered. Elvis & Lawrence (1988) present EXOSAT observations in the 2 - 10 keV range. They detect a source with a flat power-law spectrum which resembles that of typical Seyfert 1 galaxies. Within their observations they did not find evidence of variations on timescales of 30 minutes to 4 years. They use this as evidence that the direct view of the nucleus is totally obscured and the X-ray flux observed is seen only in scattered light.

NGC 2992 (MCG - 02 - 25 - 14/Arp 245): NGC 2992 is a nearby Sa galaxy ($z = 0.0077$) interacting with NGC 2993 (Gilli et al., 2000) by a tidal tail with a projected length of 2.9 arcmin and inclined about 70° to our line of sight, displaying a broad disturbed lane of dust in the equatorial plane (Onori et al., 2017). The optical spectrum of the narrow-line X-ray galaxy NGC 2992 is fairly typical of that of a normal Seyfert 2 galaxy except for the detection of a possible weak Hα broad component with no Hβ broad component counterpart (Shuder, 1980; Veron et al., 1980; Ward et al., 1980). In contrast, broad emission is clearly observed in the profile of Paβ (Rix et al., 1990; Veilleux, Goodrich & Hill, 1997). The $K-$band spectrum of NGC 2992 is characterized by weak Brγ emission but relatively strong H_2 emission. There is a slight excess of broad emission with FWHM $\approx$ 4000 km s^{-1} on each side of narrow Brγ, but it may simply reflect structure in the underlying stellar continuum or small errors in the continuum calibration. The colour excesses derived from the narrow lines of NGC 2992 show a tendency to decrease with wavelengths. This result is difficult to explain unless differential slit loss, seeing, and guiding effects are affecting the data on this object. This may be the case since the line-emitting region in NGC 2992 is known to be extended and complex (Wehrle & Morris, 1988).

NGC 5506 (MRK 1376): Broad Paβ line in NGC 5506 ($z = 0.006181$, Sturm et al., 2002) has been reported by Blanco, Ward & Wright (1990), Rix et al. (1990), and Ruiz, Rieke & Schmidt (1994), however, Veilleux, Goodrich & Hill (1997) argued that the detection of Paβ corresponds to the strong, highly reddened emission in the wings of the profile of Paβ. Goodrich, Veilleux & Hill (1994) found that the profile of Brγ is similar to that of

Paβ which presents a narrow core superposed on a broad base. Veilleux, Goodrich & Hill (1997) investigated the Brγ and Brα of NGC 5506 but found no presence of BLR emission in Brγ and Brα. The fluxes found by Veilleux, Goodrich & Hill (1997) are significantly larger than those obtained by Moorwood & Oliva (1988) and Kawara, Nishida & Phillips (1989), the origin of this discrepancy could be attributed partly to differences in the placement of the slit.

NGC 7674 (MRK 533/UGC 12608/ Arp 182/MCG-01-59-80): NGC 7674 is a SBb galaxy with redshift $z = 0.02892$ and it was observed at practically all wavelength ranges. Osterbrock & Dahari (1983) used the Lick Observatory 3 m Shane reflector telescope to take optical ($4000 < \lambda$ (Å) < 7000) spectroscopic data of NGC 7674 and classified it as a type 2 Seyfert galaxy. Bianchi et al. (2005) using the XMM-Newton satellite observations derived a flux in the 2–10 keV band of $0.70 \pm 0.07 \times 10^{-12}$ erg cm^{-2} s^{-1}. Kraemer et al. (1994) used the International Ultraviolet Explorer (IUE) to obtain the spectrum of NGC 7674 in the range $1200 < \lambda$ (Å) < 3200 where strong metal emission lines, such as [C IV] and [C III] were observed. Riffel, Rodríguez-Ardila & Pastoriza (2006) used the NASA 3 m Infrared Telescope Facility (IRTF) and obtained near infrared spectrum of NGC 7674 in the range 0.8 to 2.4 µm. Although, NGC 7674 is classified as Seyfert 2 from its optical spectrum, in the NIR region it displays broad emission components in the permitted lines, similar to what is observed in classical Seyfert 1s (Riffel, Rodríguez-Ardila & Pastoriza, 2006). The profiles of both Paβ and Brγ are characterized by a narrow core superposed on a broad base blueshifted with respect to the narrow core (Veilleux, Goodrich & Hill, 1997). However, the broad component in the profiles of both Paβ and Brγ represents emission from a NLR rather than from a genuine high-density BLR (in which [O III] λ5007 is collisionally de-excited).

I Zw 92 (Mrk 477): I Zw 92 ($z = 0.037799$, Sturm et al., 2002) is a Seyfert 2 galaxy with polarized broad Hα harboring an obscured Seyfert 1 nucleus (Tran, 1995b). The application of evolutionary population synthesis models to UV Si IV λ1400 absorption feature and the spectral energy distribution showed that star formation has occurred leading to a significant contribution to the total bolometric luminosity ($L_{Bol} \approx 4 \times 10^{10} L_{\odot}$) of Mrk 477 in a very short period of about 6 Myr ago (González Delgado et al., 1998). No obvious broad Paβ emission was detected in the $J-$band spectra (Goodrich, Veilleux & Hill, 1994), although the relatively low resolution of the spectra undoubtedly hampered their ability to detect a broad feature with FWHM$\approx$ 3000 km s^{-1} (Tran, 1995b). The $K-$band spectrum of I Zw 92 by Veilleux, Goodrich & Hill (1997), presents relatively strong, narrow H_2 2.121 µm and Brγ features and an apparent detection of broad component to Brγ. Veilleux, Goodrich & Hill (1997) proposed that the presence of broad Brγ emission combined with the lack of any broad Hα or Paβ emission at the level of at least one-fifth implies that data of higher S/N are needed to confirm the presence of broad Brγ.

NGC 2110 (MCG-01-15-4): HST imaging spectroscopy of NGC 2110 ($z = 0.00761 \pm 0.00032$, Shuder, 1980) reveals both a narrow $\sim 1''$ long jet/region of [O III] emission extending to the north of the nucleus and an S-shaped Ha emission region within the inner $4''$ (Mulchaey et al., 1994). A similar S-shaped morphology is seen in the [Fe II] map by Sosa-Brito et al. (2001). Radio emission extends symmetrically $\sim 2''$ north and south of the nucleus (Ulvestad & Wilson, 1983) while [O III] and Hα + [N II] images show more extended emission which is also elongated north-south (Wilson, Baldwin & Ulvestad, 1985, Pogge, 1989). Hard X-ray observations of its nucleus are consistent with an obscured Seyfert 1 nucleus (Malaguti et al., 1999). Quillen et al. (1999) observed NGC 2110 with NICMOS and find the molecular hydrogen emission to be extended. In agreement with these data are those by Storchi-Bergmann et al. (1999), who observed NGC 2110 with a long slit in the near-IR and found extended [Fe II] λ1.257 µm and H_2 1 − 0 S(1) emission while the data by Sosa-Brito et al. (2001) lack sufficient signal-to-noise for the observation of extended H_2 1 − 0 S(1) emission. Storchi-Bergmann et al. (1999) found that an important source of the excitation for [Fe II] λ1.257 µm may be shocks driven by the radio jet, while the H is excited by the central X-ray source and the dynamical center is displaced with respect to the peak of near-IR continuum where there is signatures of hot dust emission which is consistence with the $K-$band spectra by Sosa-Brito et al. (2001).

NGC 5929 (UGC 9851): This CfA Seyfert 2 galaxy (Huchra & Burg, 1992) resides in a strong interacting system and seems to share a common outer envelope with its neighbor, NGC 5930 (Nagar & Wilson, 1999). The $K-$band spectroscopy for this object, published by Imanishi & Alonso-Herrero (2004) and Ivanov et al. (2000), shows a continuum dominated by CO absorption features and points out towards a moderate circumnuclear starburst component. The NIR spectrum of NGC 5929 displays strong [S III] λ9531 Å, He I, and [Fe II] emission and weak H I (Riffel, Rodríguez-Ardila & Pastoriza, 2006). Conspicuous molecular hydrogen lines were detected in the $K-$band. No high ionization lines were observed. The continuum is steep with strong stellar CO absorption lines in H and K.

Mrk 463E (UGC 8850): Markarian 463 (MCG 3-36-5) ($z = 0.050802$, Sturm et al., 2002) consists of two nuclei, Mrk 463W and Mrk 463E, separated by about $4''$ (Adams, 1977 see also the $K-$band image by Sosa-Brito et al., 2001). Without distinguishing between the two nuclei, Lutz, Veilleux & Genzel (1999) utilized developed mid-infrared tools from Infrared Space Observatory (ISO) to classify Mrk 463 as an AGN. Indeed, Mrk 463E is classified as a Seyfert 2 (e.g., Shuder & Osterbrock, 1981; Hutchings & Neff, 1989) and shows in HST direct imaging what was initially described as a 0.84 arcsec long optical jet directed toward the south of the nucleus (Uomoto et al., 1993). The Seyfert 2 nucleus appears as a Seyfert 1 in reflected polarized light (Miller & Goodrich, 1990), and more recent HST imaging polarimetry has revealed that the "optical jet" is in fact a cone of polarized light extending northward from the Seyfert 1 nucleus (Tremonti et al., 1996). In

addition, the eastern component is seen to have broad Paα emission (Veilleux, Sanders & Kim, 1999; Sosa-Brito et al., 2001). Mrk 463W, on the other hand, is classified as either a Seyfert 2 (Shuder & Osterbrock, 1981; Mazzarella et al., 1991) or as a LINER (Kollatschny & Fricke, 1984). Although there are arguments in favour of other classifications, but Sosa-Brito et al. (2001) adopted the Seyfert 2 classifications for both nuclei and the unresolved nuclei seen in their $K-$band data shown to be unresolved at higher spatial resolution (Mazzarella et al., 1991).

MRK 622 (UGC 04229): Mrk 622 ($z = 0.0233$, Mazzarella & Balzano, 1986) has a Seyfert 2 nucleus whose optical emission-line properties have been studied in detail by Shuder & Osterbrock (1981). Veilleux, Goodrich & Hill (1997) displayed the spectrum of Mrk 622 near Paβ and interpolated the spectrum around 1.308 µm to get rid of a strong cosmic ray. There was no obvious sign for a broad component to Paβ, since $F(\mathrm{Pa}\beta_\mathrm{b}) < 1.4 \times 10^{-14}$ erg cm^{-2} s^{-1} with FWHM$\approx$ 2700 km s^{-1} while the width of Paβ is slightly smaller than that of [Fe II] λ 1.2567 µm (Veilleux, Goodrich & Hill, 1997).

NGC 1386 (ESO 358 - G035): Phillips & Frogel (1980) found that the very high excitation emission-line spectrum of NGC 1386 is that of a type 2 Seyfert nucleus. Braatz et al. (1997) also revealed the Seyfert 2 nucleus in this galaxy by both the water maser emission and its related FWHM as well as the strong Fe-K emission line seen in ASCA observations by Iyomoto et al. (1997). Infrared excess observations were made in the L and N bands by Sparks et al. (1986) but not in the J, H, and K bands. The $K-$band spectra by Sosa-Brito et al. (2001) provided little support for a spectrum that dilutes the fairly strong features of stellar absorption. Speckle Hα observations showed an elongated structure $\sim 3''$ long centered on the nucleus along a position angle of $\sim 30°$ consisting of several knots (Mauder et al., 1992), consistence with the broadband $H-$ and $K-$band maps elongation by Sosa-Brito et al. (2001). Ulvestad & Wilson (1984b) found that the morphology of the nuclear radio continuum is extended toward the southwest along galaxy major axis (P.A. $= 55°$) by about 400 pc. Evidence for nuclear outflow along the same axis is found by Weaver, Wilson & Baldwin (1991).

NGC 7582 (ESO291-G016): NGC 7582 is a nearby ($z = 0.005254$, Sturm et al., 2002) $(\mathrm{R}_1')\mathrm{SB(s)ab}$ member of the interacting Grus Quartet (de Vaucouleurs, 1975) as a classical Seyfert 2 galaxy, with a well-defined [O III] cone (Morris et al., 1985; Storchi-Bergmann & Bonatto, 1991) and normally narrow emission lines (e.g., Cid Fernandes, Storchi-Bergmann & Schmitt, 1998). Heisler, Lumsden & Bailey (1997) proposed that, the nucleus itself is totally obscured, even to scattered light, by an edge-on thick torus surrounding it because of NGC 7582 lack of broad lines in spectropolarimetric observations coupled with a high 60 µm/25 µm flux ratio. Aretxaga et al. (1999) reported on the sudden transition toward a type 1 Seyfert of classical Seyfert 2 galaxy NGC 7582 using ESO–La Silla with the Danish 1.54 m and ESO 3.6 m telescopes from July 11 to October 21, 1998, with the

Hα line reaching a maximum width of $\sim 12\,000$ km s^{-1}. Three scenarios were taken into consideration in espousing the appearance of the broad lines namely; the capture of a star by a supermassive black hole, a reddening change in the surrounding torus, and the radiative onset of a Type IIn supernova (SN) exploding in a compact nuclear/circumnuclear starburst. The first two of these scenarios deal specifically with the active nucleus and its obscuring environment, whereas the last one is associated with stellar processes. The SN scenario is favoured over the the first two scenarios because of reservations about reconciling the first two models with the unification scheme (Aretxaga et al., 1999). BeppoSAX observations of NGC 7582 in 1998 November revealing unseen hard X-ray component by Turner et al. (2000) gave evidence in favour of a nuclear-based details with correlated variability across the X-ray spectrum leading to the conclusion that a single component dominates the $2-100$ keV band. However, these variations do not seem to be at all correlated with those in the optical reported observations by Aretxaga et al. (1999). The $H-$ and $K-$band spectra showed Brγ as the strongest nuclear line decomposed into broad ($\sim 3\,000$ km s^{-1}) and narrow (420 km s^{-1}) components where the broad component has an additional blue wing (Reunanen, Kotilainen & Prieto, 2003), while the $K-$band spectra by Sosa-Brito et al. (2001) showed a broadening of the Brγ line, along with a reddening of the continuum in the seeing weighted aperture with observed Brγ equivalent width for the 1994 July ESO 2.2 m observations in fairly agreement with that obtained by Oliva et al. (1995).

NGC 1275 (3C 84/Perseus A): NGC 1275 ($z = 0.017559$, Sturm et al., 2002) is a giant elliptical galaxy at the core of the Perseus cluster, with an optically luminous nucleus, classified by Veron (1978) as a BL Lac object and currently classified as a Seyfert 1.5/LINER by Sosa-Brito et al. (2001). Rothschild et al. (1981) observed that the active nucleus is a hard X-ray source and it is variable on timescales of about 1 year. Intranight microvariability in the optical has been observed (Pronik, Merkulova & Metik, 1999) . NGC 1275 has a jet (Marr et al., 1989; Pedlar, Booler & Davies, 1983; Pedlar et al., 1990; Dhawan et al., 1990) and counter jet radio morphology (Vermeulen, Readhead & Backer, 1994). NGC 1275 is also a cooling flow galaxy (see, e.g., Heckman et al., 1989). This galaxy has been studied in the NIR by Krabbe et al. (2000), who found that its NIR properties can best be described as a combination of dense molecular gas, ionized emission line gas, and hot dust emission concentrated on the nucleus. Kent & Sargent (1979) studied its two velocity systems and conclude that probably the high-velocity emission line system (8200 km s^{-1}, several arcsec northwest of the nucleus) is excited by hot stars, while the low-velocity filamentary emission line structure (5300 km s^{-1}, the systemic velocity of NGC 1275) can be explained by either shocks or photoionization from the Seyfert nucleus. There is also a central population of young massive star clusters (Holtzman et al., 1992).

Circinus (ESO 97-G013): Circinus ($z = 0.001498$, Sturm et al., 2002) lies close to the galactic plane, within a window of relatively low ($A_V \approx 1.5$ mag) interstellar extinction (Freeman et al., 1977). It displays several characteristics of a typical Seyfert 2 nucleus: the observed optical line ratio (Oliva et al., 1994), an ionization cone observed in [O III] λ5007 (Marconi et al., 1994) with the corresponding countercone appearing in the line of [Si VI] 1.97 µm (Maiolino et al., 2000), narrow prominent coronal lines in its optical/near-IR spectrum (Oliva et al., 1994), and broad (FWHM$\approx$ 3300 km s^{-1}) Hα emission detected in polarized light (Oliva et al., 1998). Additional indicators of the presence of an AGN include the existence of a nonstellar source at 2.2 µm whose diameter is less than 3 pc (Maiolino et al., 1998, though these authors see no compelling evidence for a nuclear black hole), H_2O maser activity (Gardner & Whiteoak, 1982; Greenhill et al., 1997), Fe-K fluorescent line emission detected in its X-ray spectrum (Matt et al., 1996), and observed high-excitation lines of Ne, S, Mg, O, and Si in the $2.5 - 45$ µm wavelength range (Moorwood et al., 1996, but see also Binette et al., 1997 and Oliva, Marconi & Moorwood, 1999). Recent star formation in the nuclear region has been detected through the near-IR observations by Maiolino et al. (1998), who found that the luminosity due to star formation within the central few hundred parsecs is comparable to the AGN luminosity, though the central 14 pc (converted to our adopted distance) is dominated by the AGN luminosity, with star formation contributing only 2% of the light.

Centaurus A (Cen A/NGC 5128): Cen A ($z = 0.001828$, Sturm et al., 2002) is the closest AGN and a luminous radio galaxy, but with a nucleus completely optically obscured; Mirabel et al. (1999) presented a mid-infrared ISO spectrum of the nucleus . This source is resolved along the slit of the IRS, but the spectrum shown is only that of the central nucleus within the same IRS spatial resolution as an unresolved source indicating the presence of strong silicate absorption and emission lines where, the strength of [Ne V] indicates ionization by the AGN (Weedman et al., 2005).

Cygnus A (3C 405/Cyg A): Cyg A ($z = 0.05562 \pm 0.00015$, Stockton, Ridgway & Lilly, 1994) is one of the most powerful active galaxy discovered and it is an ultra-luminous radio sources in the local universe. Ward et al. (1991) measured an improved signal-to-noise ratio of Paα and Brγ lines fluxes mainly due to the different absolute flux calibration and their resolution-corrected FWHM velocity of 510 ± 60 km s^{-1} is in good agreement with the Balmer line widths reported by Osterbrock & Miller (1975). Concentrating on the nuclear regions of the Cyg A galaxy, Carilli & Barthel (1996) review the evidence for an obscured QSO and concluded that Cygnus A is anomalously radio loud. The infrared emission in Cygnus A is a combination of heated AGN and starburst dust, with the AGN contributing around ~ 90 % of the luminosity (Privon et al., 2012).

MRK 266SW (NGC 5256SW): The spectra of Markarian 266 (NGC 5256) ($z = 0.0281$ for Sy2 and $z = 0.0277$ for LINER, Mazzarella & Balzano, 1986) consists of a galac-

tic pair of a Seyfert 2 nucleus to the southwest and a LINER nucleus to the northeast namely MRK 266SW (NGC 5256SW) and its companion MRK 266NE (NGC 5256NE) (Kollatschny & Fricke, 1984; Osterbrock & Miller, 1975), respectively. Kay (1994) tentatively reported the detection of a broad Hα line in the polarized light of Mrk 266SW. No broad Paβ was detected in this galaxy by Goodrich, Veilleux & Hill (1994), nor is there any evidence for broad wings to Brγ in the spectrum by Veilleux, Goodrich & Hill (1997). The reddening derived from the narrow-line ratio Paβ_n/Hα_n differs significantly from the values based on Brγ_n/Hα_n or the Balmer decrement. This apparent discrepancy may be due to differential slit losses associated with the extended nature of the line-emitting region in this galaxy (Mazzarella et al., 1988). Slight changes in the seeing and positioning of the slit can cause variations in the flux entering the spectrograph aperture. The differences in the profiles of [Fe II] 1.2567 µm, Paβ, H_2 2.121 µm, Brγ, and [O III] λ5007 may also be explained in that way. The obvious blue wing in the profile of [O III] λ5007 (Vrtilek & Carleton, 1985) is not visible in any of the infrared line profiles. Significant structure was detected in the red wing of Paβ (Goodrich, Veilleux & Hill, 1994), but the S/N of the $K-$band data is insufficient to confirm the presence of this feature in Brγ.

MRK 1066 (UGC 02456): Goodrich & Osterbrock (1983) classified Mrk 1066 ($z = 0.0119$, Mazzarella & Balzano, 1986) as a Seyfert 2 galaxy as a result of no visible broad-line Balmer components. Regan & Mulchaey (1999) describe this Seyfert 2 galaxy (SAB) as a dusty object with a single broad dust lane dominating its morphology. In the X-ray observations presented by Cardamone, Moran & Kay (2007) indicated a flux at $2-8$ keV of 3.92×10^{-13} erg cm^{-2} s^{-1} for this object. It is a FIR luminous galaxy containing a double nucleus (Gimeno, Díaz & Carranza, 2004). The non-simultaneous $J-$ and $K-$band spectroscopy by Veilleux, Goodrich & Hill (1997) shows strong [Fe II] and Paβ, with weak excess of emission seeing at the sides of both lines. They put stringent constraints on the flux of broad Brγ and Paβ. The JHK spectrum obtained by Riffel, Rodríguez-Ardila & Pastoriza (2006) shows a flat continuum from 0.8 to 1.3 µm, where the emission line spectrum is strong and bright. [S III], He I, H I, [Fe II] and H_2 are the most conspicuous emission features. Weak high-ionization lines of [Si VI] 19630 Å and [Ca VIII] 23218Å were detected. The line profiles are narrow, with FWHM $\approx 400-500$ km s^{-1} . No evidence of broad components in the permitted lines was found. The most prominent stellar absorption features are the Ca II triplet in the blue end and the 2.3 µm CO bandhead in K. Ramos Almeida et al. (2014) found a good match between the MIR morphology of Mrk 1066 and the extended Paβ, Brγ, and [O III] λ5007 Å emission, which was interpreted that the 8.7 µm emission is probing star formation, dust in the narrow-line region, and the oval structure previously detected in the near-infrared while the Chandra soft X-ray morphology does not match any of the previous, contrary to what it is generally assumed for Seyfert galaxies.

NGC 424 (TOL 0109-383): This Seyfert 2 galaxy ($z = 0.011661$, Sturm et al., 2002) has been observed with HST by Malkan, Gorjian & Tam (1998). It contains a bright extended narrow line region (ENLR) with relatively broad and strong He II line emission detected out to ~ 10 arcsec (2.2 kpc) diameter. A Seyfert 1 nucleus is weakly detected at Hα, with prominent coronal line emission (Dopita et al., 2015). Broad Hα and Hβ has been detected in polarised light from the nucleus by Moran et al. (2000) with a width of 12 000 km s^{-1}. The nucleus is believe to be flanked by two sets of H II regions within a fast-rotating larger star-forming ring (Dopita et al., 2015).

NGC 1320 (MRK 607/MCG -1-9-36): NGC 1320 ($z = 0.0089$, Mazzarella & Balzano, 1986) is a high-inclination galaxy which has been observed in [O III] and [N II] using the Hubble Space Telescope (HST) by Ferruit, Wilson & Mulchaey (2000). It has a Seyfert 2 nucleus, compact ENLR, and active star formation largely confined to the narrow, inner NW spiral arm. The rotation curve is regular. NGC 1320 is a "warm,", high-ionization, edge-on Seyfert 2 galaxy with a weak, featureless continuum and very narrow emission lines as well as a relatively large infrared luminosity (De Robertis & Osterbrock, 1986).

NGC 1667: NGC 1667 is a fairly compact Seyfert 2 nucleus surrounded by a ring together with spiral arms of H II regions. These are fairly metal-rich and share the strong rotational signature of the galaxy. It has a near-IR bar aligned at P.A. $= 9°$ (Mulchaey, Regan & Kundu, 1997).

NGC 3393: Diaz, Prieto & Wamsteker (1988) studied the optical and UV spectra of the nuclear region of NGC 3393 ($z = 0.01315$, Cooke et al., 2000) and find no evidence for internal reddening. Further, they find that the spectral type of the dominant stellar population is sufficiently old that it does not contribute to the UV continuum, but rather contributes $\gtrsim 90\%$ of the optical continuum. Their analysis of the IRAS fluxes shows that it can be fitted with a combination of two relatively cool components, one at 130 K and the other at 30 K. For comparison, the $K-$band spectrum by Sosa-Brito et al. (2001) shows no clear evidence for hot dust emission (see also Alonso-Herrero et al., 1998). Ferguson et al. (1997), and later Cooke et al. (2000), show optical line strengths and ratios which clearly distinguish this galaxy as a Seyfert 2. The weak $20 - 100$ keV emission seen with BeppoSAX has been modeled by Maiolino et al. (1998), who favor a cold reflection-dominated (Compton thick) model.

NGC 5953: The interacting pair 91 in the catalogue of galaxies by Arp (1966), NGC 5953 (with a Seyfert type 2 nucleus) and NGC 5954 (with a LINER) (Gonzalez Delgado & Perez, 1996), surrounded by a ring of star formation with a radius of $\sim 4''$. Riffel, Rodríguez-Ardila & Pastoriza (2006) classified NGC 5953 as the edge of a Seyfert 2/LINER. Long-slit spectroscopy shows that in the circumnuclear region a starburst coexists with moderate-excitation gas ionized by the active nucleus in the interacting pair but more

conspicuous in NGC 5953 (Gonzalez Delgado & Perez, 1996). The $J-$band spectroscopy by Alonso-Herrero et al. (2000) shows a spectrum with strong [Fe II] λ 1.257 µm and Paβ emission lines. The spectrum by Riffel, Rodríguez-Ardila & Pastoriza (2006) displays low- and moderate-ionization emission lines, on top of a steep continuum with numerous stellar absorption features. The Ca II triplet in absorption dominates the blue end of the spectrum, while strong 2.3 µm CO bandheads are observed at the red edge and the CO absorption bands are also strong in H with [S III] as the highest (and most intense) forbidden line detected in addition to [Fe II] emission being prominent in the J and H, but in K, the most conspicuous emission features are from H_2. Brγ is rather weak, and Paα is severely affected by telluric absorption (Riffel, Rodríguez-Ardila & Pastoriza, 2006).

NGC 7682 (UGC 12622/MCG-0-59-47/ARP 216): NGC 7682 ($z = 0.01718 \pm 0.00004$, Brodie et al., 1987) is a CfA Seyfert 2 (Huchra & Burg, 1992) in interaction with NGC 7683 (Arp, 1966). Ionized gas in Hα + [N II] and [O III] λ5007 Å is detected on scales of kiloparsecs on this object (Brodie et al., 1987; Durret, 1994). In the NIR, only $K-$band spectroscopy was previously reported by Imanishi & Alonso-Herrero (2004). The spectrum by Riffel, Rodríguez-Ardila & Pastoriza (2006) displays conspicuous emission lines with bright [S III], He I, and H I. Low-ionization lines such as [C I], [S II], and [Fe II] as well as high-ionization lines of [S VIII] and [Si VI] were clearly detected. In the $K-$band, molecular H_2 and Paα were the brightest emission features. All lines were spectroscopically unresolved or barely resolved. The continuum emission is dominated by absorption features, including the Ca II triplet in the blue and numerous CO in $HK-$bands.

ESO428 - G014 (0714-2914/M4-1/MCG 5-18-2): ESO428-G14 (SA0+, $z = 0.00544$, Falcke et al., 1996) is a host of a Seyfert 2 nucleus (Bergvall, Johansson & Olofsson, 1986) irrespective of its being classified earlier as a planetary nebula, PK 241-7°1 by Perek & Kohoutek (1967), even though, the NLR of this object has been the subject of investigation because of the many individual, thin strands that are very closely related to the radio jet and that produce a highly complex, yet ordered, structure (Falcke et al., 1996). It also displays a two-side jet with a double helix of emission-line gas. In the NIR, ESO428 − G014 has been studied, among others, by Veilleux, Goodrich & Hill (1997) and Reunanen, Kotilainen & Prieto (2003). The latter authors reported bright, extended (up to $\approx$ 320 pc) [Fe II], Brγ, and H_2 emission, parallel to the cone. The NIR spectrum of Riffel, Rodríguez-Ardila & Pastoriza (2006), of larger wavelength coverage, shows the strongest nuclear emission lines of [S III] and He I and also reported the first detection of [S VIII] 9912 Å, and [Si X] 14300 Å as well as lines of [P II], [S II], and [Ca I] with the continuum emission smoothly decreasing in flux with the wavelength. The Ca II triplet and numerous CO bands (in both H and K) are clearly detected. The detection of strong [Si VI] 19630 Å is also confirmed (Reunanen, Kotilainen & Prieto, 2003; Riffel, Rodríguez-Ardila & Pastoriza, 2006).

We compiled from the literature flux of infrared and optical emission-lines of the Seyfert 2 nuclei previously described. In Table 2, the IR flux of hydrogen transition lines and the flux of the IR emission-lines of doubly ionized neon two fine structure lines are listed. In Table 3, the optical reddening emission line intensities (relative to Hβ = 1.0 − 100) are listed. In each table, the original papers from which the data were compiled are listed.

2.2 The hydrogen emission lines

The observed near-IR hydrogen emission lines contain transitions from the Paschen and Brackett series. In this work selection of observational measurements of Paschen and Brackett emission lines, namely, Paα to Pa10 and Brα to Br13, respectively, have been made. Although, seen in the majority of the sources, the measured second strongest observed Brackett emission line, namely, Brδ as well as Br10, Br11, Br13, and Pa8 as the least observed emission lines in the selected objects, since they are strongly affected by telluric absorption.

The Paα to Paδ and Brα to Brδ emission lines are not just the strongest emission lines found in the NIR and MIR, they are also relatively free from blending features and dust attenuation. This makes them valuable tools to derive the chemical abundances of AGNs. The optical Balmer emission lines, although stronger, can suffer blending with other lines (i.e., Hα normally blends with [N II] λ6548, λ6584 Å), and at least to some degree, are expected to be more affected by dust absorption than Paschen emission lines. All Paschen emission lines of higher order than Paα and Paβ are strongly blended with emission lines from other elements. In particular, Paγ is strongly blended with [He I] 1.0830 µm and [Fe II] 1.0863 µm, and its red wing also with [Fe II] 1.1126 µm. The Paδ emission line is heavily blended with the [Fe II] $\lambda\lambda$9956, 9998Å doublet on its blue side and with [He II] 1.0124 µm and, in objects with strong iron emission, [Fe II] 1.0132 µm and [Fe II] 1.0174 µm on its red side. The strongest narrow emission line in the NIR, namely, [S III] λ9531 contaminates the peak of emission of Pa8. Moderate to high resolution, R > 1 000, will be reliably preferable to deblend the blended emission lines (Goodrich, Veilleux & Hill, 1994). Independent measurements of the narrow component fluxes can yield important constraints on the presence of dust within the line of sight which could also affect the emitter regions of IR lines. In fact, effects of dust on hydrogen emission line measurements are clearly observable only in the Balmer emission line ratios but they cannot be detected at a significant level using the Paschen and Brackett emission lines alone.

Table 2 – Neon Mid-infrared fine structure lines and near to mid-infrared Paschen and Brackett series observational fluxes for selected Seyfert 2 nuclei in units of 10^{-14} erg cm^{-2} s^{-1}.

Object	[NeIII]15.56μm	Pa8 λ9549 Å	Paδ λ10052 Å	Paγ λ10941 Å	Paβ λ12822 Å	Paα λ18756 Å	Br13 λ16114 Å	Br11 λ16811 Å	Br10 λ17367 Å	Brδ λ19451 Å	Brγ λ21661 Å	Brβ λ26259 Å	Brα λ40523 Å	Ref.
NGC 3081	36.46 ± 1.25	—	—	—	5.46	—	—	—	—	—	—	—	1.12	[5, 6, 13]
NGC 4388	106.00 ± 1.11	0.05	0.01	0.03	8.09	0.08	—	—	—	—	1.13		3.22	[1, 5, 7]
NGC 4507	28.78 ± 0.63	—	—	—	—	—	—	—	—	—	—	—	3.65	[6, 8]
NGC 5135	58.00 ± 0.00	—	—	—	—	—	—	—	—	—	1.65 ± 0.5	—	7.9	[4, 9, 28]
NGC 5643	56.00 ± 0.00	0.009	0.02	0.05	3.5	—	—	—	—	—	—	4.0	2.92	[2, 4, 6, 7, 10]
NGC 5728	54.76 ± 0.51	—	0.545 ± 0.142	0.380 ± 0.105	0.737 ± 0.116	2.063 ± 0.192	—	—	—	—	0.211 ± 0.019	—	—	[11, 13]
IC 5063	66.30 ± 0.99	—	—	—	—	—	—	—	—	—	66.30 ± 0.99	< 5.0	—	[1, 6, 17]
IC 5135	37.00 ± 2.00	—	—	—	—	—	—	—	—	—	1.02 ± 0.08	—	8.3	[5, 9, 16, 28]
MRK 3	207.00 ± 29.00	—	—	—	11.5	—	—	—	—	—	6.20 ± 0.40	—	—	[5, 16, 25]
MRK 273	33.81 ± 0.25	—	—	—	—	8.84	—	—	—	0.70	0.73 ± 0.04	4.2	4.4	[8, 9, 12, 29]
MRK 348	25.00 ± 1.00	—	0.27 ± 0.04	0.71 ± 0.12	1.21 ± 0.06	3.55 ± 0.15	—	—	—	0.33 ± 0.13	0.301 ± 0.042	—	—	[13, 14]
MRK 573	24.0 ± 0.00	—	0.327 ± 0.016	0.611 ± 0.04	0.958 ± 0.017	4.557 ± 0.028	—	—	—	0.137 ± 0.006	0.277 ± 0.009	—	—	[10, 11]
NGC 1068	1432.20 ± 76.87	—	—	—	—	—	—	—	—	—	12.7	41.0	69.0	[5, 10, 12, 15]
NGC 2992	61.06 ± 1.98	2.6	2.65	3.7	5.1	8.8	0.28	0.56	0.73	—	1.16	—	6.65	[6, 13, 19]
NGC 5506	152.13 ± 9.13	—	—	—	85.1	—	—	—	—	—	11.8	7.0	12.0	[5, 10, 13]
NGC 7674	46.00 ± 2.00	—	0.838 ± 0.067	1.387 ± 0.131	1.036 ± 0.058	3.206 ± 1.009	—	2.566 ± 0.452	—	0.338 ± 0.051	0.313 ± 0.025	—	—	[11, 16]
I Zw 92	16.00 ± 0.00	—	—	—	10.4	—	—	—	—	—	0.953	—	—	[5, 10]
NGC 2110	47.40 ± 0.71	—	0.300 ± 0.027	1.266 ± 0.103	1.491 ± 0.086	3.295 ± 0.450	—	—	—	—	0.250 ± 0.022	—	2.11	[6, 11, 13]
NGC 5929	9.83 ± 0.31			0.379 ± 0.027	0.768 ± 0.020	—	—	—	—	—	0.135 ± 0.025	—	—	[1, 11]
MRK 463E	40.46 ± 0.73	—	—	—	3.01	—	—	—	—	—	0.272	—	—	[5, 8]
MRK 622	8.00 ± 1.00	—	—	—	1.02	—	—	—	—	—	—	—	—	[5, 16]
NGC 1386	36.6 ± 0.72	—	—	—	3.50	—	—	—	—	—	0.176 ± 0.014	—	—	[1, 2, 3]
NGC 7582	105.00 ± 2.05	—	—	—	7.8	—	—	—	—	—	4.4 ± 0.4	9.0	20.6 ± 7.0	[1, 2, 10, 18]
NGC 1275	22.37 ± 0.56	—	1.332 ± 0.108	8.353 ± 0.425	6.066 ± 0.315	14.514 ± 0.252	—	—	—	1.398 ± 0.206	0.977 ± 0.041	[2	22	8, 10, 11]
Circinus	400.00 ± 0.90	—	—	10.4	—	—	—	—	—	—	3.8	32	15.0	[8, 10, 20]
Centaurus A	147.65 ± 0.00	—	—	19	16	—	—	—	—	—	2.7	9.0	8.0	[3, 10, 13, 26]
Cygnus A	41.30 ± 0.4	—	—	—	—	2.6 ± 0.2	—	—	—	—	0.26 ± 0.08	—	—	[21, 22]
MRK 266SW	28.00 ± 0.00	—	—		5.51	—	—	—	—	—	0.367	—	4.5	[4, 5, 9]
MRK 1066	46.91 ± 0.76	—	0.974 ± 0.030	2.553 ± 0.120	5.407 ± 0.024	14.574 ± 1.060		0.398 ± 0.055	—	0.867 ± 0.004	1.416 ± 0.022	—	—	[8, 11]
NGC 424	21.00 ± 1.00	—	—	—	—	—	—	—	—	—	< 1.0	< 5.0	—	[10, 16, 17]
NGC 1320	9.00 ± 1.00	—	—	—	—	—	—	—	—	—	0.094 ± 0.01			[16, 25]
NGC 1667	7.23 ± 3.00	—	—	—	—	—	—	—	—	—	0.018 ± 0.004	—	—	[16, 25]
NGC 3393	95.00 ± 0.00	—	—	—	—	—	—	—	—	—	0.46 ± 0.005	—	—	[24, 27]
NGC 5953	21.00 ± 1.00	—	—	—	0.544	1.982 ± 0.083	—	—	—	—	0.277	—	—	[11, 16, 23]
NGC 7682	8.07 ± 0.15	—	0.118 ± 0.018	0.498 ± 0.112	0.992 ± 0.065	3.182 ± 0.081	—	—	—	—	0.194 ± 0.011	—	—	[11, 13]
ESO428 − G014	168.01 ± 0.00	—	0.919 ± 0.063	3.104 ± 0.115	4.526 ± 0.057	10.205 ± 0.078	—	0.822 ± 0.029		0.300 ± 0.049	0.898 ± 0.014	—	—	[11, 24]

References: (1) Tommasin et al. (2010), (2) Winge et al. (2000), (3) Reunanen, Kotilainen & Prieto (2002), (4) Pereira-Santaella et al. (2010), (5) Veilleux, Goodrich & Hill (1997), (6) Lutz et al. (2002), (7) Onori et al. (2017), (8) Dasyra et al. (2011), (9) Imanishi et al. (2010), (10) Sturm et al. (2002), (11) Riffel, Rodríguez-Ardila & Pastoriza (2006), (12) Goldader et al. (1995), (13) Weaver et al. (2010), (14) Ramos Almeida, Pérez García & Acosta-Pulido (2009), (15) Goulding & Alexander (2009), (16) Deo et al. (2007), (17) Moorwood & Oliva (1988), (18) Kawara, Nishida & Phillips (1989), (19) Gilli et al. (2000), (20) Oliva et al. (1994), (21) Privon et al. (2012), (22) Ward et al. (1991), (23) Rodríguez-Ardila, Riffel & Pastoriza (2005), (24) Wu, Zhao & Meng (2011), (25) van der Laan et al. (2013), (26) Bryant & Hunstead (1999), (27) Sosa-Brito et al. (2001), (28) Goldader et al. (1997), and (29) Veilleux, Sanders & Kim (1999).

For the NIR broad emission line region (BLR) of AGNs, Landt et al. (2008) obtained the dust extinction in the order of $A_V \sim 1$ to ~ 2 mag in consonance with similar results obatined by Cohen (1983), Ward et al. (1987), and Crenshaw et al. (2001, 2002). From this result, the effect of the dust causing the observed extinction of the narrow emission line region (NLR) on the broad components depends on the location of the dust, i.e., if it is mixed with the gas phase ("internal dust") or if it is located outside the NLR, for instance, in the host galaxy. Since the covering factor of the narrow emission line clouds is assumed to be very small (only a few per cent), the line of sight towards the BLR will not necessarily intercept these. However, dust external to the NLR will act as a screen and affect also the smallest scale components such as the BLR and the continuum emitted by the accretion disk.

Nevertheless, given these limitations, IR transitions offer the possibility of studying the metallicity of galaxies practically without suffering from any dust extinction effects, therefore, they should be explored and used whenever possible (Moorwood et al., 1980; 1980; Lester et al., 1987; Rubin et al., 1988; Tsamis et al., 2003). For instance, the metallicities of the central and obscured regions of starburst galaxies can only be accessed via far-IR lines, while metallicities derived via optical lines are likely to only relate to the outer, less dust-extincted part of these galaxies (Dors et al., 2013; Puglisi et al., 2017; Calabrò et al., 2018). Reddening in Seyfert galaxies by means of NIR line ratios was performed by Riffel, Rodríguez-Ardila & Pastoriza (2006), which led to the fact that Seyfert 2s tend to lie close to the locus of points of the reddening curve; with $E(B-V)$ in the interval 0.25−1.00 mag, whereas Seyfert 1s, in contrast, are predominantly populated by broad and narrow lines, which display extinction values close to zero for the H I region. The problems related to the extinction correction are most relevant to the optical line fluxes, but the extinction can be considered almost negligible for infrared data.

Table 3 – Observed reddening-uncorrected optical emission-line intensities of Seyfert 2 nuclei compiled from the literature.

Object	[O II] λ3727 Å	[Ne III] λ3869 Å	[O III] λ4363 Å	[O III] λ4959 Å	[O III] λ5007 Å	[O I] λ6300 Å	Hα λ6563 Å	Hβ λ4861 Å	[N II] λ6584 Å	[S II] λ6717 Å	[S II] λ6731 Å	Ref.
NGC 3081	1.47	0.88	0.20	4.53	13.30	0.37	4.53	1.00	3.87	0.99	1.07	1
NGC 4388	1.72	0.48	0.13	3.83	11.20	0.78	4.86	1.00	2.59	1.27	1.12	1
NGC 4507	1.64	0.71	0.27	3.17	9.53	0.86	5.16	1.00	2.80	1.10	1.23	1
NGC 5135	1.06	0.42	0.08	1.49	4.82	0.31	6.12	1.00	5.45	0.92	0.87	1
NGC 5643	2.68	0.89	0.32	4.85	16.60	1.16	6.17	1.00	7.17	2.40	2.21	1
NGC 5728	1.84	0.75	0.34	3.92	11.80	1.00	5.97	1.00	8.36	0.99	0.97	1
IC 5063	2.90	0.75	0.22	3.55	11.00	0.68	5.55	1.00	3.44	1.50	1.31	1
IC 5135	2.15	1.04	0.19	2.20	7.41	0.60	6.07	1.00	7.56	1.19	1.11	1
MRK 3	2.21	0.94	0.19	4.16	13.46	1.14	5.31	1.00	5.48	1.30	1.46	2
MRK 273	3.05	0.71	0.13	5.39	17.96	1.22	28.20	3.06	29.30	17.50	—	2, 3
MRK 348	3.05	1.23	0.21	3.96	12.33	1.58	4.27	1.00	3.54	1.74	2.01	2
MRK 573	2.11	1.01	0.15	4.01	12.64	0.43	4.30	1.00	3.62	1.12	1.21	2
NGC 1068	0.76	0.94	0.17	4.28	13.22	0.62	4.47	1.00	7.94	0.48	0.99	2
NGC 2992	0.19	0.04	0.01	0.32	1.00	0.15	1.73	0.13	1.00	0.46	0.41	4
NGC 5506	0.14	0.04	0.01	0.31	1.00	0.11	0.87	0.12	0.80	0.32	0.34	4
NGC 7674	1.08	0.98	0.11	3.99	12.82	0.38	4.62	1.00	4.62	0.69	0.81	5
I Zw 92	1.95	0.94	0.28	3.60	10.50	0.55	3.54	1.00	1.43	0.55	0.60	5
NGC 2110[a]	21.10	4.20	0.73	11.17	33.50	8.20	18.00	4.30	34.00	7.90	9.80	6
NGC 5929[a]	14.80	2.21	0.40	4.23	12.70	8.20	20.60	4.40	12.10	7.60	6.70	6
MRK 463E	0.21	0.07	0.013	0.33	1.00	0.055	0.48	0.13	0.23	0.10	0.09	7
MRK 622	0.49	0.06	0.004	0.33	1.00	0.041	1.88	0.16	1.77	0.32	0.35	7
NGC 1386[a]	1.81	0.77	0.19	3.78	11.34	0.46	4.70	1.00	5.60	1.04	1.29	8
NGC 7582	124.10	32.80	2.90	71.60	214.70	8.70	286.00	100.00	186.90	41.80	38.80	9
NGC 1275	2.90	1.43	0.33	4.33	12.99	1.48	5.44	1.00	5.44	1.33	—	10
Circinus	78.00	41.00	16.00	317.00	1048.00	46.00	565.00	100.00	154.00	128.00	113.00	11
Centaurus A	2.49	0.48	0.10	2.38	6.28	2.05	7.27	1.00	10.83	5.24	4.17	12
Cygnus A	2.44	0.66	0.16	4.08	13.11	2.10	6.61	1.00	13.07	3.65	3.29	13
MRK 266SW	5.20	0.90	0.08	1.50	4.50	0.38	3.30	1.00	3.68	0.54	0.46	14
MRK 1066	0.32	0.08	0.01	0.31	1.00	0.15	1.80	0.23	1.58	0.36	0.39	15
NGC 424	0.04	0.21	0.03	0.37	1.00	0.04	0.64	0.22	0.25	0.05	0.05	16
NGC 1320	0.38	0.49	0.29	3.57	9.86	0.38	4.86	1.00	3.36	0.93	1.07	17, 18
NGC 1667	12.08	1.98	0.42	3.99	11.10	0.94	3.03	1.00	6.59	2.86	—	19, 20
NGC 3393	155.00	77.00	10.00	341.00	1030.00	34.00	359.00	100.00	492.00	202.00	—	21
NGC 5953	2.60	0.90	0.12	1.70	4.30	0.32	2.90	1.00	4.00	0.80	0.84	22
NGC 7682[a]	575.00	158.00	77.40	1310.00	3930.00	167.00	470.00	100.00	515.00	134.00	141.00	23
ESO428 − G014	2.49	1.13	0.28	4.20	13.60	0.49	3.55	1.00	4.03	1.07	1.14	24

References: (1) Phillips, Charles & Baldwin (1983), (2) Koski (1978), (3) Malkan et al. (2017), (4) Shuder (1980), (5) Kraemer et al. (1994), (6) Ferruit et al. (1999), (7) Shuder & Osterbrock (1981), (8) Bennert et al. (2006), (9) Dopita et al. (2015), (10) Shields & Oke (1975b), (11) Oliva et al. (1994), (12) Phillips (1981), (13) Osterbrock & Miller (1975), (14) Osterbrock & Dahari (1983), (15) Goodrich & Osterbrock (1983), (16) Vaceli et al. (1997), (17) De Robertis & Osterbrock (1986), (18) Thomas et al. (2017), (19) Ho, Filippenko & Sargent (1993), (20) Radovich & Rafanelli (1996), (21) Cooke et al. (2000), (22) Gonzalez Delgado & Perez (1996), (23) Durret (1994), and (24) Bergvall, Johansson & Olofsson (1986).

Note: [a]Value of $I([\mathrm{O\,III}]\lambda4959)$ estimated from the theoretical relation $I[\mathrm{O\,III}]\lambda4959 = I[\mathrm{O\,III}]\lambda5007/3.0$ (Storey & Zeippen, 2000).

2.3 Reddening correction

The interstellar medium is mainly composed of dust and gas, and occupy the entire space between the stars. Most of the gas is composed of hydrogen ($\approx 90\%$, in number of atoms), whereas the dust is essentially composed of graphite and silicates. The grains composition of the dust are microscopic with dimensions smaller than a micrometer which cause interference in astronomical observations. Dust and gas can reduce the amount of light received from astronomical objects under observations through absorption and scattering of electromagnetic radiation. There are three ways to discover dust, through its thermal emission, its effect on the observed spectrum (extinction), and through light polarisation. This study concerns the emission lines of AGNs and, consequently, the details they provide about the physical conditions of their nuclei. Therefore, we concentrate on the extinction and consider the other two dust properties only to the degree that they are likely correlated with it.

Interstellar reddening is a different phenomenon from redshift, which is without distortion the proportional frequency shifts of the spectra. Reddening typically eliminates shorter wavelength photons from a radiated spectrum thus leaving the longer wavelength photons (in the optical, light that is redder), keeping the spectroscopic lines unchanged. Extinction arising from both the interstellar medium (ISM) and the Earth's atmosphere (wavelength regions such as X-ray, ultraviolet, and infrared) as well as circumstellar dust around an observed object are measured with photometric systems filters (passbands) as well as Balmer decrements from the spectroscopy. Extinction from Earth's atmosphere can be overcome by the use of space-based observatories. To correct extinction effect on the observed optical emission-lines, usually, the relation below is utilized.

$$\frac{I(\lambda)}{I(\mathrm{H}\beta)} = \frac{F(\lambda)}{F(\mathrm{H}\beta)} \times 10^{c(\mathrm{H}\beta)[f(\lambda)-f(\mathrm{H}\beta)]}, \tag{2.1}$$

where $I(\lambda)$ is the intensity of the emission line at a given wavelength λ (reddening corrected), $F(\lambda)$ is the measured flux of the emission line, $f(\lambda)$ is the adopted reddening curve normalized to Hβ, and $c(\mathrm{H}\beta)$ is the interstellar extinction coefficient.

The extinction coefficient of interest is normally calculated using the line ratio Hα/Hβ and comparing it with its theoretical line ratio, for instance, the one calculated by Hummer & Storey (1987) for a temperature of 10 000 K and an electron density of 100 cm^{-3}. A verification function used for transfer corrections was used by Savage & Mathis (1979), considering reddening law and the unreddened ratio Hα/Hβ = 2.86 taking into account Case B at electron temperature $T_\mathrm{e} = 10^4$ K and electron density $N_\mathrm{e} = 10^2$ cm^{-3} (Whitford, 1958; Brocklehurst, 1971; Miller & Mathews, 1972). The typical dereddening technique is to derive the logarithmic extinction at Hβ and the reddening constant c,

from the observed Hα/Hβ ratio, assuming that the intrinsic one has the theoretical value $(\mathrm{H}\alpha/\mathrm{H}\beta)_{\mathrm{B}}$ predicted for Case B recombination. Observed and corrected intensities are denoted $I_o(\lambda)$ and $I_c(\lambda)$ respectively, leading to the relation below.

$$\log I_c(\lambda) = \log I_o(\lambda) + cf(\lambda), \tag{2.2}$$

The units of $f(\lambda)$ are chosen such that $f(\lambda) = 0$ for the wavelength of the Hβ line and $f(\infty) = -1$. For any given nebula we define B to be the factor by which the observed absolute Hβ intensity must be multiplied in order to correct the interstellar absorption. With the units adopted for $f(\lambda)$ we then have $c = \log \mathrm{B}$. The equation below is yielded by rearrangements of Equation 2.2.

$$c = \frac{\log\left(\mathrm{H}\alpha/\mathrm{H}\beta\right)_{\mathrm{B}} - \log\left(\mathrm{H}\alpha/\mathrm{H}\beta\right)_{\mathrm{observed}}}{f_\alpha - f_\beta} \tag{2.3}$$

where f_α and f_β represent the values of the reddening law at the wavelengths of Hα and Hβ lines respectively. Therefore, for any observed line ratio $(F_{\lambda1}/F_{\lambda2})_{\mathrm{observed}}$ the reddening corrected value $(F_{\lambda1}/F_{\lambda2})_{\mathrm{corrected}}$ can be obtained from:

$$\log(F_{\lambda1}/F_{\lambda2})_{\mathrm{corrected}} = \log(F_{\lambda1}/F_{\lambda2})_{\mathrm{observed}} + c(f_{\lambda1} - f_{\lambda2}). \tag{2.4}$$

Ideally, the theoretical $(\mathrm{H}\alpha/\mathrm{H}\beta)_B$ value at the right temperature can be used in iteration after the electron temperature of the plasma has been determined. However, there are numerous problems associated with the iteration method. One of these drawbacks is the non-universality of the extinction law. The work by Cardelli, Clayton & Mathis (1989), shows that reddening correction depends on the ratio of total to selective absorption at V band given by the parameter $R_V = A_V/E_{(B-V)}$, where A_V is the absolute extinction or total absorption in magnitudes at V dependent on the total hydrogen column density of the material along the line-of-sight from the relation $N_H = (1.79 \pm 0.03)A_V \times 10^{21}$ cm^{-2} based on ROSAT observations (Predehl & Schmitt, 1995) and $E_{(B-V)}$ is the color excess given by the calibrated blue minus calibrated visible $\left[\text{i.e., } E_{(B-V)} = (B-V)_{\mathrm{observed}} - (B-V)_{\mathrm{intrinsic}}\right]$. While the authoritative estimation of R_V as reported by Morgan, Harris & Johnson (1953) and confirmed by Hiltner & Johnson (1956) is in the range 3 ± 0.2, the actual values are from 2.5 to 5 (Cardelli, Clayton & Mathis, 1989; Barbaro et al., 2001; Patriarchi et al., 2001). Using a consensus assumed value of $R_V = 3.1$ from the literature leads to the logarithmic extinction at Hβ, $c(\mathrm{H}\beta) = 1.452E(B-V)$ and $A_V = 2.13$ c(Hβ), however, the IR extinction and the value of R_V are not significantly different from galactic values (Howarth, 1983). Objects located in the Galactic bulge suffer extinction at a low value of R_V (e.g. Stasińska et al., 1992; Liu et al., 2001). Cardelli, Clayton & Mathis (1989) ascribed such differences in extinction

laws to the presence of systematically larger particles in dense regions between small and large values of R_V. Such R_V variations have a significant effect on line ratios when interacting with ultraviolet spectra. It is therefore convenient to link the optical and ultraviolet spectra by using line ratios with known intrinsic value, such as He II λ1640/He II λ4686. The differences seen in the VB[1] component's ratio He II λ1640/He II λ4686 indicate that, contrary to expectations, this line ratio may not be such a good indicator of reddening (Wamsteker et al., 1990).

Another problem is that dust is not generally positioned entirely between the astronomical object under investigation and the observer as in the case of stars. Some extinction may be due to dust mixed with the emitting gas. In that case, the extinction dependency on the wavelength is distinct and highly dependent on geometry (Mathis, 1983). One way to proceed, which mitigates this problem, is to use the entire set of hydrogen lines observed and fit their ratios to the theoretical value, which then gives an empirical reddening law to deredden the other emission lines. However, this is still not perfect, as the extinction of lines emitted only at the periphery of the nebula or only in the central parts is different from the extinction of hydrogen lines emitted throughout the entire nebular body. The problem is further complicated by the effects of scattering (see e.g. Henney, 1998).

In giant H II regions, where the observing slit contains stellar light, the stellar absorption in the hydrogen lines must be corrected first. This can be achieved in an iterative procedure, for instance the description by Izotov, Thuan & Lipovetsky (1994), but Hägele et al. (2006) presented opposing view to this procedure and pointed out that it is better to define a pseudo continuum in order to correct redenning in giant H II regions. However in the case of an AGN it is impossible to define a pseudo-continuum since the emission lines are too broad to see the underlying absorption line wings. On the other hand, if the effect of the underlying stellar population in the Balmer lines is visible it is relatively small even in the presence of an H II region (a few percent for Hβ and negligible for Hα although its effect depends on metallicities as pointed out by Díaz et al., 2007), so in AGNs this effect is possibly very small and negligible. Additional problem is that, the ratios of the intrinsic hydrogen line can deviate from the theory of case B. This is the Case, for example, in high electron temperature nebulae ($\sim$ 20 000 K), which could result in a significant collisional contribution to the emissivity of the lowest order Balmer lines. The line ratio for the hydrogen lines in this instance was corrected by adopting Case B,

[1] The UBV (Ultraviolet, Blue, Visual) photometric system , also known as the Johnson system (or Johnson-Morgan system), is a wide band, which is generally used to classify stars according to their colours (see details by Johnson & Morgan, 1953).

$(F_{\lambda1}/F_{\lambda1})_{\rm B}$ is related to the true line ratio $(F_{\lambda1}/F_{\lambda1})_{\rm true}$ by:

$$\log(F_{\lambda1}/F_{\lambda2})_{\rm B} - \log(F_{\lambda1}/F_{\lambda2})_{\rm true} = [\log\,({\rm H}\alpha/{\rm H}\beta)_{\rm B} - \log\,({\rm H}\alpha/{\rm H}\beta)_{\rm true}] \times \frac{f_{\lambda1} - f_{\lambda2}}{f_\alpha - f_\beta} \quad (2.5)$$

In comparison with the Case B recombination value of 2.85, Halpern (1982) and Halpern & Steiner (1983) found that Hα/Hβ is close to 3.1 in high as well as low ionization AGN models. This contradicts Heckman (1980) preposition of an anomalously high Balmer decrement in these objects. Therefore, intrinsic ratios Hα/Hβ = 2.85 and Hα/Hβ = 3.1 are estimations for H II regions and AGNs, respectively (Ferland & Netzer, 1983; Gaskell, 1984; Gaskell & Ferland, 1984; Veilleux & Osterbrock, 1987), while Dong et al. (2008) found the intrinsic value of broad-line Balmer decrements, Hα/Hβ = 3.06 with a standard deviation of 0.03 dex from the large and homogeneous sample of Seyfert 1 galaxies and quasi-stellar objects (QSOs) using spectroscopic data obtained in the Sloan Digital Sky Survey (446 DR4 data). In AGNs, however, the harder photoionizing spectrum results in a large transition zone, or partly ionized region, in which H^0 coexists with H^+ and free electrons. In this zone collisional excitation is also important in addition to recombination collisional excitation (Ferland & Netzer, 1983; Halpern & Steiner, 1983). The main effect of collisional excitation is to enhance Hα. The higher Balmer lines are less affected because of their large re-excitation energies and smaller excitation cross-sections.

In the cases where the reddening correction was not performed in the original works, consideration has to be given to the fact that the best way to find a consistent value for c is to choose a value that would at least return the unreddened ratios close to the theoretical ones for the strong and well detected lines. The error margin in Equation 2.5 can be very big at $\lambda1$, which is very different from $\lambda2$, regardless of the real extinction. For instance, a factor in the range of 1.5−2 can easily be reached for C III] λ1909/[O III] λ5007 (see Stasińska, 2002). Irrespective of the dereddening method used, it is good practice to check that the Hα/Hβ, Hγ/Hβ, and Hδ/Hβ emission line ratios have the expected values in comparison with the theoretical Case B ratios of 2.86 or 3.1, 0.468, and 0.259 (Halpern, 1982; Halpern & Steiner, 1983; Hummer & Storey, 1987; Osterbrock & Ferland, 2006), respectively; if not, a similar value of, for example, [O III] λ4363 Å/λ5007 Å will be in a similar margin of error. The extinction increases towards shorter wavelengths, thus reddening the radiation flux from an emitting source is reduced according to the equation

$$I_\lambda = I_{\lambda0} \times e^{-\tau_\lambda}, \quad (2.6)$$

where $I_{\lambda0}$ is the unreddened intensity of the light observed at Earth, I_λ is the actual observed intensity and $\tau_\lambda = cf(\lambda)$ is the optical depth at the wavelength of the observation.

It is clear hitherto that the most widely used method of estimating the dust content is based on the relative strengths of the lower Balmer lines, Hα/Hβ. When using the gas emission lines as a dust tracer, one assumes that the gas emission comes from the same position as the emission from the ionizing stars, which is usually not the case, because the gas in a spiral galaxy is contained in a plane. Generally, we must admit that little is known about the real distribution of dust in AGNs of the emission line. It seems very patchy and irregular, so assigning a single extinction value is just a rough first approximation. However, neglecting these uncertainties at first order the reddening effect can be written on the reliance of the ratio Hα/Hβ as:

$$\frac{I(\mathrm{H}\alpha)}{I(\mathrm{H}\beta)} = \frac{F(\mathrm{H}\alpha)}{F(\mathrm{H}\beta)} \times 10^{c(\mathrm{H}\beta)[f(\lambda)-f(\mathrm{H}\beta)]}, \tag{2.7}$$

where $c(\mathrm{H}\beta)$ is the measure of the amount of reddening ($E(B-V) = 0.77c(\mathrm{H}\beta)$), $f(\lambda)$ is the reddening curve, $I(\lambda)$ indicates the (unreddened) intrinsic flux and $F(\lambda)$ is the flux measured. Note that only the difference in optical depths at the two wavelengths enters in this equation; so the correction depends on the form of the interstellar extinction curve (with arbitrary normalization) and on the amount of extinction ($c(\mathrm{H}\beta)$). If the Whitford (1958) reddening curve as parameterized by Miller & Mathews (1972) is used one can thus derive an extinction of the Hβ by measuring the intensity ratio Hα/Hβ, and assuming an interstellar extinction curve, as follows.

Expressing the intensity reduction in magnitudes, the total extinction at some wavelength λ is given by

$$\mathrm{A}_\lambda = -2.5 \log(\mathrm{I}_\lambda/\mathrm{I}_{\lambda 0}) = \mathrm{m} - \mathrm{m}_0, \tag{2.8}$$

where m is the magnitude observed and m_0 is the intrinsic magnitude,

$$\mathrm{A}(\mathrm{H}\alpha) = -2.5 \log(\mathrm{F}(\mathrm{H}\alpha)_{\mathrm{observed}}/\mathrm{F}(\mathrm{H}\alpha)_{\mathrm{emitted}}), \tag{2.9}$$

$$\mathrm{A}(\mathrm{H}\beta) = -2.5 \log(\mathrm{F}(\mathrm{H}\beta)_{\mathrm{observed}}/\mathrm{F}(\mathrm{H}\beta)_{\mathrm{emitted}}), \tag{2.10}$$

$$\mathrm{A}(\mathrm{H}\beta) - \mathrm{A}(\mathrm{H}\alpha) = \mathrm{E}(\beta-\alpha) = 2.5 \times \left[\log\left(\frac{F(\mathrm{H}\alpha)_{\mathrm{observed}}}{F(\mathrm{H}\alpha)_{\mathrm{emitted}}}\right) - \log\left(\frac{F(\mathrm{H}\beta)_{\mathrm{observed}}}{F(\mathrm{H}\beta)_{\mathrm{emitted}}}\right)\right] \tag{2.11}$$

$$E(\beta-\alpha) = 2.5 \times \left[\log\left(\frac{F(\mathrm{H}\alpha)_{\mathrm{observed}}}{F(\mathrm{H}\alpha)_{\mathrm{emitted}}}\frac{F(\mathrm{H}\beta)_{\mathrm{emitted}}}{F(\mathrm{H}\beta)_{\mathrm{observed}}}\right)\right], \tag{2.12}$$

$$E(\beta-\alpha) = 2.5 \times \left[\log\left(\frac{F(\mathrm{H}\alpha)}{F(\mathrm{H}\beta)}\right)_{\mathrm{observed}} - \log\left(\frac{F(\mathrm{H}\alpha)}{F(\mathrm{H}\beta)}\right)_{\mathrm{emitted}}\right], \tag{2.13}$$

$$R_V = \frac{A_V}{E_{B-V}} = \frac{2.5c(\mathrm{H}\beta) - 0.425E(\beta-\alpha)}{0.863E(\beta-\alpha)}, \tag{2.14}$$

$$c(\mathrm{H}\beta) = \frac{0.425E(\beta-\alpha) + 0.863E(\beta-\alpha)R_V}{2.5}, \tag{2.15}$$

$$c(\mathrm{H}\beta) = 3.10 \times \left[\log\left(\frac{F(\mathrm{H}\alpha)}{F(\mathrm{H}\beta)}\right) - \log\left(\frac{I(\mathrm{H}\alpha)}{I(\mathrm{H}\beta)}\right)\right]. \tag{2.16}$$

The intrinsic flux ratio for H II region-like objects from the Case B Balmer recombination decrement $I(\mathrm{H}\alpha/\mathrm{H}\beta) = 2.85$ for $T_\mathrm{e} = 10^4$ K and $N_e = 10^4\,\mathrm{cm}^{-3}$ is usually adopted. For AGN we must take into account that the harder photoionizing spectrum results in a large transition zone, or partly ionized region, in which H^0 coexists with H^+ and free electrons. In this zone collisional excitation is also important in addition to recombination collisional excitation. The main effect of collisional excitation and harder ionizing continuum is to enhance Hα (Gaskell & Ferland, 1984; Osterbrock & Ferland, 2006). The higher Balmer lines are less affected because of their large excitation energies and smaller excitation cross sections. Again, the intrinsic Hα/Hβ ratio in most Seyfert 1 and Seyfert 2 galaxies is significantly larger than the prediction of Case B recombination 2.86 (Malkan, 1983). Also, Lu et al. (2019) investigated 554 selected AGNs from SDSS DR7 and concluded that the best Gaussian fit estimates of BLR Balmer decrement of $\mathrm{H}\alpha/\mathrm{H}\beta = 3.16 \pm 0.07$ dex, and NLR Balmer decrement of $\mathrm{H}\alpha/\mathrm{H}\beta = 4.37 \pm 0.10$ dex with a perfect correlation between broad-line Balmer decrements and Seyfert sub-type. Furthermore, we investigated the use of the Balmer decrement in the Narrow Line Region (NLR) of Seyfert 2 nuclei and found that the use of $I(\mathrm{H}\alpha/\mathrm{H}\beta) = 2.85$ gives T_e values of $\sim 700 \pm 30$ K higher than the T_e values from $I(\mathrm{H}\alpha/\mathrm{H}\beta) = 3.1$. Therefore, for the intrinsic ratio of Seyfert 2 nuclei we adopt $I(\mathrm{H}\alpha/\mathrm{H}\beta) = 3.1$ and the reddening correction at the different wavelengths can thus be obtained from:

$$\log I(\lambda) = \log F(\lambda) + c(\mathrm{H}\beta)f(\lambda), \tag{2.17}$$

Once $c(\mathrm{H}\beta)$ is derived as represented by Equation 2.16 above, the observed emission lines (often in units relative to Hβ=100) are corrected for interstellar extinction by

$$I_\lambda = F(\lambda) \times 10^{c(\mathrm{H}\beta)f(\lambda)} \tag{2.18}$$

or

$$(I_\lambda/I_{\mathrm{H}\beta})_{\mathrm{corr}} = (I_\lambda/I_{\mathrm{H}\beta})_{\mathrm{obs}} \times 10^{c(\mathrm{H}\beta)f(\lambda)}. \tag{2.19}$$

The wavelength dependence in the optical domain, $f(\lambda)$ is the reddening value for the line derived from the curve given by Whitford (1958), defined such the $f(\infty) = -1$ and $f(\mathrm{H}\beta) = 0$. An analytical estimation from values established by Kaler (1976) can be expressed as:

$$f(\lambda) = 2.5659\lambda^2 - 4.8545\lambda + 1.7545, \tag{2.20}$$

with λ in the units of micrometers within the range of $0.30 < \lambda(\mu\mathrm{m}) < 0.70$.

The intrinsic ratio for AGNs, $\mathrm{H}\alpha/\mathrm{H}\beta = 3.1$ is in good agreement with the results of photoionization models (Ferland & Netzer, 1983; Pequignot, 1984) and observational determinations (Gaskell, 1984; Gaskell & Ferland, 1984). Therefore, it is imperative to reiterate that the theoretical intrinsic ratio $\mathrm{H}\alpha/\mathrm{H}\beta = 3.1$ was compared with the observed $\mathrm{H}\alpha/\mathrm{H}\beta$ ratio in the literature for reddening correction in this work. The reddening correction relations used to complete Table 4 based on the effect of reddening on the ratio $\mathrm{H}\alpha/\mathrm{H}\beta$ are Equation 2.16, Equation 2.19, and Equation 2.20 above. In order to have an internally consistent sample, we applied this method to each of our objects where necessary, using only the ratio of the two strongest Balmer lines, $\mathrm{H}\alpha/\mathrm{H}\beta$, to determine the amount of extinction. We adopted negligible intrinsic reddening when the apparent Balmer decrement from the original work is below 3.10 and the extinction correction constant indicates a value of zero as shown in Table 4, thus $c(\mathrm{H}\beta) = 0$. The amount of interstellar extinction obtained using this method generally agrees relatively well with the amount of extinction determined using other line ratios such as He II λ3203/He II λ4686 (Shuder & Osterbrock, 1981) or [S II] λ4071/[S II] λ10320 (Wampler, 1971; Shields & Oke, 1975a; Koski, 1978). However, the problem with the latter Balmer-line method is the large uncertainty in the measured strengths of $\mathrm{H}\gamma$, $\mathrm{H}\delta$, etc., because of their intrinsic weakness and the possibility of being affected strongly by the underlying stellar Balmer absorption lines.

In the optical regime, [O III]λ5007/$\mathrm{H}\beta$ versus [N II]λ6584/$\mathrm{H}\alpha$ and [O III]λ5007/$\mathrm{H}\beta$ versus [S II](λ6716+λ6731)/$\mathrm{H}\alpha$ diagnostic diagrams (see Figure 10) have been used to distinguish objects whose main ionization mechanisms are by massive stars or Planetary Nebulae (PNe) from those that are mainly ionized by gas shocks or an active galactic nucleus. In order to separate the distinct classes of objects following the standard Baldwin-Phillips-Terlevich (BPT) diagrams (Baldwin, Phillips & Terlevich, 1981; Veilleux

& Osterbrock, 1987), the criteria proposed by Kewley et al. (2001) where all objects with

$$\log([\mathrm{O\,III}]\lambda5007/\mathrm{H}\beta) > \frac{0.61}{[\log([\mathrm{N\,II}]\lambda6584/\mathrm{H}\alpha) - 0.47]} + 1.19 \tag{2.21}$$

and

$$\log([\mathrm{O\,III}]\lambda5007/\mathrm{H}\beta) > \frac{0.72}{[\log([\mathrm{S\,II}]\lambda6725/\mathrm{H}\alpha) - 0.32]} + 1.30 \tag{2.22}$$

have AGNs as their main ionization mechanism were used. Figure 10 further confirms that the sources of ionization for the objects under consideration in this work are indeed Seyfert 2 nuclei.

Figure 10 – Reddening-corrected diagnostic diagrams for [O III] λ5007 Å/Hβ versus [N II] λ6584 Å/Hα (left-hand-side) and [O III] λ5007 Å/Hβ versus [S II] ($\lambda\lambda$6716, 6731 Å)/Hα (right-hand-side). The green solid lines, taken from Kewley et al. (2001), separate objects ionized by massive stars or PNe (H II-like objects) from those that are mainly ionized by gas shocks or AGN-like objects.

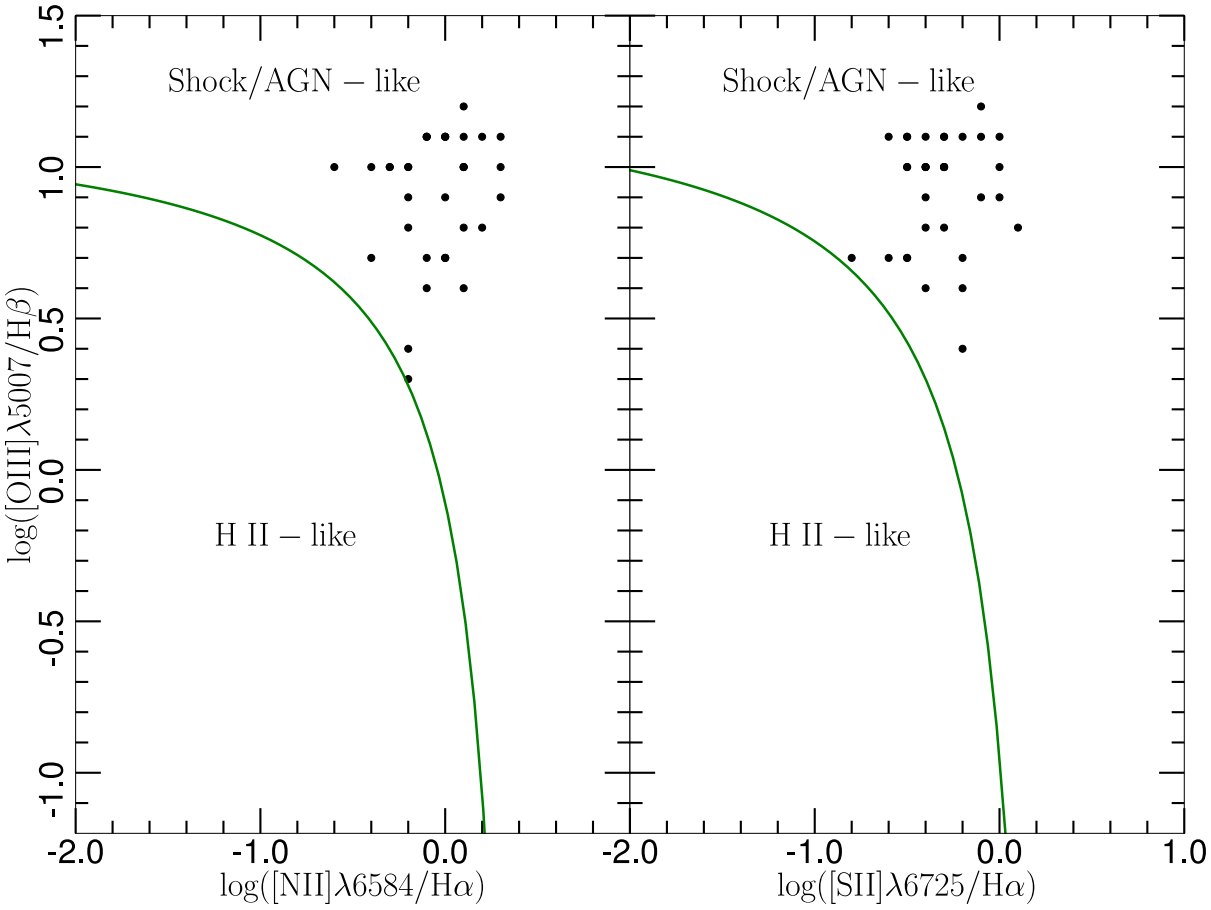

Table 4 – Reddening-corrected optical emission-line intensities of Seyfert 2 nuclei relative to Hβ = 1.00 compiled from the literature.

Object	[O II] λ3727 Å	[Ne III] λ3869 Å	[O III] λ4363 Å	[O III] λ4959 Å	[O III] λ5007 Å	[O I] λ6300 Å	Hα λ6563 Å	[N II] λ6584 Å	[S II] λ6717 Å	[S II] λ6731 Å	c(Hβ)
f(λ)	0.298	0.257	0.123	− 0.022	− 0.033	− 0.285	− 0.326	− 0.330	− 0.349	− 0.351	
NGC 3081	2.10	1.20	0.23	4.42	12.80	0.26	3.10	2.63	0.66	0.71	0.5107
NGC 4388	2.62	0.69	0.15	3.71	10.70	0.52	3.10	1.64	0.78	0.69	0.6054
NGC 4507	2.64	1.07	0.33	3.06	9.05	0.55	3.10	1.66	0.63	0.71	0.6861
NGC 5135	2.00	0.73	0.10	1.42	4.50	0.17	3.10	2.72	0.44	0.42	0.9158
NGC 5643	5.10	1.55	0.42	4.63	15.48	0.63	3.10	3.55	1.14	1.05	0.9268
NGC 5728	3.40	1.27	0.44	3.75	11.04	0.56	3.10	4.28	0.49	0.48	0.8824
IC 5063	5.00	1.20	0.28	3.41	10.37	0.41	3.10	1.90	0.80	0.70	0.7842
IC 5135	4.03	1.79	0.25	2.10	6.92	0.33	3.10	3.81	0.58	0.53	0.9048
MRK 3	3.66	1.45	0.23	4.01	12.74	0.71	3.10	3.16	0.73	0.81	0.7246
MRK 273	2.76	0.56	0.06	1.64	5.25	0.15	3.10	3.15	1.76	—	1.4670
MRK 348	4.12	1.59	0.24	3.88	11.93	1.19	3.10	2.55	1.23	1.42	0.4311
MRK 573	2.87	1.32	0.17	3.92	12.23	0.32	3.10	2.59	0.79	0.85	0.4406
NGC 1068	1.07	1.26	0.20	4.18	12.74	0.45	3.10	5.46	0.32	0.67	0.4928
NGC 2992	5.71	1.10	0.18	2.23	6.63	0.32	3.10	1.74	0.73	0.65	1.9617
NGC 5506	2.58	0.65	0.13	2.44	7.64	0.43	3.10	2.80	1.06	1.13	1.1439
NGC 7674	1.57	1.35	0.13	3.88	12.31	0.27	3.10	3.07	0.45	0.53	0.5372
I Zw 92	2.21	1.05	0.29	3.57	10.36	0.49	3.10	1.25	0.48	0.52	0.1787
NGC 2110	6.50	1.24	0.19	2.54	7.56	1.46	3.10	5.82	1.33	1.64	0.4044
NGC 5929	4.95	0.70	0.11	0.94	2.77	1.29	3.10	1.81	1.11	0.97	0.5551
MRK 463E	1.90	0.58	0.11	2.51	7.56	0.36	3.10	2.12	0.62	0.57	0.2354
MRK 622	10.65	1.17	0.04	1.88	5.46	0.08	3.10	2.84	0.47	0.51	1.7941
NGC 1386	2.67	1.08	0.22	3.68	10.87	0.32	3.10	3.66	0.66	0.82	0.5603
NGC 7582	1.15	0.31	0.03	0.72	2.16	0.09	3.10	2.03	0.46	0.42	0.0000
NGC 1275	4.91	2.25	0.41	4.17	12.27	0.90	3.10	3.06	0.72	2.45	0.7572
Circinus	1.37	0.67	0.20	3.04	9.86	0.27	3.10	0.83	0.67	0.59	0.8082
Centaurus A	5.53	0.96	0.14	2.25	5.76	0.96	3.10	4.54	2.09	1.65	1.1476
Cygnus A	4.95	1.22	0.21	3.88	12.14	1.07	3.10	6.03	1.61	1.45	1.0195
MRK 266SW	5.51	0.95	0.08	1.49	4.47	0.36	3.10	3.45	0.50	0.43	0.0842
MRK 1066	3.31	0.70	0.07	1.27	3.96	0.29	3.10	2.67	0.58	0.62	1.2469
NGC 424	0.17	0.91	0.13	1.69	4.57	0.19	3.10	1.21	0.24	0.24	0.0000
NGC 1320	0.57	0.70	0.35	3.46	9.42	0.26	3.10	2.12	0.57	0.66	0.6054
NGC 1667	11.82	1.94	0.42	4.00	11.13	0.96	3.10	6.75	2.93	9.97	0.0000
NGC 3393	1.78	0.87	0.11	3.38	10.15	0.30	3.10	4.24	1.72	5.86	0.1976
NGC 5953	2.44	0.85	0.12	1.71	4.33	0.34	3.10	4.28	0.86	0.90	0.0000
NGC 7682	8.49	2.21	0.91	12.74	37.67	1.16	3.10	3.37	0.85	0.90	0.5603
ESO428 − G014	2.83	1.13	0.30	4.16	13.41	0.43	3.10	3.51	0.92	0.98	0.1825

3 Methodology

The main goal of this work is to understand the temperature problem in AGNs, thus, the cause of higher electron temperature values usually derived from observational R_{O3} ratio than those predicted by photoionization models.

In the light of the foregoing, we proposed that a comparison between the neon abundance derived through infrared emission-lines and by using the T_e-method is a better methodology than using photoionization models, such as the oxygen abundances comparison carried out by Dors et al. (2020a). This is because in photoionization model, different assumptions are required to simulate several AGN physical parameters, typical examples are to assume a given spectral energy distribution (SED), electron density of the gas, ionization parameter, etc., see Dors et al. (2017). In fact, Feltre, Charlot & Gutkin (2016) showed that the increase in certain line ratios, such as [O III]λ5007/Hβ, is mainly due to the combination of metallicity with the ionization parameter and a secondary dependence between the hardness of the SED and the electron density with the line ratios is also found. In Figure 11, taken from Feltre, Charlot & Gutkin (2016), results of photoionization models built with the Cloudy code (Ferland et al., 2013) are compared with observational data taken from the Sloan Digital Sky Survey in some diagnostic diagrams. It can clearly be seen that different emission lines depend on different nebular parameters, which could not be representative of real AGN parameters (see also Carvalho et al., 2020). Another conspicuous example of this problem is the difference between the model predicted and observed slope of the SED of AGNs, especially the power law slope. Dors et al. (2017), by using the Cloudy code performed detailed modelling of a sample of 44 local Seyfert 2 nuclei ($z < 0.1$). These authors derived the slope for the SED, represented by α_{ox}, values in the range $-1.6 \lesssim \alpha_{ox} \lesssim -0.1$, with an average value of -1.1. In Figure 12, a histogram containing the distribution of observational values of α_{ox}, obtained by Miller et al. (2011) is shown, where a range of $-2.1 \lesssim \alpha_{ox} \lesssim -0.9$ is derived, with an average value of -1.40. Thus, photoionization models can predict a harder SED than the real energy distribution of AGNs.

Figure 11 – Diagnostic diagrams containing observational data from SDSS DR7.

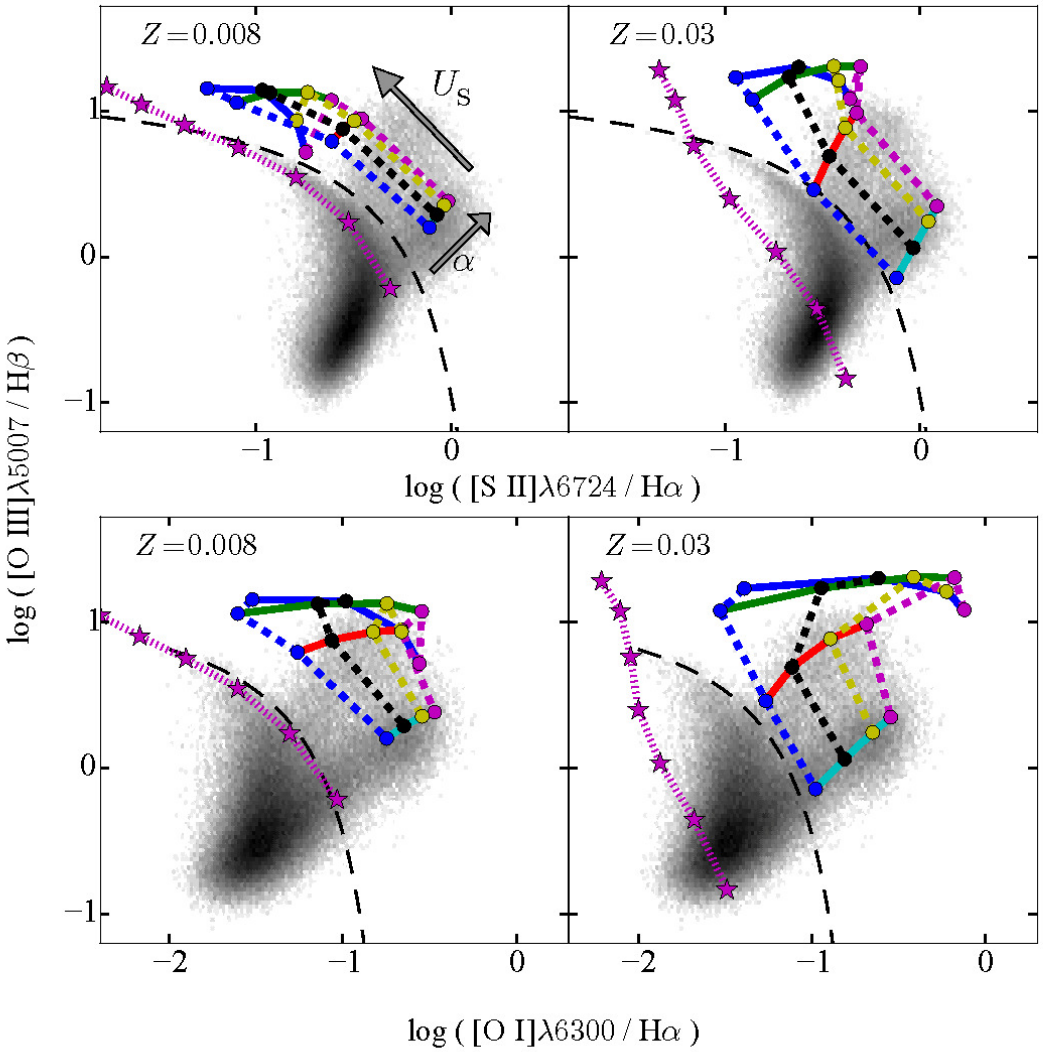

Source: Feltre, Charlot & Gutkin (2016)

Figure 12 – Histogram containing the distribution of the spectral index α_{ox} derived by Miller et al. (2011) for about 700 radio-intermediate and radio-loud quasars.

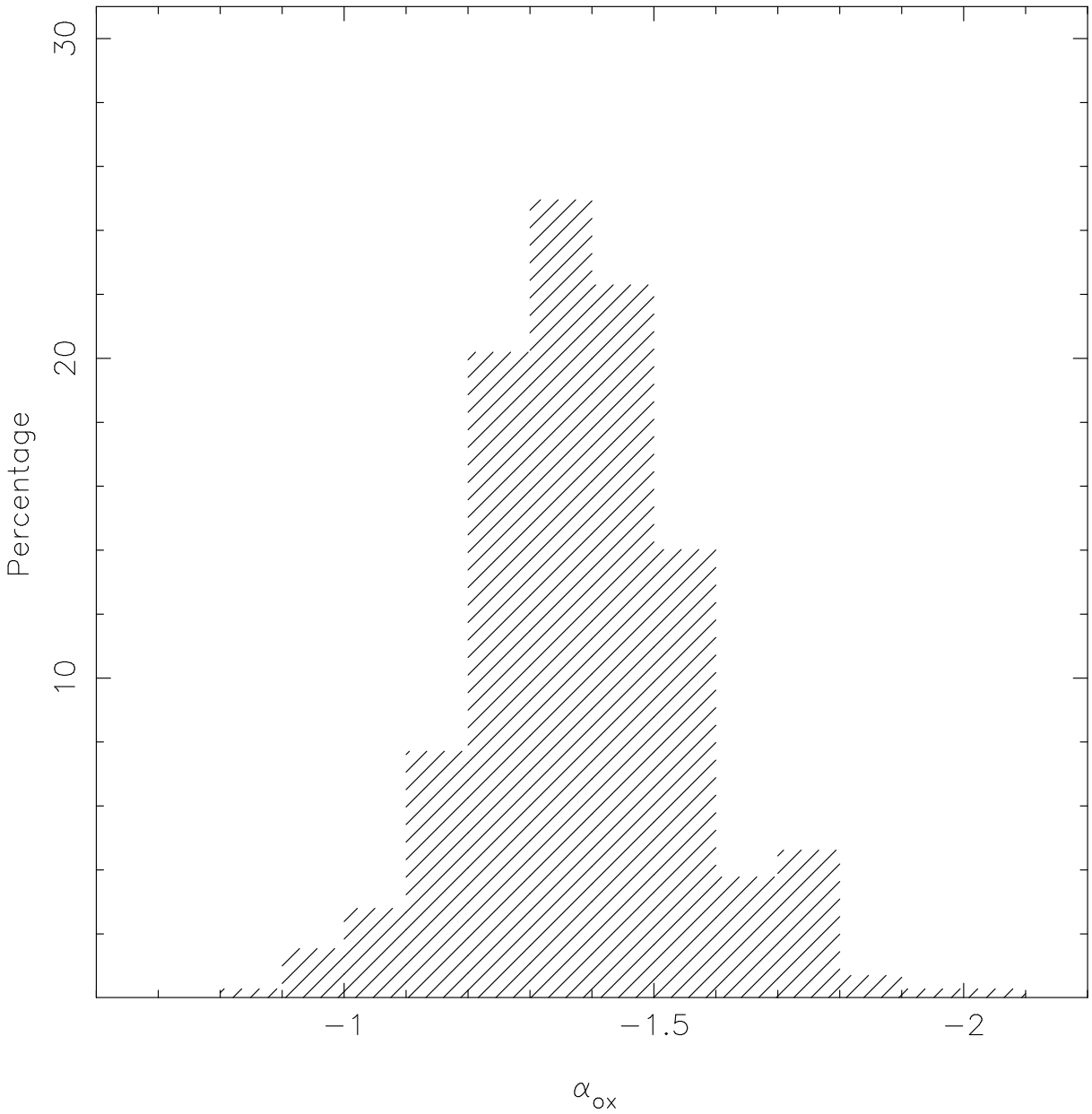

Source: Dors et al. (2019)

In summary, these (input) model parameters could not be representative for real AGNs, yielding unreliable results. In fact, the presence of gas shocks and their magnitudes or influences, for example, makes it difficult to better understand the physical processes present in Seyfert 2 AGNs. Contini (2017), by using the SUMA code (Contini & Aldrovandi, 1983), built detailed photoionization models to reproduce optical emission lines of a sample of 23 Seyfert 2. This author found the presence of gas shock with velocities ranging from 100 to 400 km s^{-1} in the NLRs of the objects considered. The effect of the gas shock is to increase the electron temperature and ionization of the gas and, consequently, to increase the emission line intensities. The analysis of temperature problem carried out by Dors et al. (2015, 2020a, 2020b) is based on photoionization models built with the CLOUDY code, which does not consider gas shock. Thus, the temperature or abundance discrepancy found by these authors with values derived through the $T_{\rm e}-$method and from photoionization models could be somewhat uncertain.

To circumvent the limitation in photoionization models, we adopt a comparison between neon abundances derived through infrared and optical emission lines without using photoionization models. Similar methodology was used in H II region studies of neon abundances by Dors et al. (2013) and sulphur abundances by Dors et al. (2016). Basically, in this methodology, the ionic abundance of a given element, for instance, the Ne^{2+}, is calculated using the T_e-method, e.g.

$$\left(\frac{\rm Ne^{2+}}{\rm H^{+}}\right)_{\rm Op.} = f\left[T_e, I\left(\rm Ne^{2+}\right)_{\rm Op.}\right], \tag{3.1}$$

where $I\left(\rm Ne^{2+}\right)_{\rm Op.}$ is the intensity (in relation to Hβ) of an optical line emitted by the Ne^{2+} ion and $T_{\rm e}$ is the temperature of the free electrons that are exciting the Ne^{2+}. In general, $T_{\rm e}$ is derived through the dependence of this parameter and the [O III](λ4959 + λ5007)/λ4363 line ratio. That is, $T_{\rm e}$ is estimated using the [O III] electron temperature as representative one of the emitter gas region of the [Ne III] λ3868 Å emission line. In principle, the [O III] and [S III] electron temperatures could be very similar (and in general are assumed to be equal) but the relation given by Hägele et al. (2006) showed that there are some differences depending on the temperatures of the objects. Moreover, Binette et al. (2012) also demonstrated that the difference depends on the metallicity of the objects and the difference could be due to the presence of temperature fluctuations and they also considered the possibility of a non-Maxwell-Boltzmann energy distribution (a Kappa-distribution) for the electron energies. However, in the case of neon we are unable to calculate the electron temperature since an optical auroral emission line of neon is not available, the only reliable assumption is the electron temperature of [O III] as representative of the high-ionization zone (i.e., $T_{\rm e}$([Ne III]) $\approx T_{\rm e}$([O III], see Peimbert & Costero, 1969).

Thereafter the ionic neon optical estimations, the Ne^{2+} abundance is also calculated by using infrared emission lines, i.e.

$$\left(\frac{Ne^{2+}}{H^+}\right)_{IR} = f\left[j_\lambda(Ne^{2+}), I\left(Ne^{2+}\right)_{IR}\right], \tag{3.2}$$

where $j_\lambda(Ne^{2+})$ is the emissivity of a given neon line and $I(Ne^{2+})_{IR}$ is the intensity (in relation to some hydrogen infrared lines) of an infrared line emitted by the Ne^{2+} ion. Abundance determinations based on infrared lines are practically independent from the electron temperature, and therefore, in principle, they are more precise than the ones via the T_e-method. In this scenario, let us assume the $(Ne^{2+}/H^+)_{IR}$ abundance as real ionic value.

In general, for H II regions, it has been found that $(Ne^{2+}/H^+)_{IR}$ is higher than $(Ne^{2+}/H^+)_{Op.}$ (see Dors et al., 2013), in other words, $(Ne^{2+}/H^+)_{Op.}$ is underestimated. The origin of this underestimation can be attributed to the gas shock presence or electron temperature fluctuation, in which lower and unreal values of $(Ne^{2+}/H^+)_{Op.}$ are derived. To quantify the effects of gas shock presence or electron temperature on T_e-method, we calculate the electron temperature value to conciliate $(Ne^{2+}/H^+)_{Op.}$ with $(Ne^{2+}/H^+)_{IR}$. We define this value as T_0 and consider it as the real electron temperature. Obviously, we must find $T_e > T_0$. Esteban and collaborators carried out a related procedure, which over the years measured oxygen and carbon abundances in H II regions resulting from excited and recombination lines (see Esteban et al., 2020 and references therein).

In the present work, we investigate the discrepancy between the aforementioned temperature values assuming the existence of electron temperature fluctuation in the NLRs of AGNs. A description of the methodology used in calculating the neon ionic abundance, T_e and T_0 is presented in succeeding subsections.

3.1 Determination of neon ionic abundances

3.1.1 T_e-method

The T_e-method, fundamentally, consists of deriving the electron temperature and the electron density of the gas and using these values to derive the ionic abundance of heavy elements (Osterbrock, 1989). The basic methodology of this method is presented below.

The T_e-method basically utilizes the following relation:

$$\frac{N(X^{i+})}{N(H^+)} = \frac{I(\lambda)}{I(H\beta)} \times \frac{\epsilon(H\beta)}{\epsilon(\lambda)}\ , \tag{3.3}$$

where $N(X^{i+})$ is the abundance of any ion (X^{i+}) related to H^+, $I(\lambda)$ is the intensity of the ion emission line, $I(H\beta)$ is the intensity of the Hβ emission line, and $\epsilon(\lambda)$ is the emission coefficient of the ion line under study with wavelength equal to λ.

In the case of collisionally excited lines, at the low density limit, the emission coefficient is given by

$$\epsilon(\lambda) = \mathrm{h}\,\nu\,q_{\mathrm{col}}(\lambda) = \frac{\mathrm{h\,c}}{\lambda} \times 8.63 \times 10^{-6} \times \frac{\Omega}{\omega_1} \times T_{\mathrm{e}}^{-0.5} \times e^{-\chi/\mathrm{k}\,T_{\mathrm{e}}}, \tag{3.4}$$

where, h is the Planck's constant, ν is the frequency, q_{col} is the collisional transition rate, Ω is the collision force for the observed transitions, ω_1 is the statistical weight of the lower level, χ is the excitation energy, k is the Boltzmann's constant, and T_{e} is the electron temperature. It can be seen that, the emission coefficient for collisionally excited lines depends strongly on the temperature, so it is essential to calculate the ionic abundance.

The electron temperature can be estimated through, for instance, [O III](λ4959Å + λ5007Å)/λ4363Å and [N II](λ6548Å + λ6884Å)/λ5755Å line ratios, since the relative excitation rates for the upper and lower levels depend strongly on the temperature. However, the [O III] λ4363 Å and [N II] λ5755 Å auroral emission lines are generally very weak, about 20 to 100 times weaker than Hβ (see Hägele et al., 2006, 2008, 2012; Sanders et al., 2016, 2020) in relatively low metallicity objects. For high metallicity objects the auroral [O III] λ4363 Å is undetectable (see Díaz et al., 2007; Hägele et al., 2007, 2009, 2010, 2013).

Figure 13 shows an example of the optical spectrum of an H II region. Another distinctive characteristic of these objects is the smaller range of ionization levels compared to Seyfert galaxies. Typical electron temperatures within the H II regions are in order of 10 000 K while in Seyferts are $\sim$ 15 000 K, with the cooler objects showing higher abundances of heavy elements. Typical electron density values in H II regions are of the order of 100−500 cm^{-3} (Beckmann & Shrader, 2012) and in the NLRs of Seyfert 2 galaxies 100−2 000 cm^{-3} (Dors et al., 2012).

Figure 13 – Spectrum of the region No.2 in NGC 2541.

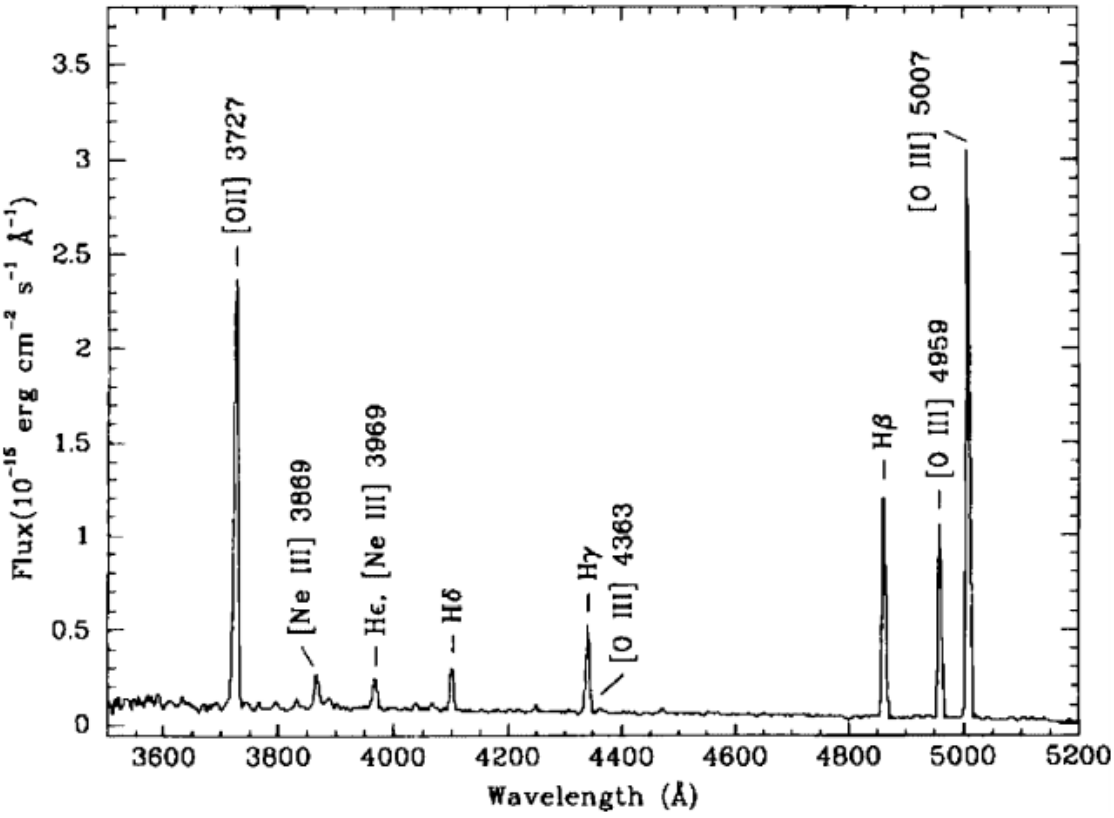

Source: Zaritsky, Kennicutt Robert C. & Huchra (1994)

Hägele et al. (2008) obtained from the task TEMDEN of IRAF[1](De Robertis, Dufour & Hunt, 1987; Shaw & Dufour, 1995) functions to determine electron temperatures. It is considered that, t_3 and t_2 are the electron temperatures (in units of 10^4 K) for the electrons that are excitating the O^{2+} and O^+ ions in the high and low ionization zones, respectively. We will consider only the electron temperature in the high-ionization zone (t_3) determination in this work. The relation by Hägele et al. (2008) is given as:

$$t_3 = 0.8254 - 0.0002415 \times R_{O3} + \frac{47.77}{R_{O3}}, \tag{3.5}$$

where, R_{O3}= [O III](λ4959Å + λ5007Å)/λ4363Å. This relation is valid for a range of temperature 7 000 − 23 000 K or 700 $\lesssim$ R_{O3} $\lesssim$ 30. The equation to estimate ionic abundance of the twice ionized neon in the optical was originally derived by Pagel et al.

[1] Image Reduction and Analysis Facility (IRAF) is distributed by the National Optical Astronomy Observatories, which are operated by the Association of Universities for Research in Astronomy, Inc., under cooperative agreement with the National Science Foundation.

(1992) and in its current form given by Hägele et al. (2008) as:

$$12 + \log\left(\frac{\mathrm{Ne}^{2+}}{\mathrm{H}^{+}}\right)_{\mathrm{Op.}} = \log\left[\frac{I(3869)}{I(\mathrm{H}\beta)}\right] + 6.486 + \frac{1.558}{t_3} - 0.504 \times \log t_3. \qquad (3.6)$$

In the optical spectrum of AGNs and H II regions we can only measure the unblended neon line [Ne III] λ3869 Å and, consequently, we are able to estimate only the $\mathrm{Ne}^{2+}/\mathrm{H}^{+}$ ionic abundance. The abundance of other neon ions can only be calculated from infrared lines. For example, in Figure 14, the optical spectrum of one object of our sample, Mrk 573, obtained by Kraemer et al. (2010) is shown, which indicates the presence of lines from a wide range of ionization states.

Figure 14 – STIS G430L spectrum of the central NLR knot in Mrk 573.

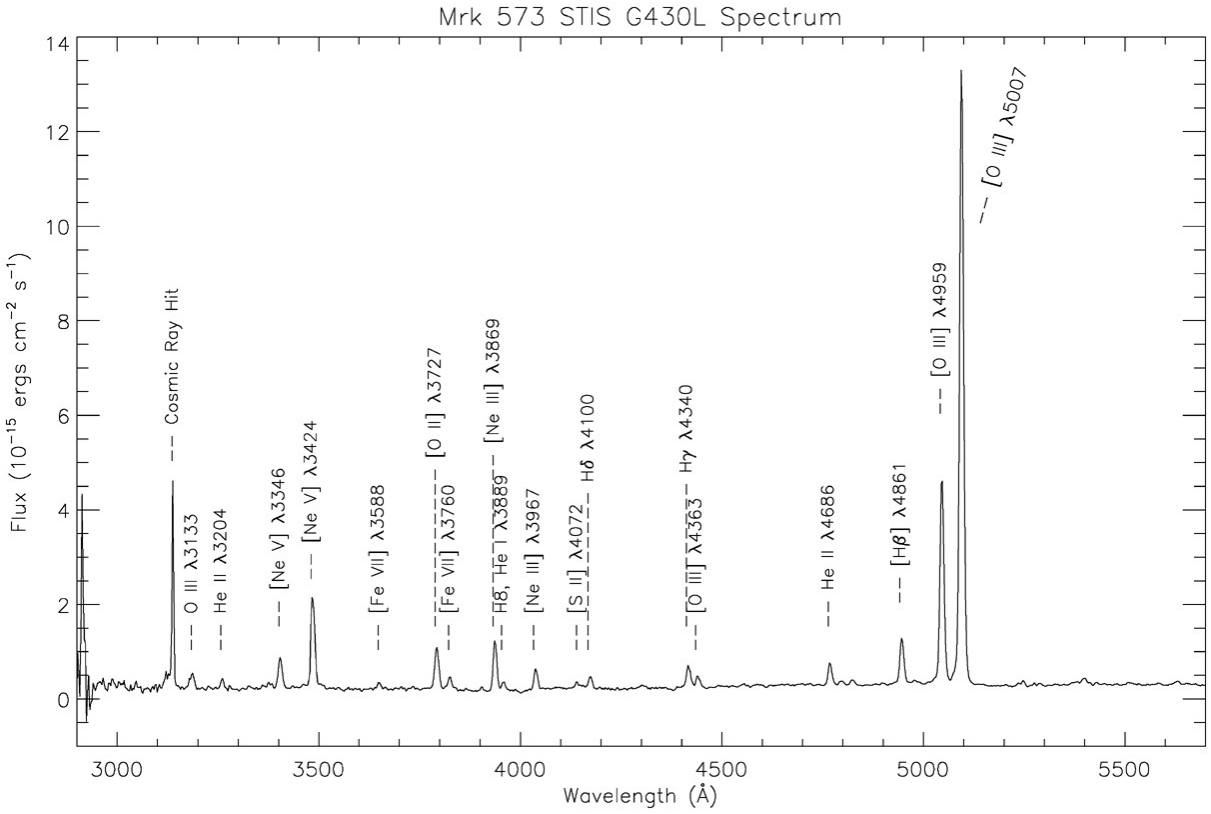

Source: Kraemer et al. (2010)

3.1.2 Infrared – lines method

Infrared−lines method (hereafter, IR−method) is based on determining the abundance of a given element using intensities of emission lines in the infrared spectral region. In the case of H II regions, emission lines in the range of 4 µm to 40 µm are generally used. The intensity of lines in the infrared is weakly dependent on the electron temperature, which makes this method advantageous since it is often difficult to determine this parameter.

The Ne^{+} and Ne^{2+} ionic fractions can be determined using the intensities of the [Ne II] 12.81 µm and [Ne III] 15.56 µm emission lines, respectively, following a similar methodology presented by Dors et al. (2013). Considering two ions X^{i+} and H^{+}, the ratio of their ionic abundance is determined by:

$$\frac{n_{X^{i+}}}{n_{H^{+}}} = \frac{I_{\lambda}(X^{i+})N_{e}j_{\lambda(H^{+})}}{I_{\lambda}(H^{+})N_{e}j_{\lambda(X^{i+})}}, \tag{3.7}$$

where, $n_{(X^{i+})}$ and $n_{H^{+}}$ are the densities of the X^{i+} and H^{+} ions, $I_{\lambda}(X^{i+})$ is the intensity of a given emission line emitted by X^{i+}, $I_{\lambda}(H^{+})$ is the intensity of a reference hydrogen line, while $j_{\lambda(X^{i+})}$ and $j_{\lambda(H^{+})}$ are the emissivity values. In Dors et al. (2013) the emissivity values were obtained from the IONIC routine of the nebular package of IRAF, which uses the Ne atomic parameters from Mendoza (1983), Saraph & Tully (1994), Galavis, Mendoza & Zeippen (1997), Badnell et al. (2006), Griffin, Mitnik & Badnell (2001), Kaufman & Sugar (1986), Butler & Zeippen (1994), and McLaughlin & Bell (2000). In all abundance determinations, these emissivity values are believed to be constant as they differ by less than 5% over a wide temperature range (Simpson, 1975). Using this method, any error in the determination of these emissivities directly translates in a systematic shift in the derived Ne^{+} and Ne^{2+} ionic abundances. To obtain the ionic abundances with respect to hydrogen, H^{+} emission nebula-associated is required and these can be derived from the mid-infrared H I recombination lines, such as Pα, Pβ, Pδ, Brγ, Brδ, and Br_{10}, which are detected in most of the objects under consideration.

The calculation of the Ne^{2+} ion abundance can be done using the line in the infrared [Ne III]λ15.56 µm. The emission coefficient of emission for lines in the infrared has a weak dependence on the electronic temperature, which, in general, is disregarded. Therefore, abundance of a given ion can be obtained directly from an emission line observed in the infrared using a hydrogen reference line. Thus, for neon, we have

$$\frac{Ne^{2+}}{H^{+}} = \frac{I(15.56\,\mu m)}{I(H\beta)} \times 6.323 \times 10^{-5}. \tag{3.8}$$

Taking into account all the above assumptions together with the values of the hydrogen

line emissivities relative to Hβ listed in Table 5 and Equation 3.8, we derive the following relations:

$$\frac{\mathrm{Ne^{2+}}}{\mathrm{H^{+}}} = \frac{I(15.56\,\mu\mathrm{m})}{I(\mathrm{Pa}\alpha)} \times 2.099 \times 10^{-5}, \tag{3.9}$$

$$\frac{\mathrm{Ne^{2+}}}{\mathrm{H^{+}}} = \frac{I(15.56\,\mu\mathrm{m})}{I(\mathrm{Pa}\beta)} \times 1.024 \times 10^{-5}, \tag{3.10}$$

$$\frac{\mathrm{Ne^{2+}}}{\mathrm{H^{+}}} = \frac{I(15.56\,\mu\mathrm{m})}{I(\mathrm{Pa}\gamma)} \times 5.697 \times 10^{-6}, \tag{3.11}$$

$$\frac{\mathrm{Ne^{2+}}}{\mathrm{H^{+}}} = \frac{I(15.56\,\mu\mathrm{m})}{I(\mathrm{Pa}\delta)} \times 3.503 \times 10^{-6}, \tag{3.12}$$

$$\frac{\mathrm{Ne^{2+}}}{\mathrm{H^{+}}} = \frac{I(15.56\,\mu\mathrm{m})}{I(\mathrm{Pa8})} \times 2.368 \times 10^{-6}, \tag{3.13}$$

$$\frac{\mathrm{Ne^{2+}}}{\mathrm{H^{+}}} = \frac{I(15.56\,\mu\mathrm{m})}{I(\mathrm{Br}\alpha)} \times 4.919 \times 10^{-6}, \tag{3.14}$$

$$\frac{\mathrm{Ne^{2+}}}{\mathrm{H^{+}}} = \frac{I(15.56\,\mu\mathrm{m})}{I(\mathrm{Br}\beta)} \times 2.826 \times 10^{-6}, \tag{3.15}$$

$$\frac{\mathrm{Ne^{2+}}}{\mathrm{H^{+}}} = \frac{I(15.56\,\mu\mathrm{m})}{I(\mathrm{Br}\gamma)} \times 1.739 \times 10^{-6}, \tag{3.16}$$

$$\frac{\mathrm{Ne^{2+}}}{\mathrm{H^{+}}} = \frac{I(15.56\,\mu\mathrm{m})}{I(\mathrm{Br}\delta)} \times 1.144 \times 10^{-6}, \tag{3.17}$$

$$\frac{\mathrm{Ne^{2+}}}{\mathrm{H^{+}}} = \frac{I(15.56\,\mu\mathrm{m})}{I(\mathrm{Br10})} \times 5.754 \times 10^{-7}, \tag{3.18}$$

$$\frac{\mathrm{Ne^{2+}}}{\mathrm{H^{+}}} = \frac{I(15.56\,\mu\mathrm{m})}{I(\mathrm{Br11})} \times 4.401 \times 10^{-7}, \tag{3.19}$$

and

$$\frac{\mathrm{Ne^{2+}}}{\mathrm{H^{+}}} = \frac{I(15.56\,\mu\mathrm{m})}{I(\mathrm{Br13})} \times 2.681 \times 10^{-7}. \tag{3.20}$$

In Figure 15, the infrared spectrum of Mrk 573 obtained by Ramos Almeida et al. (2008) is shown, where the Paγ and other lines have been observed.

Figure 15 – Normalized spectrum in the 0.88 − 1.35 µm wavelength of the nuclear region of Mrk 573 in the *ZJ* range. Detections of the permitted Fe II 9200Å lines and the Fe II 1 µm lines, together with the O I $\lambda\lambda$ 1.128, 1.317 narrow lines are clear.

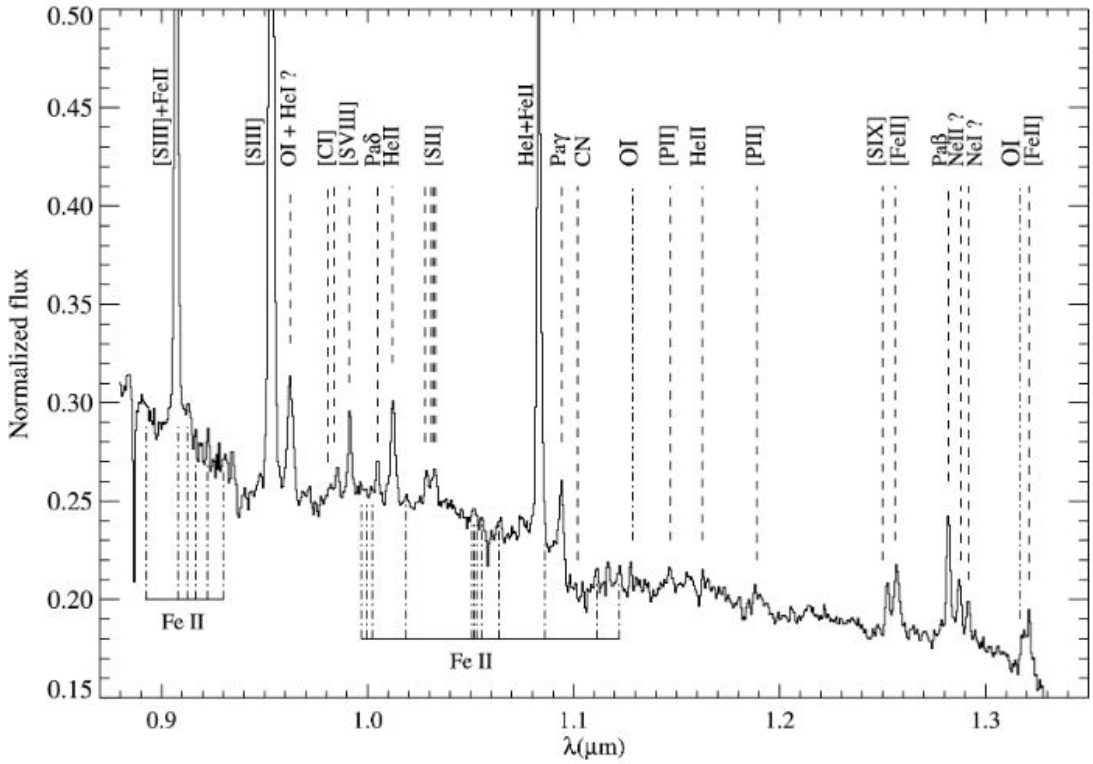

Source: Ramos Almeida et al. (2008)

Table 5 – H I emissivity ratio values (Case B).

$n_e(10^4$ **cm**$^{-3})$	**T**$(10^4$ **K)**
Paschen-line intensities relative to Hβ	
$j_{P\alpha}/j_{H\beta}$	0.33200
$j_{P\beta}/j_{H\beta}$	0.16200
$j_{P\gamma}/j_{H\beta}$	0.09010
$j_{P\delta}/j_{H\beta}$	0.05540
$j_{P8}/j_{H\beta}$	0.03745
Brackett-line intensities relative to Hβ	
$j_{Br\alpha}/j_{H\beta}$	0.07780
$j_{Br\beta}/j_{H\beta}$	0.04470
$j_{Br\gamma}/j_{H\beta}$	0.02750
$j_{Br\delta}/j_{H\beta}$	0.01810
$j_{Br10}/j_{H\beta}$	0.00910
$j_{Br11}/j_{H\beta}$	0.00696
$j_{Br13}/j_{H\beta}$	0.00424

Source: Osterbrock & Ferland (2006)

The Case B was assumed to derived the above equations. This approximation assumes that none of the ionizing photons are expected to escape from the nebula, meaning after many scatterings and absorptions and recombinations the photons are reconverted into more than one photon (e.g., see Osterbrock & Ferland, 2006; Gaskell, 2017). Moreover, as opposed to the broad-line region gas, much of the narrow-line region gas is believed to be optically thick to the ionizing radiation, even though studies of the He II λ4686/Hβ ratio indicate the presence of some optically thin gas (Murdin, 2003).

The [Ne III] 15.56 µm line is always chosen over the [Ne III] 36.0 µm when both are measured because the spectrum is noisier at the long wavelength end of the long high-resolution (LH) module in the Infrared Spectrograph (IRS). Therefore, we preferred to use the [Ne III] 15.56 µm line flux for the abundance determination of this ion which also has a larger transition probability and critical density.

In this study, the importance of using infrared lines when deriving chemical abundances are highlighted and summarized as follows. Infrared light lies just beyond the red portion of the visible spectrum ("below red") with wavelengths ranging from about 0.7 to 350 microns. In near infrared light direct observations through the gas and dust to view the stars forming within the cloud. In mid and far infrared light it is possible to observe the glow of the dust itself, emission from cold dust, central regions of galaxies, and very cold molecular clouds. As opposed to optical or UV lines, infrared lines are little affected by extinction. Uncertainties in the electron temperature or temperature fluctuations within the nebula are not significant when using infrared lines because they originate from levels very close to the ground level. In addition, many ions emit in the infrared, and the use of ionization correction factors (ICFs, not available for AGNs in the literature) can be substantially minimized by making infrared observations. This applies especially to neon, sulphur, and argon. Infrared observations have made it possible to access the far infrared AGN spectra, which present strong metal emission lines, thereby fostering the investigation of MIR/FIR transitions as metallicity tracers. Last but not least, although not detailed in this work, dust emission in this portion of the electromagnetic spectrum can be studied. In the study of neon, no optical or infrared observation of Ne I and Ne IV lines have been made in the literature reviewed hitherto, because of their high excitation energies. For the AGN objects which do not show an O IV line it is unlikely that there is any Ne^{3+} because the latter requires a higher energy radiation field than the former. The AGNs which show the O IV line a correction must be made in order to derive the total abundance of the neon, which is out of the scope of the present work.

3.1.3 Temperature fluctuations measure (t^2)

More often than not, the temperature in a gas nebulae is nonuniform, therefore chemical abundances derived from $T_{\rm e}-$based methodology are biased. To evaluated such biases, we utilized the mathematical formalism developed by Peimbert (1967) to ascertain the level of temperature fluctuations in the Ne^{2+}/H^{+} ionic abundances of our Seyfert 2 nuclei samples. This formalism is based on the Taylor expansion of the average temperature given by

$$T_0(\mathrm{X^{i+}}) = \frac{\int T_e n_e n(\mathrm{X^{i+}}) dV}{\int n_e n(\mathrm{X^{i+}}) dV}, \tag{3.21}$$

and defined for each ion $n(\mathrm{X^{i+}})$, using the root mean square (r.m.s.) temperature variation

$$t^2(X^{i+}) = \frac{\int (T_e - T_0(\mathrm{X^{i+}}))^2 n_e n(X^{i+}) dV}{T_0(\mathrm{X^{i+}})^2 \int n_e n(\mathrm{X^{i+}}) dV}. \tag{3.22}$$

where V, the observed volume is the product of the observed solid angle (Ω) and the distance inside the nebula (l) along the line of sight in units of parsecs, $n_{\rm e}$ and n are the local number density of electrons and protons in units of $\mathrm{cm^{-3}}$ respectively, finally, T_0 and $T_{\rm e}$ are the high ionization region average and electron temperatures defined over the entire volume under consideration. Since the variations in the density terms do not affect the nebular auroral emission line ratios, the mean electron temperature in the high ionization zone can be expressed as:

$$T_e(\mathrm{O^{2+}}) = T_0 \left[1 + \frac{1}{2}\left(\frac{90\,800}{T_0} - 3\right) t^2\right]. \tag{3.23}$$

We estimate T_0 at the point where the doubly ionized neon abundances in optical and infrared are equal. Therefore, from Equation 3.6 we obtain,

$$12 + \log\left(\frac{\mathrm{Ne^{2+}}}{\mathrm{H^{+}}}\right)_{\rm IR} = \log\left[\frac{I(3869)}{I(\mathrm{H}\beta)}\right] + 6.486 + \frac{1.558}{T_0} - 0.504 \times \log T_0. \tag{3.24}$$

4 Results and discussions

Customarily, knowledge of elemental abundances originates from two complementary sciences - astronomy and cosmochemistry. Astronomy or astrophysics deals with the studies of observations and the measurements relating to radio, microwave, infrared (IR), visible, ultraviolet, x-ray, gamma ray, neutrino, gravity-wave studies that measure positions, brightness, spectra, structure of gas clouds, planets, stars, galaxies, globular clusters of galaxies, superclusters, quasars, etc., or developing physical models to predict and explain the radiation detected from astronomical objects, and the application of physics to these observations to understand and interpret them, specifically, the composition of the sun and other stars, while cosmochemistry encompasses hands-on studies of meteorites, interplanetary, as well as interstellar dust within the interstellar medium (ISM). These two disciplines together make up a whole in order to validate, supplement, and optimize solar system abundance data which are widely used as a reference composition in both disciplines. During the 1920s, hydrogen was discovered to be predominated in the sun and other stars, and Payne (1925a, 1925b) found the logarithm of the relative abundance of hydrogen to be greater than 11 for the sun and equal to 12.5 for her set of analyzed stars. Payne (1925a) defined the fractional logarithmic to the base 10 abundance of hydrogen to be equal to 11 in her PhD dissertation. Presently, the astronomical abundance scale uses hydrogen, the most abundant element in the sun, ISM, and other stars as reference element. Ionic or elemental abundances are normalized to 10^{12} ions of hydrogen. In order to avoid negative logarithmic values for elements of low abundance, which presented numerical problems in the first computers during the last 5 decades, Claas (1951) is known to be the first to have undertaken the normalization of abundances with hydrogen (i.e., the metallicity of H = 12). Therefore, the ratio of the number of ions of a given element $N(X^{i+})$, relative to the number of hydrogen ion $N(H^{i+})$, is given in an astronomical logarithmic abundance scale:

$$A\left(X^{i+}\right) = \left[\log N(X^{i+})/N(H^{i+})\right] + 12. \tag{4.1}$$

In Table 6, the ionic Ne^{2+}/H^{+} abundance values for our sample obtained using the IR-lines method from different H I transition lines are listed. The IR Ne^{2+}/H^{+} shown in Figure 16 are the averaged values obtained using different reference hydrogen lines as described in the previous section (see section 2.2). In the bottom panel of Figure 16, a comparison between the ionic abundance 12+log(Ne^{2+}/H^{+}) obtained using the T_e and IR methods are shown (see section 3.1). In the top panel of Figure 16, the mean differences between the estimations are also shown.

Table 6 – 12+log(Ne^{2+}/H^+) abundances derived by using the IR−method (see subsection 3.1.2) taken into account the reference lines from different transitions of H I.

Object	Pa8 λ9549 Å	Paδ λ10052 Å	Paγ λ10941 Å	Paβ λ12822 Å	Paα λ18756 Å	Br13 λ16114 Å	Br11 λ16811 Å	Br10 λ17367 Å	Brδ λ19451 Å	Brγ λ21661 Å	Brβ λ26259 Å	Brα λ40523 Å
NGC 3081	—	—	—	7.8345 ± 0.0155	—	—	—	—	—	—	—	8.2041 ± 0.0155
NGC 4388	9.7096 ± 0.0076	10.5785 ± 0.0076	10.3126 ± 0.0076	10.1413 ± 0.0077	—	—	—	—	—	8.2214 ± 0.0076	—	8.2182 ± 0.0076
NGC 4507	—	—	—	—	—	—	—	—	—	—	—	7.5859 ± 0.03617
NGC 5135	—	—	—	—	—	—	—	—	—	7.7866 ± 0.0137	—	7.5578 ± 0.0061
NGC 5643	10.1682 ± 0.0061	9.9915 ± 0.0061	9.8047 ± 0.0061	8.2143 ± 0.0061	—	—	—	—	—	—	7.5972 ± 0.0061	7.9745 ± 0.0061
NGC 5728	—	8.5466 ± 0.0119	8.9145 ± 0.0125	8.8813 ± 0.0078	8.7459 ± 0.0056	—	—	—	—	8.6545 ± 0.0055	—	—
IC 5063	—	—	—	—	—	—	—	—	—	8.1066 ± 0.0303	7.6185 ± 0.0274	—
IC 5135	—	—	—	—	—	—	—	—	—	7.8001 ± 0.0421	—	7.3399 ± 0.0239
MRK 3	—	—	—	8.2615 ± 0.0625	—	—	—	—	—	7.7599 ± 0.0625	—	—
MRK 273	—	—	—	—	7.9046 ± 0.0054	—	—	—	7.7423 ± 0.0054	7.9065 ± 0.0242	7.3569 ± 0.00535	7.5774 ± 0.0053
MRK 348	—	8.4319 ± 0.0679	8.2244 ± 0.0778	8.2417 ± 0.0274	8.0857 ± 0.0249	—	—	—	7.8535 ± 0.0239	8.0799 ± 0.0647	—	—
MRK 573	—	8.4103 ± 0.0218	8.3505 ± 0.0288	8.4093 ± 0.0088	8.0435 ± 0.0051	—	—	—	8.3023 ± 0.0194	8.1782 ± 0.0147	—	—
NGC 1068	—	—	—	—	—	—	—	—	—	8.2917 ± 0.0239	7.9937 ± 0.0240	8.008 ± 0.0239
NGC 2992	7.7448 ± 0.0147	7.9066 ± 0.0147	7.9728 ± 0.0147	8.0881 ± 0.0146	8.1629 ± 0.0146	7.7666 ± 0.0148	7.6807 ± 0.0147	7.6820 ± 0.0147	—	7.9612 ± 0.0147	—	7.6544 ± 0.0146
NGC 5506	—	—	—	7.2618 ± 0.0267	—	—	—	—	—	7.3499 ± 0.0268	7.7876 ± 0.0283	7.7940 ± 0.0267
NGC 7674	—	8.2853 ± 0.0395	8.2785 ± 0.0451	8.6583 ± 0.0309	8.4791 ± 0.0236	—	—	—	8.1985 ± 0.0697	8.4087 ± 0.0397	—	—
I Zw 92	—	—	—	7.1974 ± 0.0061	—	—	—	—	—	7.4652 ± 0.0061	—	—
NGC 2110	—	8.7444 ± 0.0400	8.3299 ± 0.0362	8.5129 ± 0.0256	8.4840 ± 0.0616	—	—	—	—	8.5193 ± 0.0386	—	8.0432 ± 0.0078
NGC 5929	—	—	8.1704 ± 0.0336	8.1174 ± 0.0178	—	—	—	—	—	8.1107 ± 0.0851	—	—
MRK 463E	—	—	—	8.1386 ± 0.0091	—	—	—	—	—	—	7.4560 ± 0.0091	—
MRK 622	—	—	—	7.9047 ± 0.0116	—	—	—	—	—	—	—	—
NGC 1386	—	—	—	8.0295 ± 0.0095	—	—	—	—	—	8.5590 ± 0.0360	—	—
NGC 7582	—	—	—	8.1392 ± 0.0185	—	—	—	—	—	7.6191 ± 0.0438	7.5177 ± 0.0186	7.3990 ± 0.0233
NGC 1275	—	7.7712 ± 0.0371	7.1842 ± 0.0246	7.5782 ± 0.0251	7.5100 ± 0.0132	—	—	—	7.2681 ± 0.0679	7.6005 ± 0.0210	7.4998 ± 0.0118	7.6992 ± 0.0117
Circinus	—	—	8.3405 ± 0.0108	—	—	—	—	—	—	8.2623 ± 0.0108	7.5479 ± 0.0107	8.1176 ± 0.0107
Centaurus A	—	—	7.6230 ± 0.0057	7.9523 ± 0.0057	—	—	—	—	—	7.9550 ± 0.0056	7.6431 ± 0.0057	7.9349 ± 0.0057
Cygnus A	—	—	—	—	8.5242 ± 0.0339	—	—	—	—	8.4413 ± 0.0140	—	—
MRK 266SW	—	—	—	7.8851 ± 0.0060	—	—	—	—	—	8.2915 ± 0.0061	—	7.6545 ± 0.0060
MRK 1066	—	8.2272 ± 0.0150	8.0201 ± 0.0217	7.9485 ± 0.0073	7.8315 ± 0.0325	—	7.7181 ± 0.0622	—	7.7916 ± 0.0073	7.7604 ± 0.0098	—	—
NGC 424	—	—	—	—	—	—	—	—	—	7.5624 ± 0.0209	7.0742 ± 0.0209	—
NGC 1320	—	—	—	—	—	—	—	—	—	8.2211 ± 0.0685	—	—
NGC 1667	—	—	—	—	—	—	—	—	—	8.8546 ± 0.1056	—	—
NGC 3393	—	—	—	—	—	—	—	—	—	8.5552 ± 0.0064	—	—
NGC 5953	—	—	—	8.5965 ± 0.0215	8.3471 ± 0.0281	—	—	—	—	8.1197 ± 0.0215	—	—
NGC 7682	—	7.7541 ± 0.0126	7.9653 ± 0.0126	7.9211 ± 0.0297	7.7260 ± 0.0136	—	—	—	—	7.8595 ± 0.0256	—	—
ESO428 − G014	—	8.80711 ± 0.0298	8.4894 ± 0.0167	8.5798 ± 0.0069	8.5385 ± 0.0054	—	7.9542 ± 0.0159	—	8.8130 ± 0.0734	8.5124 ± 0.0080	—	—

In Table 7, the Ne^{2+}/H^{+} ionic abundance values for our sample obtained using the T_e-method and the averaged values from the IR−lines method together with differences between the optical and infrared ionic abundance estimations are listed. Also, listed in this Table are the t_3 (referred as T_e), T_0, and the t^2 parameter values calculated from Equation 3.23.

Table 7 – Doubly ionized neon chemical abundances. Col. (1): AGN objects names from the literature; Col. (2): electron temperature; Col. (3): average temperature derived from Equation 3.24; Col. (4): root mean square temperature variations, t^2; Col. (5): mean neon ionic abundances from the values listed in Table 6 derived from NIR and MIR emission lines; Col. (6): neon ionic abundances derived from optical reddening corrected emission lines (see subsection 3.1.1, typical error in these values is ± 0.01 dex); Col. (7): difference (D, in dex) between the values listed in columns (5) and (6).

Object	Temperature		t^2 Parameter	$12 + \log(X^{2+}/H^{+})$		D (dex)
	T_e (10^4 K)	T_0 (10^4 K)		$(Ne^{2+})_{IR}$	$(Ne^{2+})_{Op.}$	
NGC 3081	1.4455 ± 0.0083	1.0543 ± 0.0099	0.1322 ± 0.0038	8.01 ± 0.01	7.55 ± 0.01	0.4612 ± 0.0196
NGC 4388	1.2994 ± 0.0065	0.8513 ± 0.0028	0.1373 ± 0.0021	9.53 ± 0.01	7.46 ± 0.01	2.0636 ± 0.0151
NGC 4507	2.1183 ± 0.0166	1.3518 ± 0.0112	0.3051 ± 0.0071	7.58 ± 0.03	7.08 ± 0.01	0.4976 ± 0.0384
NGC 5135	1.6181 ± 0.0104	1.1402 ± 0.0065	0.1689 ± 0.0040	7.67 ± 0.01	7.20 ± 0.01	0.4712 ± 0.0139
NGC 5643	1.8131 ± 0.0128	0.7194 ± 0.0019	0.3159 ± 0.0037	8.95 ± 0.00	7.40 ± 0.01	1.5561 ± 0.0116
NGC 5728	2.2386 ± 0.0182	0.7417 ± 0.0022	0.4365 ± 0.0053	8.74 ± 0.01	7.10 ± 0.01	1.6424 ± 0.0109
IC 5063	1.7492 ± 0.0120	1.1966 ± 0.0081	0.2013 ± 0.0049	7.86 ± 0.02	7.32 ± 0.01	0.5337 ± 0.0301
IC 5135	2.1409 ± 0.0170	1.6387 ± 0.0421	0.2404 ± 0.0153	7.57 ± 0.02	7.29 ± 0.01	0.2721 ± 0.0308
MRK 3	1.4638 ± 0.0087	1.1185 ± 0.0434	0.1205 ± 0.0128	8.01 ± 0.06	7.62 ± 0.01	0.3840 ± 0.0644
MRK 273	1.2136 ± 0.0057	1.0992 ± 0.0039	0.0395 ± 0.0023	7.69 ± 0.01	7.46 ± 0.01	0.2296 ± 0.0164
MRK 348	1.5351 ± 0.0093	1.0026 ± 0.0155	0.1753 ± 0.0049	8.15 ± 0.02	7.60 ± 0.01	0.5438 ± 0.0292
MRK 573	1.3053 ± 0.0068	0.9339 ± 0.0046	0.1182 ± 0.0024	8.28 ± 0.01	7.73 ± 0.01	0.5443 ± 0.0162
NGC 1068	1.3699 ± 0.0075	1.0219 ± 0.0139	0.1156 ± 0.0045	8.09 ± 0.02	7.65 ± 0.01	0.4434 ± 0.0270
NGC 2992	1.7295 ± 0.0118	1.1565 ± 0.0109	0.2042 ± 0.0050	7.86 ± 0.01	7.30 ± 0.01	0.5616 ± 0.0177
NGC 5506	1.4228 ± 0.0080	1.1969 ± 0.0212	0.0822 ± 0.0073	7.54 ± 0.02	7.31 ± 0.01	0.2384 ± 0.0290
NGC 7674	1.1789 ± 0.0052	0.8919 ± 0.0116	0.0896 ± 0.0035	8.38 ± 0.02	7.90 ± 0.02	0.4817 ± 0.0297
I Zw 92	1.8082 ± 0.0127	1.6533 ± 0.0098	0.0751 ± 0.0074	7.33 ± 0.01	7.23 ± 0.01	0.0966 ± 0.0117
NGC 2110	1.7110 ± 0.0115	0.8527 ± 0.0073	0.2631 ± 0.0038	8.43 ± 0.01	7.37 ± 0.01	1.0667 ± 0.0201
NGC 5929	2.2336 ± 0.0180	0.8775 ± 0.0147	0.4206 ± 0.0059	8.13 ± 0.03	6.85 ± 0.01	1.2803 ± 0.0346
MRK 463E	1.3251 ± 0.0068	0.7847 ± 0.0084	0.1606 ± 0.0027	8.00 ± 0.01	7.35 ± 0.01	0.6473 ± 0.0214
MRK 622	1.0413 ± 0.0039	1.0413 ± 0.0039	0.0006 ± 0.0000	7.90 ± 0.01	8.00 ± 0.02	0.1334 ± 0.0219
NGC 1386	1.5320 ± 0.0094	0.8868 ± 0.0088	0.2010 ± 0.0035	8.29 ± 0.01	7.43 ± 0.01	0.8555 ± 0.0226
NGC 7582	1.2998 ± 0.0066	0.9262 ± 0.0070	0.1186 ± 0.0028	7.66 ± 0.02	7.11 ± 0.01	0.5496 ± 0.0249
NGC 1275	2.0070 ± 0.0152	1.9165 ± 0.0310	0.0537 ± 0.0194	7.51 ± 0.01	7.46 ± 0.01	0.0536 ± 0.0181
Circinus	1.5505 ± 0.0096	0.8934 ± 0.0050	0.2053 ± 0.0031	8.06 ± 0.01	7.21 ± 0.01	0.8529 ± 0.0157
Centaurus A	1.6467 ± 0.0107	1.1216 ± 0.0034	0.1837 ± 0.0038	7.82 ± 0.00	7.30 ± 0.01	0.5211 ± 0.0118
Cygnus A	1.4331 ± 0.0082	0.8291 ± 0.0074	0.1832 ± 0.0029	8.48 ± 0.01	7.57 ± 0.01	0.9061 ± 0.0223
MRK 266SW	1.4487 ± 0.0085	1.1543 ± 0.0049	0.1048 ± 0.0033	7.94 ± 0.00	7.45 ± 0.01	0.4856 ± 0.0134
MRK 1066	1.4467 ± 0.0083	0.9741 ± 0.0071	0.1535 ± 0.0032	7.89 ± 0.01	7.32 ± 0.01	0.5785 ± 0.0179
NGC 424	1.8042 ± 0.0126	1.4402 ± 0.0234	0.1527 ± 0.0092	7.31 ± 0.02	7.17 ± 0.01	0.1390 ± 0.0235
NGC 1320	2.0774 ± 0.0159	0.8370 ± 0.0274	0.3777 ± 0.0060	8.22 ± 0.06	6.91 ± 0.01	1.3075 ± 0.0689
MRK 1667	2.1430 ± 0.0169	0.7686 ± 0.0368	0.4055 ± 0.0065	8.85 ± 0.10	7.33 ± 0.01	1.5219 ± 0.1062
MRK 3393	1.1840 ± 0.0053	0.7518 ± 0.0025	0.1266 ± 0.0016	8.55 ± 0.01	7.70 ± 0.02	0.8505 ± 0.0166
NGC 5953	1.7622 ± 0.0122	0.8197 ± 0.0086	0.2846 ± 0.0040	8.35 ± 0.02	7.17 ± 0.01	1.1784 ± 0.0240
NGC 7682	1.6744 ± 0.0111	1.2949 ± 0.0169	0.1461 ± 0.0067	7.84 ± 0.01	7.64 ± 0.01	0.1992 ± 0.0160
ESO428−G014	1.5993 ± 0.0103	0.8195 ± 0.0050	0.2355 ± 0.0032	8.52 ± 0.01	7.45 ± 0.01	1.0698 ± 0.0170

The validity of derived abundances is based on the accuracy of the data and the methodology used while typical uncertainty values for Ne/H are known to be in order of 0.10 to 0.25 dex with a little less for Ne/O (Stasińska, 2004).

Presented in Table 6 are the results obtained for the neon abundance twice ionized Ne^{2+}/H^{+} from the different Paschen and Brackett lines in our sample obtained using the IR-lines method (see subsection 3.1.2). In Table 7 the mean Ne^{2+}/H^{+} values for each objects, calculated from the values listed in Table 6, are compared with those derived by using the T_e-method (see subsection 3.1.1). It must be noted that, $(Ne^{2+}/H^{+})_{IR}$ has higher values than $(Ne^{2+}/H^{+})_{Op.}$ by a factor of about 5. A similar result was obtain for H II regions by Dors et al. (2013), who found Ne^{2+}/H^{+} abundances via IR method are higher than those via the T_e-method by a factor of 4. In Figure 16, the Ne^{2+}/H^{+} abundance values, listed in Table 7, are compared with each other (green points). Also, in this plot the H II region estimations (red points) obtained by Dors et al. (2013) are shown. It can be noted that, the discrepancy in ionic abundances for Seyfert 2 is slightly higher than the one found in H II regions ($\sim$ 0.01 dex higher), even-though there are few outliers (NGC 4388, NGC 5643, NGC 5728, and NGC 1667) which show the highest Ne^{2+}/H^{+} abundances via the IR$-$method, although it must be noted that Dors et al. (2013) also derived such a difference for one of their objects. The averaged differences for AGNs and the one derived for H II regions correspond to factors of 5 and 4 respectively. For H II regions, the abundances derived from collisionally excited lines under the assumption of constant temperature, typically underestimate the abundances relative to hydrogen by a factor of $\sim$0.30 dex in comparison to those derived from recombination lines (see Esteban et al., 2020 and references therein).

Vermeij & van der Hulst (2002) obtained optical (by using the Boller & Chivens spectrograph on the ESO 1.52 meter telescope) and infrared spectra (by using Short Wavelength Spectrometer$-$SWS and Long Wavelength Spectrometer$-$LWS on board the Infrared Space Observatory$-$ISO) of 15 H II regions located in the Magellanic Clouds. From these objects, it was possible to derive the Ne^{2+} ionic abundances via both IR and T_e-method for 13 of them. The difference (D) between these estimations ranges from -0.6 to $+0.6$, thus, for some objects the T_e-method resulted in higher abundances. The averaged value of D was about zero. Obviously, the Vermeij & van der Hulst (2002) is in disagreement with the findings by Dors et al. (2013). In any case, the $12 + \log(Ne^{2+}/H^{+})$ abundances via IR method for our sample are in the range of $\sim$7.30 to $\sim$9.50, while the abundances derived by Vermeij & van der Hulst (2002) for H II regions ranges from 6.6 to 7.8. This comparison indicates that, the Ne^{2+}/H^{+} abundance in Seyfert 2 is higher than those in H II regions, probably due to harder radiation field existent in AGNs. This conclusion, based on abundance determination via IR lines, is free from the uncertainties produced by the T_e-problem existence in AGNs (see Dors et al. 2015, 2020b). Additional

studies about the total abundance of Ne/H is necessary to compare the values in the two object class. It is worth to mention that the total neon abundance in Seyfert 2 is unknown. We infer from Figure 16 that, Ne^{2+}/H^{+} ionic abundances from the NLR of Seyfert 2 nuclei are higher in both optical and infrared as compared to H II regions.

Figure 16 – Bottom panel: Comparison between ionic abundance of the Ne^{2+}/H^{+} derived using Visible−lines and IR−lines methods. Yellow squares represent estimations for the objects presented in this work and black squares are H II region estimations by Dors et al. (2013). Solid line represents equality of the two estimates. Dashed line is the equality line shifted by the average of the differences between the ionic abundances. Top panel: Difference (D = x − y) between the estimations. Black line represents the null difference, while the average difference (< D >) is shown. The hatched area indicates the uncertainty of ±0.1 derived in the abundance estimation.

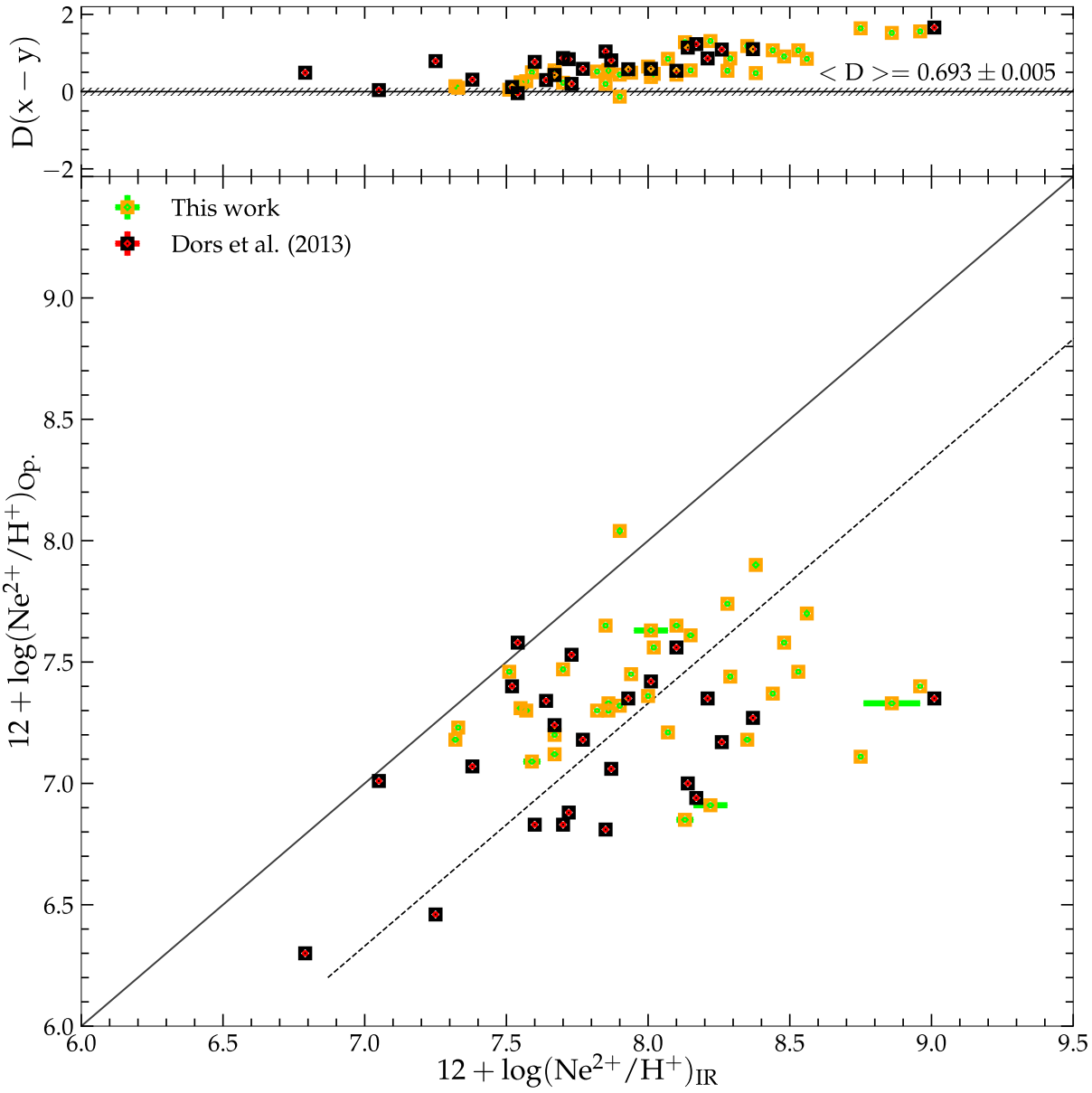

We have observed large uncertainties between the optical and infrared neon ionic estimations with the mix of the Paschen and Brackett series. Separating the Paschen and Brackett series ionic estimations with or without discriminating against the outliers (i.e., NGC 5643, NGC 5728, and NGC 1667), we do not find any significant change in the disparity of electron temperature trend in H II regions and AGNs as shown in Figure 17. We therefore find the use of either only Paschen or only Bracket series or both to be reliable estimations of neon ionic abundance in Seyfert 2 nuclei.

Figure 17 – Bottom panel: Comparison between ionic abundance of the Ne^{2+}/H^{+} derived via IR−lines methods separating the Paschen and Brackett Series. Green and cyan squares represent Paschen or Brackett only estimation, while yellow squares represent estimations for both presented in this work and black squares still remain H II region estimations by Dors et al. (2013). Solid line represents equality of the two estimates. Dashed line is the equality line shifted by the average of the differences between the ionic abundances. Top panel: Difference (D = x − y) between the estimations. Black line represents the null difference, while the average differences (< D >) are shown. The hatched area indicates the uncertainty of ±0.1 derived in abundance estimation.

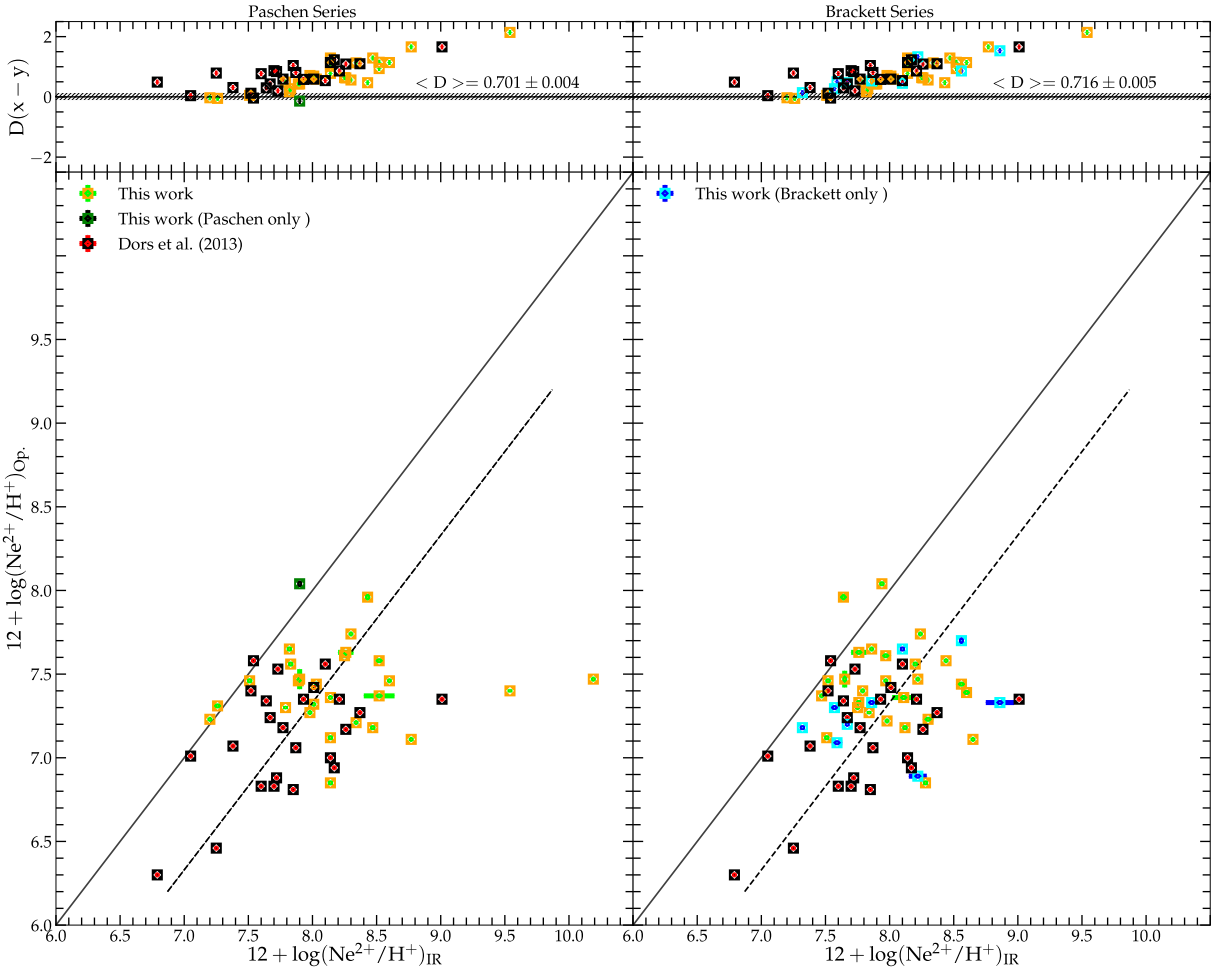

Carvalho et al. (2020) proposed a relation between the logarithm of the ionization parameter (U) and [O III]λ5007Å/[O II]λ3727Å line ratio, to be applied to Seyfert 2 objects. The linear regression obtained is:

$$\log U = (0.57 \pm 0.01\, x^2) + (1.38 \pm 0.01\, x) - (3.14 \pm 0.01), \tag{4.2}$$

where $x = \log([\text{O III}]\lambda5007\text{Å}/[\text{O II}]\lambda3727\text{Å})$. Using the optical line intensities of our sample (see Table 4) and the relation above (Equation 4.2), we derived the U parameter which measures the level of ionization of the gas for the objects in our sample. In Figure 18, the derived U values versus the difference (D) of the ionic neon abundance (see Table 7) are shown. It can be seen from Figure 18 that there is very little dependence of U on temperature fluctuations (if this is the source of D) over the whole range of D.

Figure 18 – Logarithm of the ionization parameter U versus the Ne^{2+}/H^+ abundance difference (D). U values were obtained by using Equation 4.2 obtained by Carvalho et al. (2020) and the optical intensity lines listed in Table 3. The values representing D are listed in Table 7.

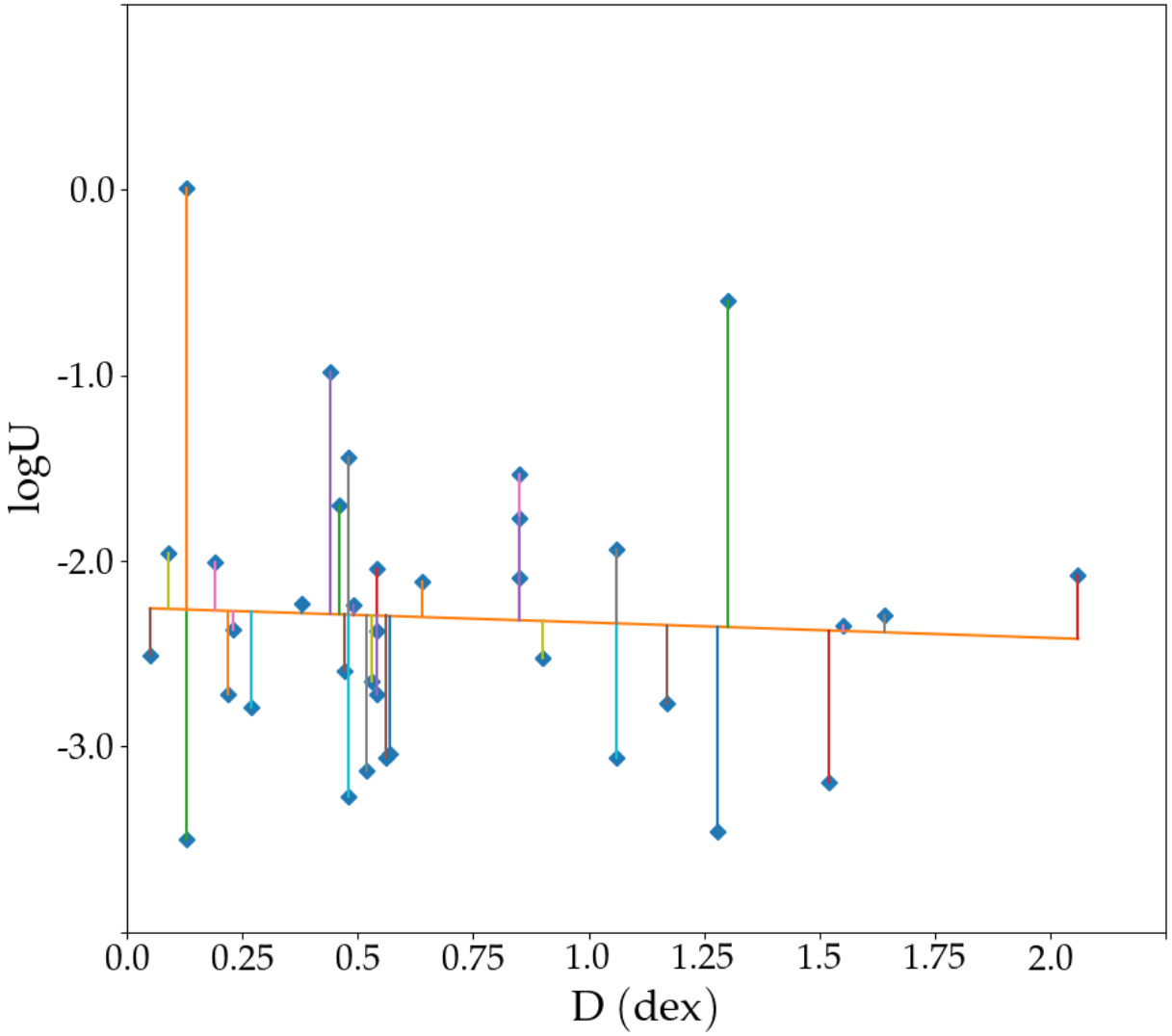

The electron temperatures corresponding to the estimations from optical and infrared Ne^{2+}/H^+ are shown in Figure 19. As usual it is clear from this figure that the high Ne^{2+}/H^+ ionic abundances are derived from lower electron temperatures and vice versa. The temperature fluctuation parameter t^2 has been estimated in this work from T_0 and T_e (see subsection 3.1.3 for details) in the range from 0.0006 to 0.4365 ± 0.0053 with an average value of 0.1859 ± 0.0011.

The t^2 values predicted from photoionization models by CLOUDY CODE for Planetary Nebulae (PNe) and H II regions are in the range from 0.000 to 0.015 with a typical value of about 0.004 (Ferland et al., 2013, 2017). Peimbert, Peña-Guerrero & Peimbert (2012) found $0.019 < t^2 < 0.120$ from 37 galactic and extragalactic H II regions with an average value of 0.044. Peña-Guerrero et al. (2012) also derived the presence of temperature inhomogeneities in two H II regions in the Small Magellanic Cloud (SMC) by comparing the temperature derived using oxygen forbidden lines with the temperature derived using helium recombination lines (RLs) and by comparing the abundances derived from oxygen forbidden lines with those derived from oxygen RLs. These authors derived an averaged $t^2 = 0.067 \pm 0.013$ for NGC 456 and $t^2 = 0.036 \pm 0.027$ for NGC 460. From 5 H II regions in the LMC, Toribio San Cipriano et al. (2017) found $0.028 < t^2 < 0.069$ with an average value of 0.038, and from 4 H II regions in the SMC found that $0.075 < t^2 < 0.107$ with an average value of 0.089.

According to Peimbert (1967) and Peimbert & Costero (1969), a t^2 value of about 0.04 typically results in an underestimation of C/H, O/H, and Ne/H, by about 0.2 to 0.3 dex. It is therefore extremely important to ascertain whether the fluctuations in temperature exist or whether they are an inherent potential errors from the techniques used. If temperature variations exist, it is imperative to better understand their nature and possibly derive some methodology to mitigate or reconcile them in chemical abundance derivations. It is worthy to note that, hitherto, the t^2 values available in the literature are always indirectly based on the comparison of different methods to the estimation of T_e. Only mapping the AGNs with appropriate sensitivity and spatial resolution in the temperature diagnostic lines could give direct evidence of small scale fluctuations. Unfortunately, such studies for AGNs are rare in the literature and the few studies in this direction have found electron temperature to be almost constant along the radius of AGNs, as derived by Revalski et al. (2018a, 2018b).

As previously presented (refer to chapter 2), we used data from different sources to derive the neon ionic abundances, i.e. different aperture in the slit may have been used in the optical and infrared observations which could introduce uncertainties in the results. However, our sample consist of objects in the redshift range ($z < 0.1$) and we found almost the same difference in Ne^{2+} abundances like those derived in the nearby H II regions, for most part located in the Magellanic Clouds. Thus, this indicates that the aperture effect has no influence on our results and that it is possible to have the same level of electron temperature fluctuation in H II regions and AGNs. Peimbert, Peimbert & Delgado-Inglada (2017) expounded the possible sources of temperature inhomogeneities in gaseous nebulae of PNe and H II regions as: presence of shock wave, shadowed regions, spatially distributed ionization sources, density inhomogeneities, time dependent ionization, cosmic rays, over-estimation of the intensity of weak lines, and magnetic re-connection (see also Dors et al., 2020b). However, the origin of the electron temperature fluctuation is an open problem in nebular astrophysics. Observations using future class of giant telescopes (e.g. Giant Magellanic Telescope) and data to be obtained with the James Webb Telescope could reveal clumps of distinct temperature in NLRs of AGNs which could bring more clarity to the problem of abundance discrepancy in AGNs.

Figure 19 – Bottom panel: Comparison between electron temperature (T_e) and the average temperature (T_0). Points represent T_e values estimated from R_{O3} (t_3; see subsection 3.1.1) versus T_0 calculated through the assumption that $(Ne^{2+}/H^+)_{IR}$ is equal to $(Ne^{2+}/H^+)_{Op.}$ (see subsection 3.1.3). Solid line represents the equality between both estimates. Top panel: Difference between these estimations (D=x–y) versus T_e. The solid line represents the zeroth difference between the estimations.

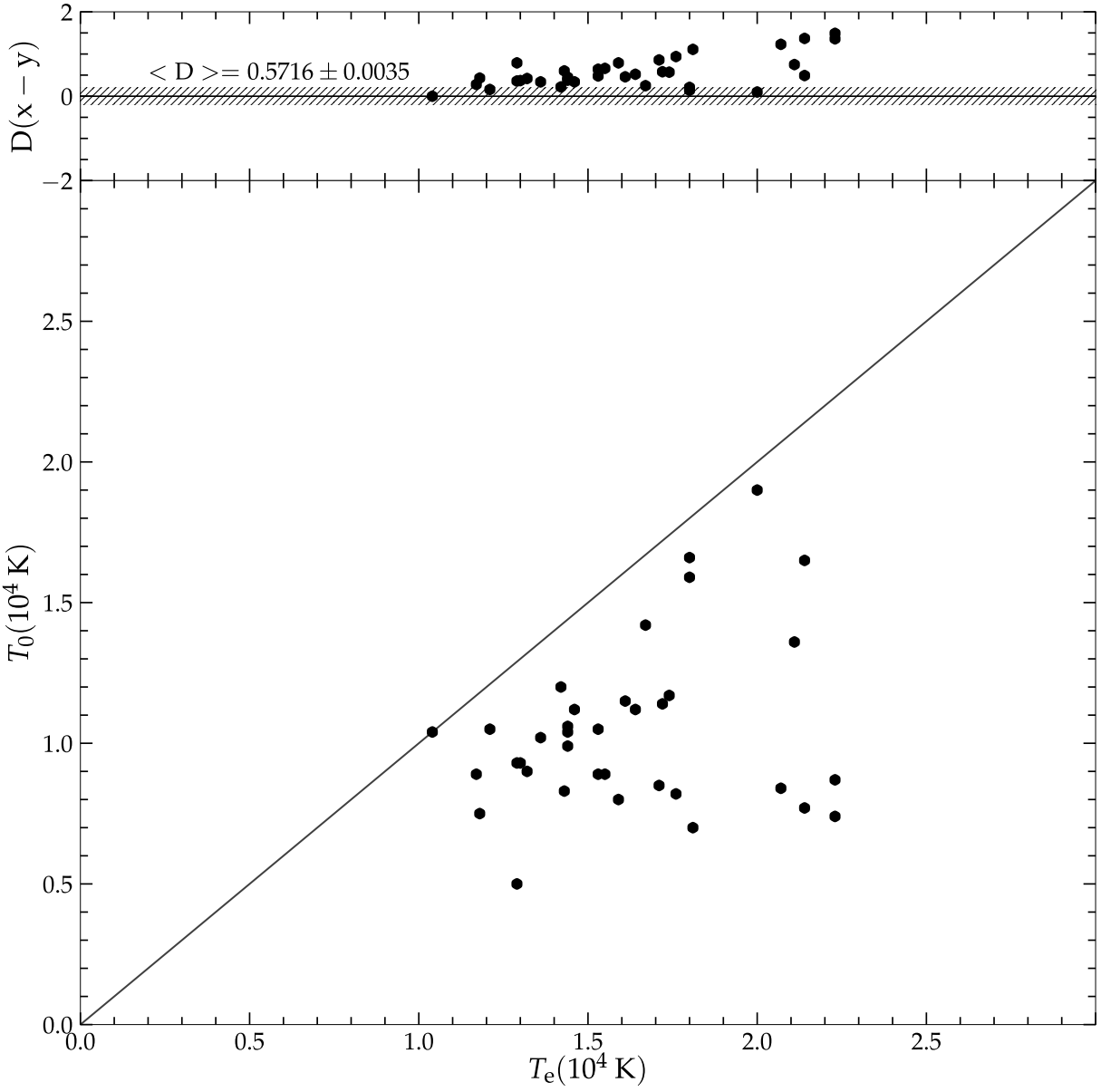

5 Conclusions

We summarize the major findings from the discussions in Chapter 4 in this concluding chapter and then focus on potential implications of study in this field.

5.1 Summary

We compiled from the literature infrared and optical emission lines of 36 Seyfert 2 nuclei located in the local universe (redshift, $z < 0.1$). These emission lines were used to derive the Ne^{2+}/H^{+} ionic abundances through the T_e-method and the IR$-$method. These estimations were compared with each other and we obtained the following conclusions:

1. We investigated the use of the Balmer decrement observed ratio of intensities of the $3 \rightarrow 2$ (Hα λ6563 Å) and $4 \rightarrow 2$ (Hβ λ4861 Å) transitions of the hydrogen atom compared to their intrinsic intensity ratio so as to yield a relative extinction in the Narrow Line Region (NLR) of Seyfert 2 nuclei and find that the use of $I(\mathrm{H}\alpha/\mathrm{H}\beta) = 2.85$ gives T_e values of 700 ± 30 K higher than the T_e values derived from $I(\mathrm{H}\alpha/\mathrm{H}\beta) = 3.1$.

2. We derived Ne^{2+}/H^{+} ionic abundances using optical and IR emission lines emitted from different Paschen and Brackett hydrogen transitions as reference lines. Differences in order of 0.6931 ± 0.0052 dex are derived from the different estimations.

3. The Ne^{2+}/H^{+} ionic fractions obtained using direct optical measurements of the electron temperature are underestimated by a factor of about 5 in comparison with those measured by NIR/MIR emissions lines.

4. The Ne^{2+}/H^{+} abundance differences derived from the comparison between the T_e-method and the IR$-$method estimations are slightly higher than those derived in nearby H II regions ($\sim 0.01 \pm 0.01$ dex higher).

5. We did not find any relation between the ionic abundance difference (D) and the ionization parameter U, therefore, there is very little dependence of U on temperature fluctuations over the whole range of D.

6. The derived Ne^{2+}/H^{+} ionic abundance differences could be interpreted as a result of the presence of electron temperature fluctuations in the NLRs of AGNs. Therefore, we estimate the level of fluctuations in terms of the t^2 parameter in the range from 0.0006 to 0.4365 ± 0.0053 with an average value of 0.1859 ± 0.0011.

7. In view of the root mean square temperature inhomogeneities, we conclude that, if electron temperature fluctuations are present in Seyfert 2 nuclei, they would be somewhat more predominant than in H II regions.

5.2 Future work

While we have made considerable strides, there is so much work to be done. Therefore, we outline a few paths here we believe should be pursued in light of the findings discussed in this study.

1. Determination of the total Ne abundance (Ne/H) of Seyfert 2 nuclei from either optical or IR-method by taking into account the unobserved ions. This can be done in two ways. First, estimation of ionization correction factors (ICFs), which represent the unseen ionization stages of each ion. Since some of the neon ions such as Ne^{+} and Ne^{3+} have not been observed in the optical a significant fraction of Ne likely lies in the Ne^{+} and Ne^{3+} states and it is impossible to obtain a direct contribution from these states to the total neon abundance without ICF. A second way for determining the Ne/H could be done by summing all the observed ionic species of the ionization stages of neon, for instance, looking at the neon abundances in the sample for which every ion from Ne^{+} to Ne^{5+} (highly possible in IR observations) has been measured so that lines representing all important stages of ionization are found, such that no correction for unseen ionization stages needed to be made. The latter approach would be highly reliable than the former because miscalculation of ICF is a potential source of abundance discrepancy.

2. Additionally, it is important to estimate the Ne/O and Ar/O abundance ratios hence Ne and Ar are products of the late stages in the evolution of massive stars. Neon is produced during carbon burning in the final stages of the evolution of massive stars and on the other hand, argon, like sulphur, is produced by oxygen burning and, therefore, neon and argon are expected to track oxygen abundance (O/H) very closely.

3. Finally, we propose to extend this study to the NLR of Seyfert 1 nuclei in the near future by decomposing the superimposed narrow permitted lines from the broad emission lines. Photoionization models can be used to reproduce emission lines from the NLRs of Seyfert 1 nuclei which will be very useful if a good agreement is found by comparison with some observed intensities relative to permitted lines, especially the Balmer lines for the NLRs of Seyfert 1 nuclei.

Bibliography

Adams, T. F. A Survey of the Seyfert Galaxies Based on Large-Scale Image-Tube Plates. ApJS, v. 33, p. 19, Jan. 1977.

Alloin, D.; Pelat, D.; Phillips, M. M.; Fosbury, R. A. E.; Freeman, K. Recurrent Outbursts in the Broad-Line Region of NGC 1566. ApJ, v. 308, p. 23, Sep. 1986.

Alonso-Herrero, A.; Rieke, M. J.; Rieke, G. H.; Shields, J. C. The Nature of LINERS. ApJ, v. 530, n. 2, p. 688–703, Feb. 2000.

Alonso-Herrero, A.; Shastri, P.; Singh, V. An Infrared Test of Seyfert Unification. In: *37th COSPAR Scientific Assembly*. [S.l.: s.n.], 2008. v. 37, p. 69.

Alonso-Herrero, A.; Simpson, C.; Ward, M. J.; Wilson, A. S. A Near-Infrared Imaging Study of Seyfert Galaxies with Extended Emission-Line Regions. ApJ, v. 495, n. 1, p. 196–221, Mar. 1998.

Ambartsumian, V. A. On Multiple Galaxies. *Izvestiya Akademiya Nauk Armyanskoi*, v. 9, p. 23–43, Jan 1956.

_____. On the Evolution of Galaxies. In: *La structure et l'évolution de l'universe*. [S.l.: s.n.], 1958. p. 241–249.

_____. Problems of Extra-Galactic Research. *Transactions of the International Astronomical Union, Series B*, v. 11B, p. 145, Jan 1962.

Antonucci, R. Unified models for active galactic nuclei and quasars. ARA&A, v. 31, p. 473–521, Jan 1993.

_____. A panchromatic review of thermal and nonthermal active galactic nuclei. *Astronomical and Astrophysical Transactions*, v. 27, n. 4, p. 557–602, Jan. 2012.

Antonucci, R. R. J.; Cohen, R. D. Time development of the emission lines and continuum of NGC 4151. ApJ, v. 271, p. 564–574, Aug. 1983.

Antonucci, R. R. J.; Miller, J. S. Spectropolarimetry and the nature of NGC 1068. ApJ, v. 297, p. 621–632, Oct 1985.

Aretxaga, I.; Joguet, B.; Kunth, D.; Melnick, J.; Terlevich, R. J. Seyfert 1 Mutation of the Classical Seyfert 2 Nucleus NGC 7582. ApJ, v. 519, n. 2, p. L123–L126, Jul. 1999.

Arp, H. Atlas of Peculiar Galaxies. ApJS, v. 14, p. 1, Nov. 1966.

Awaki, H.; Koyama, K.; Inoue, H.; Halpern, J. P. X-Ray Implications of a Unified Model of Seyfert Galaxies. PASJ, v. 43, p. 195–212, Apr. 1991.

Baade, W.; Minkowski, R. Identification of the Radio Sources in Cassiopeia, Cygnus A, and Puppis A. ApJ, v. 119, p. 206, Jan 1954.

Badnell, N. R.; Bautista, M. A.; Berrington, K. A.; Burke, V. M.; Butler, K.; Galavís, M. E.; Graziani, M.; Griffin, D. C.; Lennon, D. J.; Mendoza, C.; Mitnik, D. M.; Pelan, J. C.; Pradhan, A. K.; Saraph, H. E.; Storey, P. J.; Tully, J. A.; Zeippen, C. J.; Zhang, H. L. Iron Project: atomic data for IR lines. In: Barlow, M. J.; Méndez, R. H. (Ed.). *Planetary Nebulae in our Galaxy and Beyond*. [S.l.: s.n.], 2006. (IAU Symposium, v. 234), p. 211–218.

Baldwin, J. A.; Phillips, M. M.; Terlevich, R. Classification parameters for the emission-line spectra of extragalactic objects. PASP, v. 93, p. 5–19, Feb 1981.

Barbaro, G.; Mazzei, P.; Morbidelli, L.; Patriarchi, P.; Perinotto, M. Classification and properties of UV extinction curves. A&A, v. 365, p. 157–164, Jan 2001.

Bassani, L.; Dadina, M.; Maiolino, R.; Salvati, M.; Risaliti, G.; Della Ceca, R.; Matt, G.; Zamorani, G. A Three-dimensional Diagnostic Diagram for Seyfert 2 Galaxies: Probing X-Ray Absorption and Compton Thickness. ApJS, v. 121, n. 2, p. 473–482, Apr. 1999.

Beckmann, V.; Shrader, C. R. *Active Galactic Nuclei*. [S.l.]: John Wiley & Sons, 2012.

Begelman, M. C.; Blandford, R. D.; Rees, M. J. Theory of extragalactic radio sources. Rev. Mod. Phys., v. 56, n. 2, p. 255–351, Apr 1984.

Bennert, N.; Jungwiert, B.; Komossa, S.; Haas, M.; Chini, R. Size and properties of the NLR in the Seyfert-2 galaxy <ASTROBJ>NGC 1386</ASTROBJ>. A&A, v. 446, n. 3, p. 919–932, Feb. 2006.

Bennett, A. S. The preparation of the revised 3C catalogue of radio sources. MNRAS, v. 125, p. 75, Jan 1962.

Bergvall, N.; Johansson, L.; Olofsson, K. ESO 428-G14 : a new Seyfert 2 galaxy. A&A, v. 166, p. 92–96, Sep. 1986.

Bianchi, S.; Antonucci, R.; Capetti, A.; Chiaberge, M.; Laor, A.; Bassani, L.; Carrera, F. J.; La Franca, F.; Marinucci, A.; Matt, G.; Middei, R.; Panessa, F. HST unveils a compact mildly relativistic broad-line region in the candidate true type 2 NGC 3147. MNRAS, v. 488, n. 1, p. L1–L5, Sep. 2019.

Bianchi, S.; Corral, A.; Panessa, F.; Barcons, X.; Matt, G.; Bassani, L.; Carrera, F. J.; Jiménez-Bailón, E. NGC 3147: a 'true' type 2 Seyfert galaxy without the broad-line region. MNRAS, v. 385, n. 1, p. 195–199, Mar. 2008.

Bianchi, S.; Guainazzi, M.; Matt, G.; Chiaberge, M.; Iwasawa, K.; Fiore, F.; Maiolino, R. A search for changing-look AGN in the Grossan catalog. A&A, v. 442, n. 1, p. 185–194, Oct. 2005.

Bianchi, S.; Marinucci, A.; Matt, G.; Middei, R.; Barcons, X.; Bassani, L.; Carrera, F. J.; La Franca, F.; Panessa, F. The NuSTAR view of the true type 2 Seyfert NGC 3147. MNRAS, v. 468, n. 3, p. 2740–2744, Jul. 2017.

Bianchi, S.; Panessa, F.; Barcons, X.; Carrera, F. J.; La Franca, F.; Matt, G.; Onori, F.; Wolter, A.; Corral, A.; Monaco, L.; Ruiz, Á.; Brightman, M. Simultaneous X-ray and optical observations of true type 2 Seyfert galaxies. MNRAS, v. 426, n. 4, p. 3225–3240, Nov. 2012.

Binette, L.; Matadamas, R.; Hägele, G. F.; Nicholls, D. C.; Magris C., G.; Peña-Guerrero, M. Á.; Morisset, C.; Rodríguez-González, A. Discrepancies between the [O III] and [S III] temperatures in H II regions. A&A, v. 547, p. A29, Nov. 2012.

Binette, L.; Wilson, A. S.; Raga, A.; Storchi-Bergmann, T. Photoionization of very high excitation gas in the Circinus galaxy and other active galactic nuclei. A&A, v. 327, p. 909–920, Nov. 1997.

Blanco, P. R.; Ward, M. J.; Wright, G. S. Broad infrared line emission from the nuclei of Seyfert 2 galaxies. MNRAS, v. 242, p. 4P–8, Jan. 1990.

Blandford, R. D. Physical processes in active galactic nuclei. In: Blandford, R. D.; Netzer, H.; Woltjer, L.; Courvoisier, T. J. L.; Mayor, M. (Ed.). *Active Galactic Nuclei*. [S.l.: s.n.], 1990. p. 161–275.

Blietz, M.; Cameron, M.; Drapatz, S.; Genzel, R.; Krabbe, A.; van der Werf, P.; Sternberg, A.; Ward, M. Near-Infrared Spectroscopic Imaging of the Circumnuclear Environment of NGC 1068. ApJ, v. 421, p. 92, Jan. 1994.

Boller, T.; Brandt, W. N.; Fink, H. Soft X-ray properties of narrow-line Seyfert 1 galaxies. A&A, v. 305, p. 53, Jan 1996.

Bolton, J. G.; Gardner, F. F.; Mackey, M. B. The Parkes catalogue of radio sources, declination zone -20° to -60°. *Australian Journal of Physics*, v. 17, p. 340, Sep 1964.

Bolton, J. G.; Stanley, G. J. Variable Source of Radio Frequency Radiation in the Constellation of Cygnus. Nature, v. 161, n. 4087, p. 312–313, Feb. 1948.

Bolton, J. G.; Stanley, G. J.; Slee, O. B. Positions of Three Discrete Sources of Galactic Radio-Frequency Radiation. Nature, v. 164, n. 4159, p. 101–102, Jul. 1949.

Bondi, M.; Pérez-Torres, M. A.; Dallacasa, D.; Muxlow, T. W. B. A supernova factory in Mrk 273? MNRAS, v. 361, n. 2, p. 748–752, Aug. 2005.

Braatz, J.; Greenhill, L.; Moran, J.; Wilson, A.; Herrnstein, J. A VLBA Map of the H_2O Maser in the Nucleus of Seyfert 2 Galaxy NGC 1386. In: *American Astronomical Society Meeting Abstracts*. [S.l.: s.n.], 1997. (American Astronomical Society Meeting Abstracts, v. 191), p. 104.02.

Brocklehurst, M. Calculations of level populations for the low levels of hydrogenic ions in gaseous nebulae. MNRAS, v. 153, p. 471, Jan 1971.

Brodie, J.; Willick, J. A.; Bowyer, S.; Henry, J. P. Narrowband Imaging and Spectroscopy Close to the Nucleus of the Seyfert Galaxy NGC 7682. AJ, v. 93, p. 1054, May 1987.

Bryant, J. J.; Hunstead, R. W. An infrared study of Centaurus A $\hat{*}$. MNRAS, v. 308, n. 2, p. 431–446, Sep. 1999.

Buta, R.; Purcell, G. B. NGC 3081: Surface Photometry and Kinematics of a Classic Resonance Ring Barred Galaxy. AJ, v. 115, n. 2, p. 484–501, Feb. 1998.

Butler, K.; Zeippen, C. J. Atomic data from the IRON Project. V. Effective collision strengths for transitions in the ground configuration of oxygen-like ions. A&AS, v. 108, p. 1–8, Nov 1994.

Calabrò, A.; Daddi, E.; Cassata, P.; Onodera, M.; Gobat, R.; Puglisi, A.; Jin, S.; Liu, D.; Amorín, R.; Arimoto, N.; Boquien, M.; Carraro, R.; Elbaz, D.; Ibar, E.; Juneau, S.; Mannucci, F.; Méndez Hernánez, H.; Oliva, E.; Rodighiero, G.; Valentino, F.; Zanella, A. Near-infrared Emission Lines in Starburst Galaxies at 0.5 < z < 0.9: Discovery of a Merger Sequence of Extreme Obscurations. ApJ, v. 862, n. 2, p. L22, Aug. 2018.

Capetti, A.; Axon, D. J.; Macchetto, F.; Sparks, W. B.; Boksenberg, A. Radio Outflows and the Origin of the Narrow-Line Region in Seyfert Galaxies. ApJ, v. 469, p. 554, Oct. 1996.

Cardamone, C. N.; Moran, E. C.; Kay, L. E. "Hidden" Seyfert 2 Galaxies in the Chandra Deep Field North. AJ, v. 134, n. 3, p. 1263–1275, Sep. 2007.

Cardelli, J. A.; Clayton, G. C.; Mathis, J. S. The Relationship between Infrared, Optical, and Ultraviolet Extinction. ApJ, v. 345, p. 245, Oct 1989.

Carilli, C. L.; Barthel, P. D. Cygnus A. A&A Rev., v. 7, n. 1, p. 1–54, Jan. 1996.

Carilli, C. L.; Taylor, G. B. The Extreme Compact Starburst in Markarian 273. ApJ, v. 532, n. 2, p. L95–L99, Apr. 2000.

Carvalho, S. P.; Dors, O. L.; Cardaci, M. V.; Hägele, G. F.; Krabbe, A. C.; Pérez-Montero, E.; Monteiro, A. F.; Armah, M.; Freitas-Lemes, P. Chemical abundances of Seyfert 2 AGNs − II. N2 metallicity calibration based on SDSS. MNRAS, v. 492, n. 4, p. 5675–5683, Mar. 2020.

Castro, C. S.; Dors, O. L.; Cardaci, M. V.; Hägele, G. F. New metallicity calibration for Seyfert 2 galaxies based on the N2O2 index. MNRAS, v. 467, n. 2, p. 1507–1514, May 2017.

Chen, Y.-C.; Hwang, C.-Y. Morphology of Seyfert galaxies. Ap&SS, v. 362, n. 12, p. 230, Dec. 2017.

Cid Fernandes, R.; Storchi-Bergmann, T.; Schmitt, H. R. The Stellar Content of Active Galaxies. MNRAS, v. 297, n. 2, p. 579–616, Jun. 1998.

Cid Fernandes, R.; Terlevich, R. The origin of the blue continuum in type 2 Seyferts: reflection or star-forming tori? MNRAS, v. 272, n. 2, p. 423–441, Jan. 1995.

Claas, W. J. *The composition of the solar atmosphere.* [S.l.]: csa, 1951.

Cohen, M.; Hudson, H. S.; Odell, S. L.; Stein, W. A. A study of the planetary nebulae Abell 30 and Abell 78. MNRAS, v. 181, p. 233, Oct. 1977.

Cohen, R. D. The narrow-line region of intermediate Seyfet galaxies. ApJ, v. 273, p. 489–504, Oct 1983.

Cohen, R. D.; Rudy, R. J.; Puetter, R. C.; Ake, T. B.; Foltz, C. B. Variability of Markarian 1018: Seyfert 1.9 to Seyfert 1. ApJ, v. 311, p. 135, Dec. 1986.

Colina, L.; Arribas, S.; Borne, K. D. Integral Field Spectroscopy of Markarian 273: Mapping High-Velocity Gas Flows and an Off-Nucleus Seyfert 2 Nebula. ApJ, v. 527, n. 1, p. L13–L16, Dec. 1999.

Contini, M. N/O abundance ratios in gamma-ray burst and supernova host galaxies at z < 4. Comparison with AGN, starburst and H II regions. MNRAS, v. 469, n. 3, p. 3125–3140, Aug 2017.

Contini, M.; Aldrovandi, S. M. V. Composite models for the narrow emission line region of active galactic nuclei. I. The infalling filament. A&A, v. 127, p. 15–24, Nov 1983.

Cooke, A. J.; Baldwin, J. A.; Ferland, G. J.; Netzer, H.; Wilson, A. S. The Narrow-Line Region in the Seyfert 2 Galaxy NGC 3393. ApJS, v. 129, n. 2, p. 517–545, Aug. 2000.

Crenshaw, D. M.; Kraemer, S. B.; Bruhweiler, F. C.; Ruiz, J. R. Absorption and Reddening in the Seyfert Galaxy NGC 3227. ApJ, v. 555, n. 2, p. 633–640, Jul. 2001.

Crenshaw, D. M.; Kraemer, S. B.; Turner, T. J.; Collier, S.; Peterson, B. M.; Brandt, W. N.; Clavel, J.; George, I. M.; Horne, K.; Kriss, G. A.; Mathur, S.; Netzer, H.; Pogge, R. W.; Pounds, K. A.; Romano, P.; Shemmer, O.; Wamsteker, W. Reddening, Emission-Line, and Intrinsic Absorption Properties in the Narrow-Line Seyfert 1 Galaxy Arakelian 564. ApJ, v. 566, n. 1, p. 187–194, Feb. 2002.

Curran, S. J. Differences in the dense gas between type 1 and type 2 Seyferts. A&AS, v. 144, p. 271–284, Jun 2000.

Curtis, H. D. Descriptions of 762 Nebulae and Clusters Photographed with the Crossley Reflector. *Publications of Lick Observatory*, v. 13, p. 9–42, Jan 1918.

Cusumano, G.; La Parola, V.; Segreto, A.; Ferrigno, C.; Maselli, A.; Sbarufatti, B.; Romano, P.; Chincarini, G.; Giommi, P.; Masetti, N.; Moretti, A.; Parisi, P.; Tagliaferri, G. The Palermo Swift-BAT hard X-ray catalogue. III. Results after 54 months of sky survey. A&A, v. 524, p. A64, Dec. 2010.

Dasyra, K. M.; Ho, L. C.; Netzer, H.; Combes, F.; Trakhtenbrot, B.; Sturm, E.; Armus, L.; Elbaz, D. A View of the Narrow-line Region in the Infrared: Active Galactic Nuclei with Resolved Fine-structure Lines in the Spitzer Archive. ApJ, v. 740, n. 2, p. 94, Oct. 2011.

Davies, R. I.; Sugai, H.; Ward, M. J. Star formation in the circumnuclear environment of NGC1068. MNRAS, v. 300, n. 2, p. 388–396, Oct. 1998.

De Robertis, M. M.; Dufour, R. J.; Hunt, R. W. A five-level program for ions of astrophysical interest. JRASC, v. 81, p. 195–220, Dec. 1987.

De Robertis, M. M.; Osterbrock, D. E. NGC 1320: A Feeble, High-Ionization Seyfert 2 Galaxy. ApJ, v. 301, p. 98, Feb. 1986.

de Vaucouleurs, G. Nearby Groups of Galaxies. In: _____. *Galaxies and the Universe*. [S.l.: s.n.], 1975. p. 557.

Deo, R. P.; Crenshaw, D. M.; Kraemer, S. B.; Dietrich, M.; Elitzur, M.; Teplitz, H.; Turner, T. J. Spitzer IRS Observations of Seyfert 1.8 and 1.9 Galaxies: A Comparison with Seyfert 1 and Seyfert 2. ApJ, v. 671, n. 1, p. 124–135, Dec. 2007.

Dhawan, V.; Bartel, N.; Rogers, A. E. E.; Krichbaum, T. P.; Witzel, A.; Graham, D. A.; Pauliny-Toth, I. I. K.; Roennaeng, B. O.; Hirabayashi, H.; Inoue, M.; Lawrence, C. R.; Shapiro, I. I.; Burke, B. F.; Booth, R. S.; Readhead, A. C. S.; Morimoto, M.; Johnston, K. J.; Spencer, J. H.; Marcaide, J. M. Further 7 Millimeter VLBI Observations of 3C 84 and Other Sources with 100 Microarcsecond Angular Resolution. ApJ, v. 360, p. L43, Sep. 1990.

Diaz, A. I.; Prieto, M. A.; Wamsteker, W. The optical and UV spectrum of the Seyfert type 2 galaxy NGC 3393. A&A, v. 195, p. 53–59, Apr. 1988.

Díaz, Á. I.; Terlevich, E.; Castellanos, M.; Hägele, G. F. The metal abundance of circumnuclear star-forming regions in early-type spirals. Spectrophotometric observations. MNRAS, v. 382, n. 1, p. 251–269, Nov. 2007.

Dong, X.; Wang, T.; Wang, J.; Yuan, W.; Zhou, H.; Dai, H.; Zhang, K. Broad-line Balmer decrements in blue active galactic nuclei. MNRAS, v. 383, n. 2, p. 581–592, Jan. 2008.

Dopita, M. A. What Physics Drives the Unified Model? In: Terzian, Y.; Khachikian, E.; Weedman, D. (Ed.). *Activity in Galaxies and Related Phenomena*. [S.l.: s.n.], 1999. (IAU Symposium, v. 194), p. 199.

Dopita, M. A.; Shastri, P.; Davies, R.; Kewley, L.; Hampton, E.; Scharwächter, J.; Sutherland, R.; Kharb, P.; Jose, J.; Bhatt, H.; Ramya, S.; Jin, C.; Banfield, J.; Zaw, I.; Juneau, S.; James, B.; Srivastava, S. Probing the Physics of Narrow Line Regions in Active Galaxies. II. The Siding Spring Southern Seyfert Spectroscopic Snapshot Survey (S7). ApJS, v. 217, n. 1, p. 12, Mar 2015.

Dors, O. L.; Cardaci, M. V.; Hägele, G. F.; Rodrigues, I.; Grebel, E. K.; Pilyugin, L. S.; Freitas-Lemes, P.; Krabbe, A. C. On the central abundances of active galactic nuclei and star-forming galaxies. MNRAS, v. 453, n. 4, p. 4102–4111, Nov 2015.

Dors, O. L.; Freitas-Lemes, P.; Amôres, E. B.; Pérez-Montero, E.; Cardaci, M. V.; Hägele, G. F.; Armah, M.; Krabbe, A. C.; Faúndez-Abans, M. Chemical abundances of Seyfert 2 AGNs − I. Comparing oxygen abundances from distinct methods using SDSS. MNRAS, v. 492, n. 1, p. 468–479, Feb 2020a.

Dors, O. L.; Hägele, G. F.; Cardaci, M. V.; Pérez-Montero, E.; Krabbe, Â. C.; Vílchez, J. M.; Sales, D. A.; Riffel, R.; Riffel, R. A. Optical and mid-infrared neon abundance determinations in star-forming regions. MNRAS, v. 432, n. 3, p. 2512–2528, Jul 2013.

Dors, O. L.; Hägele, G. F.; Cardaci, M. V.; Krabbe, A. C. Effective temperature of ionizing stars of extragalactic H II regions. MNRAS, v. 466, n. 1, p. 726–737, Apr. 2017.

Dors, O. L.; Maiolino, R.; Cardaci, M. V.; Hägele, G. F.; Krabbe, A. C.; Pérez-Montero, E.; Armah, M. Chemical abundances of Seyfert 2 AGNs − III. Reducing the oxygen abundance discrepancy. MNRAS, v. 496, n. 3, p. 3209–3221, Jun. 2020b.

Dors, O. L.; Monteiro, A. F.; Cardaci, M. V.; Hägele, G. F.; Krabbe, A. C. Semi-empirical metallicity calibrations based on ultraviolet emission lines of type-2 AGNs. MNRAS, v. 486, n. 4, p. 5853–5866, Jul. 2019.

Dors, O. L.; Perez-Montero, E.; Hagele, G. F.; Cardaci, M. V.; Krabbe, A. C. VizieR Online Data Catalog: Star forming regions sulphur ICFs (Dors+, 2016). *VizieR Online Data Catalog*, p. J/MNRAS/456/4407, Oct. 2016.

Dors, O. L. J.; Riffel, R. A.; Cardaci, M. V.; Hägele, G. F.; Krabbe, Á. C.; Pérez-Montero, E.; Rodrigues, I. X-rays as the dominant excitation mechanism of [Fe II] and H_2 emission lines in active galaxies. MNRAS, v. 422, n. 1, p. 252–260, May 2012.

Downes, D.; Solomon, P. M. Rotating Nuclear Rings and Extreme Starbursts in Ultraluminous Galaxies. ApJ, v. 507, n. 2, p. 615–654, Nov. 1998.

Durret, F. Nuclear and extranuclear ionized gas in nine Seyfert 2 galaxies. A&AS, v. 105, p. 57–66, May 1994.

Edelson, R. A. Broad-Band Properties of the CfA Seyfert Galaxies. I. Radio Properties. ApJ, v. 313, p. 651, Feb 1987.

Edge, D. O.; Shakeshaft, J. R.; McAdam, W. B.; Baldwin, J. E.; Archer, S. A survey of radio sources at a frequency of 159 Mc/s. MmRAS, v. 68, p. 37–60, Jan 1959.

Eilek, J. A. *Cosmic Ray Acceleration of Gas in Active Galactic Nuclei.* Thesis (Doctoral) — THE UNIVERSITY OF BRITISH COLUMBIA (CANADA)., Dec 1975.

Ekers, J. A. The Parkes catalogue of radio sources, declination zone +20 to -90 . *Australian Journal of Physics Astrophysical Supplement*, v. 7, p. 3–75, Jan 1969.

Elitzur, M.; Ho, L. C. On the Disappearance of the Broad-Line Region in Low-Luminosity Active Galactic Nuclei. ApJ, v. 701, n. 2, p. L91–L94, Aug. 2009.

Elvis, M.; Lawrence, A. Hard X-Ray Emission from a Type 2 Seyfert Galaxy (NGC 1068). ApJ, v. 331, p. 161, Aug. 1988.

Epinat, B.; Amram, P.; Marcelin, M.; Balkowski, C.; Daigle, O.; Hernandez, O.; Chemin, L.; Carignan, C.; Gach, J. L.; Balard, P. GHASP: an Hα kinematic survey of spiral and irregular galaxies - VI. New Hα data cubes for 108 galaxies. MNRAS, v. 388, n. 2, p. 500–550, Aug. 2008.

Esteban, C.; Bresolin, F.; García-Rojas, J.; Toribio San Cipriano, L. Carbon, nitrogen, and oxygen abundance gradients in M101 and M31. MNRAS, v. 491, n. 2, p. 2137–2155, Jan. 2020.

Esteban, C.; García-Rojas, J.; Peimbert, M.; Peimbert, A.; Ruiz, M. T.; Rodríguez, M.; Carigi, L. Carbon and Oxygen Galactic Gradients: Observational Values from H II Region Recombination Lines. ApJ, v. 618, n. 2, p. L95–L98, Jan. 2005.

Evans, I. N.; Ford, H. C.; Kinney, A. L.; Antonucci, R. R. J.; Armus, L.; Caganoff, S. HST Imaging of the Inner 3 Arcseconds of NGC 1068 in the Light of [O iii] lambda 5007. ApJ, v. 369, p. L27, Mar. 1991.

Falcke, H.; Wilson, A. S.; Simpson, C. Hubble Space Telescope and VLA Observations of Seyfert 2 Galaxies: The Relationship between Radio Ejecta and the Narrow-Line Region. ApJ, v. 502, n. 1, p. 199–217, Jul 1998.

Falcke, H.; Wilson, A. S.; Simpson, C.; Bower, G. A. Helical Strands in the Jetlike Narrow-Line Region of ESO 428-G14. ApJ, v. 470, p. L31, Oct. 1996.

Fath, E. A. The Spectra of Some Spiral Nebulæ and Globular Star Clusters. PASP, v. 21, n. 126, p. 138–143, Jun 1909.

Feltre, A.; Charlot, S.; Gutkin, J. Nuclear activity versus star formation: emission-line diagnostics at ultraviolet and optical wavelengths. MNRAS, v. 456, n. 3, p. 3354–3374, Mar. 2016.

Ferguson, J. W.; Korista, K. T.; Baldwin, J. A.; Ferland, G. J. Locally Optimally Emitting Clouds and the Narrow Emission Lines in Seyfert Galaxies. ApJ, v. 487, n. 1, p. 122–141, Sep. 1997.

Ferland, G. J.; Chatzikos, M.; Guzmán, F.; Lykins, M. L.; van Hoof, P. A. M.; Williams, R. J. R.; Abel, N. P.; Badnell, N. R.; Keenan, F. P.; Porter, R. L.; Stancil, P. C. The 2017 Release Cloudy. Rev. Mexicana Astron. Astrofis., v. 53, p. 385–438, Oct. 2017.

Ferland, G. J.; Netzer, H. Are there any shock-heated galaxies ? ApJ, v. 264, p. 105–113, Jan 1983.

Ferland, G. J.; Porter, R. L.; van Hoof, P. A. M.; Williams, R. J. R.; Abel, N. P.; Lykins, M. L.; Shaw, G.; Henney, W. J.; Stancil, P. C. The 2013 Release of Cloudy. Rev. Mexicana Astron. Astrofis., v. 49, p. 137–163, Apr. 2013.

Ferruit, P.; Wilson, A. S.; Mulchaey, J. Hubble Space Telescope WFPC2 Imaging of a Sample of Early-Type Seyfert Galaxies. ApJS, v. 128, n. 1, p. 139–169, May 2000.

Ferruit, P.; Wilson, A. S.; Whittle, M.; Simpson, C.; Mulchaey, J. S.; Ferland, G. J. Hubble Space Telescope/Faint Object Spectrograph Spectroscopy of Spatially Resolved Narrow-Line Regions in the Seyfert 2 Galaxies NGC 2110 and NGC 5929. ApJ, v. 523, n. 1, p. 147–162, Sep. 1999.

Flury, S. R.; Moran, E. C. Chemical abundances in active galaxies. MNRAS, v. 496, n. 2, p. 2191–2203, Jun. 2020.

Frank, J.; King, A.; Raine, D. *Accretion power in astrophysics.* [S.l.: s.n.], 1992.

Freeman, K. C.; Karlsson, B.; Lynga, G.; Burrell, J. F.; van Woerden, H.; Goss, W. M.; Mebold, U. A large new galaxy in Circinus. A&A, v. 55, p. 445–458, Mar. 1977.

Galavis, M. E.; Mendoza, C.; Zeippen, C. J. Atomic data from the IRON Project. XXII. Radiative rates for forbidden transitions within the ground configuration of ions in the carbon and oxygen isoelectronic sequences. A&AS, v. 123, p. 159–171, May 1997.

García-Barreto, J. A.; Franco, J.; Carrillo, R.; Venegas, S.; Escalante-Ramírez, B. Spatial Distribution of Ionized Gas in Bright Barred Spiral Galaxies: H&alpha Images. Rev. Mexicana Astron. Astrofis., v. 32, p. 89–130, Oct. 1996.

Gardner, F. F.; Whiteoak, J. B. The Circinus galaxy - A second case of intense nuclear H2O emission. MNRAS, v. 201, p. 13P–15P, Oct. 1982.

Gaskell, C. M. Reddening of the Narrow-Line Regions of Active Galactic Nuclei and the Intrinsic Balmer Decrement II. Astrophys. Lett., v. 24, p. 43, Jan 1984.

_____. The case for cases B and C: intrinsic hydrogen line ratios of the broad-line region of active galactic nuclei, reddenings, and accretion disc sizes. MNRAS, v. 467, n. 1, p. 226–238, May 2017.

Gaskell, C. M.; Ferland, G. J. Theoretical hydrogen-line ratios for the narrow-line regions of active galactic nuclei. PASP, v. 96, p. 393–397, Jun 1984.

Genzel, R.; Lutz, D.; Sturm, E.; Egami, E.; Kunze, D.; Moorwood, A. F. M.; Rigopoulou, D.; Spoon, H. W. W.; Sternberg, A.; Tacconi-Garman, L. E.; Tacconi, L.; Thatte, N. What Powers Ultraluminous IRAS Galaxies? ApJ, v. 498, n. 2, p. 579–605, May 1998.

Gilli, R.; Maiolino, R.; Marconi, A.; Risaliti, G.; Dadina, M.; Weaver, K. A.; Colbert, E. J. M. The variability of the Seyfert galaxy NGC 2992: the case for a revived AGN. A&A, v. 355, p. 485–498, Mar. 2000.

Gimeno, G. N.; Díaz, R. J.; Carranza, G. J. Catalog of Double Nucleus Disk Galaxies. AJ, v. 128, n. 1, p. 62–67, Jul 2004.

Goldader, J. D.; Joseph, R. D.; Doyon, R.; Sand ers, D. B. Spectroscopy of Luminous Infrared Galaxies at 2 Microns. I. The Ultraluminous Galaxies (L IR 2pt>-11.5pt-3pt approximately 10 12 L_{sun}). ApJ, v. 444, p. 97, May 1995.

_____. Spectroscopy of Luminous Infrared Galaxies at 2 Microns. II. Data for Galaxies with $11.2 \lesssim \log(L_{\rm IR}/L_{\odot}) \lesssim 11.9$. ApJS, v. 108, n. 2, p. 449–470, Feb. 1997.

González Delgado, R. M.; Heckman, T.; Leitherer, C.; Meurer, G.; Krolik, J.; Wilson, A. S.; Kinney, A.; Koratkar, A. Ultraviolet-Optical Observations of the Seyfert 2 Galaxies NGC 7130, NGC 5135, and IC 3639: Implications for the Starburst-Active Galactic Nucleus Connection. ApJ, v. 505, n. 1, p. 174–198, Sep. 1998.

Gonzalez Delgado, R. M.; Perez, E. The circumnuclear region in the Seyfert 2 galaxy NGC 5953. MNRAS, v. 281, n. 3, p. 781–798, Aug. 1996.

Goodrich, R. W. Spectropolarimetry and Variability of Seyfert 1.8 and 1.9 Galaxies. ApJ, v. 340, p. 190, May 1989.

_____. Unification of AGN. In: Aretxaga, I.; Kunth, D.; Mújica, R. (Ed.). *Advanced Lectures on the Starburst-AGN*. [S.l.: s.n.], 2001. p. 69.

Goodrich, R. W.; Osterbrock, D. E. MRK 744 and MRK 1066 : two Seyfert galaxies with strong absorption-line spectra. ApJ, v. 269, p. 416–422, Jun 1983.

Goodrich, R. W.; Veilleux, S.; Hill, G. J. Infrared Spectroscopy of Seyfert 2 Galaxies: A Look through the Obscuring Torus? ApJ, v. 422, p. 521, Feb. 1994.

Goulding, A. D.; Alexander, D. M. Towards a complete census of AGN in nearby Galaxies: a large population of optically unidentified AGN. MNRAS, v. 398, n. 3, p. 1165–1193, Sep. 2009.

Gower, J. F. R.; Scott, P. F.; Wills, D. A survey of radio sources in the declination ranges —07° to 20° and 40° to 80°. MmRAS, v. 71, p. 49, Jan 1967.

Greenhill, L. J.; Ellingsen, S. P.; Norris, R. P.; Gough, R. G.; Sinclair, M. W.; Moran, J. M.; Mushotzky, R. Extremely Rapid Variations of Water Maser Emission from the Circinus Galaxy. ApJ, v. 474, n. 2, p. L103–L106, Jan. 1997.

Greenstein, J. L. Red-Shift of the Unusual Radio Source: 3C 48. Nature, v. 197, n. 4872, p. 1041–1042, Mar 1963.

Greenstein, J. L.; Matthews, T. A. Redshift of the Radio Source 3C 48. AJ, v. 68, p. 279, Jan 1963.

Griffin, D. C.; Mitnik, D. M.; Badnell, N. R. Electron-impact excitation of Ne^{+}. *Journal of Physics B Atomic Molecular Physics*, v. 34, n. 22, p. 4401–4415, Nov 2001.

Grupe, D.; Thomas, H. C.; Leighly, K. M. RX J1624.9+7554: a new X-ray transient AGN. A&A, v. 350, p. L31–L34, Oct. 1999.

GU, Q.; MAIOLINO, R.; DULTZIN-HACYAN, D. Nuclear obscuration and scattering in seyfert 2 galaxies. *Astronomy & Astrophysics*, EDP Sciences, v. 366, n. 3, p. 765–770, 2001.

Gu, Q. S.; Huang, J. H.; Su, H. J.; Shang, Z. H. New infrared Seyfert galaxies. A&A, v. 319, p. 92–97, Mar. 1997.

Hägele, G. F.; Díaz, Á. I.; Cardaci, M. V.; Terlevich, E.; Terlevich, R. Kinematics of gas and stars in the circumnuclear star-forming ring of NGC3351. MNRAS, v. 378, n. 1, p. 163–178, Jun. 2007.

_____. On the derivation of dynamical masses of the stellar clusters in the circumnuclear region of NGC2903. MNRAS, v. 396, n. 4, p. 2295–2312, Jul. 2009.

_____. The circumnuclear environment of the peculiar galaxy NGC3310. MNRAS, v. 402, n. 2, p. 1005–1026, Feb. 2010.

Hägele, G. F.; Díaz, Á. I.; Terlevich, E.; Terlevich, R.; Pérez-Montero, E.; Cardaci, M. V. Precision abundance analysis of bright HII galaxies. MNRAS, v. 383, n. 1, p. 209–229, Jan. 2008.

Hägele, G. F.; Díaz, Á. I.; Terlevich, R.; Terlevich, E.; Bosch, G. L.; Cardaci, M. V. Implications of the kinematical structure of circumnuclear star-forming regions on their derived properties. MNRAS, v. 432, n. 1, p. 810–821, Jun. 2013.

Hägele, G. F.; Firpo, V.; Bosch, G.; Díaz, Á. I.; Morrell, N. High-resolution spectroscopy of the blue compact dwarf galaxy Haro 15 - II. Chemodynamics. MNRAS, v. 422, n. 4, p. 3475–3494, Jun. 2012.

Hägele, G. F.; Pérez-Montero, E.; Díaz, Á. I.; Terlevich, E.; Terlevich, R. The temperature and ionization structure of the emitting gas in HII galaxies: implications for the accuracy of abundance determinations. MNRAS, v. 372, n. 1, p. 293–312, Oct. 2006.

Halpern, J. P. *X-ray spectra of active galactic nuclei*. Thesis (Doctoral) — Harvard University, Cambridge, MA., Mar 1982.

Halpern, J. P.; Kay, L. E.; Leighly, K. M. NGC 7582. IAU Circ., v. 7027, p. 2, Oct. 1998.

Halpern, J. P.; Steiner, J. E. Low ionization active galactic nuclei : X-ray or shock heated ? ApJ, v. 269, p. L37–L41, Jun 1983.

Hanbury Brown, R.; Jennison, R. C.; Gupta, M. K. D. Apparent Angular Sizes of Discrete Radio Sources: Observations at Jodrell Bank, Manchester. Nature, v. 170, n. 4338, p. 1061–1063, Dec. 1952.

Haniff, C. A.; Wilson, A. S.; Ward, M. J. High-Resolution Emission-Line Imaging of Seyfert Galaxies. I - Observations. ApJ, v. 334, p. 104, Nov. 1988.

Hazard, C.; Mackey, M. B.; Shimmins, A. J. Investigation of the Radio Source 3C 273 By The Method of Lunar Occultations. Nature, v. 197, n. 4872, p. 1037–1039, Mar 1963.

Heckman, M.; Sancisi, R.; Sullivan W. T., I.; Balick, B. High-resolution mapping of the giant H I envelope of the Seyfert galaxy MKN 348. MNRAS, v. 199, p. 425–433, May 1982.

Heckman, T. M. An optical and radio survey of the nuclei of bright galaxies. Activity in normal galactic nuclei. A&A, v. 500, p. 187–199, Jul 1980.

Heckman, T. M.; Baum, S. A.; van Breugel, W. J. M.; McCarthy, P. Dynamical, Physical, and Chemical Properties of Emission-Line Nebulae in Cooling Flows. ApJ, v. 338, p. 48, Mar. 1989.

Heisler, C. A.; Lumsden, S. L.; Bailey, J. A. Visibility of scattered broad-line emission in Seyfert 2 galaxies. Nature, v. 385, n. 6618, p. 700–702, Feb. 1997.

Henney, W. J. Dust Scattering of Emission Lines in H II Regions. I. Plane-parallel Models and Application to the Orion Nebula (M42). ApJ, v. 503, n. 2, p. 760–779, Aug 1998.

Hey, J. S.; Parsons, S. J.; Phillips, J. W. Fluctuations in Cosmic Radiation at Radio-Frequencies. Nature, v. 158, n. 4007, p. 234, Aug 1946.

Hill, G. J.; Goodrich, R. W.; Depoy, D. L. Observations of Paschen alpha in a Complete Sample of Radio Galaxies. ApJ, v. 462, p. 163, May 1996.

Hiltner, W. A.; Johnson, H. L. The Law of Interstellar Reddening and Absorption. ApJ, v. 124, p. 367, Sep 1956.

Ho, L. C.; Filippenko, A. V.; Sargent, W. L. W. A Reevaluation of the Excitation Mechanism of LINERs. ApJ, v. 417, p. 63, Nov. 1993.

_____. A Search for "Dwarf" Seyfert Nuclei. III. Spectroscopic Parameters and Properties of the Host Galaxies. ApJS, v. 112, n. 2, p. 315–390, Oct. 1997.

Holtzman, J. A.; Faber, S. M.; Shaya, E. J.; Lauer, T. R.; Groth, J.; Hunter, D. A.; Baum, W. A.; Ewald, S. P.; Hester, J. J.; Light, R. M.; Lynds, C. R.; O'Neil E. J., J.; Westphal, J. A. Planetary Camera Observations of NGC 1275: Discovery of a Central Population of Compact Massive Blue Star Clusters. AJ, v. 103, p. 691, Mar. 1992.

Howarth, I. D. LMC and galactic extinction. MNRAS, v. 203, p. 301–304, Apr. 1983.

Hubble, E. P. Extragalactic nebulae. ApJ, v. 64, p. 321–369, Dec. 1926.

Huchra, J.; Burg, R. The Spatial Distribution of Active Galactic Nuclei. I. The Density of Seyfert Galaxies and Liners. ApJ, v. 393, p. 90, Jul 1992.

Humason, M. L. The Emission Spectrum of the Extra-Galactic Nebula N. G. C. 1275. PASP, v. 44, n. 260, p. 267, Aug 1932.

Hummer, D. G.; Storey, P. J. Recombination-line intensities for hydrogenic ions - I. Case B calculations for H I and He II. MNRAS, v. 224, p. 801–820, Feb 1987.

Hutchings, J. B.; Neff, S. G. The Double Nucleus Galactic Merger MKN 463. AJ, v. 97, p. 1306, May 1989.

Imanishi, M.; Alonso-Herrero, A. Near-infrared K-Band Spectroscopic Investigation of Seyfert 2 Nuclei in the CfA and 12 Micron Samples. ApJ, v. 614, n. 1, p. 122–134, Oct. 2004.

Imanishi, M.; Nakagawa, T.; Shirahata, M.; Ohyama, Y.; Onaka, T. AKARI IRC Infrared 2.5-5 μm Spectroscopy of a Large Sample of Luminous Infrared Galaxies. ApJ, v. 721, n. 2, p. 1233–1261, Oct. 2010.

Inglis, M. D.; Brindle, C.; Hough, J. H.; Young, S.; Axon, D. J.; Bailey, J. A.; Ward, W. J. Evidence for an obscured broad-line region in the early-type radio galaxy IC 5063. MNRAS, v. 263, p. 895–902, Aug. 1993.

Ivanov, V. D.; Rieke, G. H.; Groppi, C. E.; Alonso-Herrero, A.; Rieke, M. J.; Engelbracht, C. W. Testing the AGN-Starburst Connection in Seyfert Galaxies. ApJ, v. 545, n. 1, p. 190–204, Dec. 2000.

Iwasawa, K. An X-ray investigation of powerful far-infrared galaxies. MNRAS, v. 302, n. 1, p. 96–110, Jan. 1999.

Iwasawa, K.; Mazzarella, J. M.; Surace, J. A.; Sand ers, D. B.; Armus, L.; Evans, A. S.; Howell, J. H.; Komossa, S.; Petric, A.; Teng, S. H.; U, V.; Veilleux, S. The location of an active nucleus and a shadow of a tidal tail in the ULIRG Mrk 273. A&A, v. 528, p. A137, Apr. 2011.

Iwasawa, K.; U, V.; Mazzarella, J. M.; Medling, A. M.; Sanders, D. B.; Evans, A. S. Testing a double AGN hypothesis for Mrk 273. A&A, v. 611, p. A71, Apr. 2018.

Iyomoto, N.; Makishima, K.; Fukazawa, Y.; Tashiro, M.; Ishisaki, Y. Detection of Strong Fe-K Lines from the Spiral Galaxies NGC 1365 and NGC 1386. PASJ, v. 49, p. 425–434, Aug. 1997.

Izotov, Y. I.; Thuan, T. X.; Lipovetsky, V. A. The Primordial Helium Abundance from a New Sample of Metal-deficient Blue Compact Galaxies. ApJ, v. 435, p. 647, Nov 1994.

JANSKY, K. G. Directional studies of atmospherics at high frequencies. *Proceedings of the Institute of Radio Engineers*, IEEE, v. 20, n. 12, p. 1920–1932, Dec. 1932.

_____. Electrical disturbances apparently of extraterrestrial origin. *Proceedings of the Institute of Radio Engineers*, IEEE, v. 21, n. 10, p. 1387–1398, 1933.

_____. A note on the source of interstellar interference. *Proceedings of the Institute of Radio Engineers*, IEEE, v. 23, n. 10, p. 1158–1163, 1935.

Johnson, H. L.; Morgan, W. W. Fundamental stellar photometry for standards of spectral type on the Revised System of the Yerkes Spectral Atlas. ApJ, v. 117, p. 313, May 1953.

Kaler, J. B. A catalog of relative emission line intensities observed in planetary and diffuse nebulae. ApJS, v. 31, p. 517, Aug. 1976.

Kauffmann, G.; Heckman, T. M.; Tremonti, C.; Brinchmann, J.; Charlot, S.; White, S. D. M.; Ridgway, S. E.; Brinkmann, J.; Fukugita, M.; Hall, P. B.; Ivezić, Ž.; Richards, G. T.; Schneider, D. P. The host galaxies of active galactic nuclei. MNRAS, v. 346, n. 4, p. 1055–1077, Dec. 2003.

Kaufman, V.; Sugar, J. Forbidden Lines in ns^2np^k Ground Configurations and nsnp Excited Configurations of Beryllium through Molybdenum Atoms and Ions. *Journal of Physical and Chemical Reference Data*, v. 15, n. 1, p. 321–426, Jan 1986.

Kawara, K.; Nishida, M.; Phillips, M. M. Brackett alpha and gamma Observations of Starburst and Seyfert Galaxies. ApJ, v. 337, p. 230, Feb. 1989.

Kay, L. E. Blue Spectropolarimetry of Seyfert 2 Galaxies. I. Analysis and Basic Results. ApJ, v. 430, p. 196, Jul. 1994.

Keel, W. C. Inclination effects on the recognition of Seyfert galaxies. AJ, v. 85, p. 198–203, Mar. 1980.

Kellermann, K. I.; Sramek, R.; Schmidt, M.; Shaffer, D. B.; Green, R. VLA Observations of Objects in the Palomar Bright Quasar Survey. AJ, v. 98, p. 1195, Oct 1989.

Kellermann, K. I.; Sramek, R. A.; Schmidt, M.; Green, R. F.; Shaffer, D. B. The Radio Structure of Radio Loud and Quiet Quasars in the Palomar Bright Quasar Survey. AJ, v. 108, p. 1163, Oct 1994.

Kent, S. M.; Sargent, W. L. W. Ionization and excitation mechanisms in the filaments around NGC 1275. ApJ, v. 230, p. 667–680, Jun. 1979.

Kewley, L. J.; Dopita, M. A. Using Strong Lines to Estimate Abundances in Extragalactic H II Regions and Starburst Galaxies. ApJS, v. 142, n. 1, p. 35–52, Sep 2002.

Kewley, L. J.; Dopita, M. A.; Sutherland, R. S.; Heisler, C. A.; Trevena, J. Theoretical Modeling of Starburst Galaxies. ApJ, v. 556, n. 1, p. 121–140, Jul 2001.

Kewley, L. J.; Groves, B.; Kauffmann, G.; Heckman, T. The host galaxies and classification of active galactic nuclei. MNRAS, v. 372, n. 3, p. 961–976, Nov. 2006.

Khachikian, E. Y.; Weedman, D. W. A New Cloud of Hydrogen Emission in a Bright Galactic Nucleus. ApJ, v. 164, p. L109, Mar. 1971.

Khachikyan, É. Y.; Weedman, D. W. A spectroscopic study of luminous galactic nuclei. *Astrophysics*, v. 7, n. 3, p. 231–240, Jul. 1971.

_____. An atlas of Seyfert galaxies. ApJ, v. 192, p. 581–589, Sep. 1974.

Kinney, A. L.; Bohlin, R. C.; Calzetti, D.; Panagia, N.; Wyse, R. F. G. An Atlas of Ultraviolet Spectra of Star-forming Galaxies. ApJS, v. 86, p. 5, May 1993.

Knapen, J. H.; Laine, S.; Yates, J. A.; Robinson, A.; Richards, A. M. S.; Doyon, R.; Nadeau, D. Resolved Structure in the Nuclear Region of the Ultraluminous Infrared Galaxy Markarian 273. ApJ, v. 490, n. 1, p. L29–L32, Nov. 1997.

Kollatschny, W.; Fricke, K. J. IUE observations of multiple nucleus galaxies. In: Rolfe, E. (Ed.). *Fourth European IUE Conference*. [S.l.: s.n.], 1984. (ESA Special Publication, v. 218), p. 91–95.

_____. The group environment of Seyfert galaxies. I. A&A, v. 219, p. 34–52, Jul. 1989.

Komossa, S. Narrow-line Seyfert 1 Galaxies. In: Rev. Mexicana Astron. Astrofis.. [S.l.: s.n.], 2008. (Revista Mexicana de Astronomia y Astrofisica Conference Series, v. 32), p. 86–92.

Korovyakovskii, Y. P.; Petrosyan, A. R.; Saakyan, K. A.; Khachikyan, É. E. Morphology of Nine Galaxies with Ultraviolet Continuum and Double and Multiple Nuclei. *Astrophysics*, v. 17, n. 2, p. 121–128, Apr. 1981.

Koski, A. T. Spectrophotometry of Seyfert 2 galaxies and narrow-line radio galaxies. ApJ, v. 223, p. 56–73, Jul 1978.

Krabbe, A.; Sams B. J., I.; Genzel, R.; Thatte, N.; Prada, F. Near infrared imaging spectroscopy of NGC 1275. A&A, v. 354, p. 439–452, Feb. 2000.

Kraemer, S. B.; Crenshaw, M.; Schmitt, H.; Trippe, M.; Melendez, M.; Fischer, T. Exploring the Inner Narrow-Line Regions of Seyfert Galaxies. In: *American Astronomical Society Meeting Abstracts #215*. [S.l.: s.n.], 2010. (American Astronomical Society Meeting Abstracts, v. 215), p. 433.01.

Kraemer, S. B.; Wu, C.-C.; Crenshaw, D. M.; Harrington, J. P. IUE Spectra and Photoionization Models of the Seyfert 2 Galaxies NGC 7674 and I ZW 92. ApJ, v. 435, p. 171, Nov 1994.

Krolik, J. H.; Begelman, M. C. An X-ray heated wind in NGC 1068. ApJ, v. 308, p. L55–L58, Sep. 1986.

Landt, H.; Bentz, M. C.; Ward, M. J.; Elvis, M.; Peterson, B. M.; Korista, K. T.; Karovska, M. The Near-Infrared Broad Emission Line Region of Active Galactic Nuclei. I. The Observations. ApJS, v. 174, n. 2, p. 282–312, Feb. 2008.

Lawrence, A. Classification of active galaxies and the prospect of a unified phenomenology. PASP, v. 99, p. 309–334, May 1987.

Lester, D. F.; Dinerstein, H. L.; Werner, M. W.; Watson, D. M.; Genzel, R.; Storey, J. W. V. Far-Infrared Measurements of N/O in H II Regions: Evidence for Enhanced CN Process Nucleosynthesis in the Inner Galaxy. ApJ, v. 320, p. 573, Sep. 1987.

Liu, W.; Veilleux, S.; Iwasawa, K.; Rupke, D. S. N.; Teng, S.; U, V.; Tombesi, F.; Sanders, D.; Max, C. E.; Meléndez, M. Elliptical Galaxy in the Making: The Dual Active Galactic Nuclei and Metal-enriched Halo of Mrk 273. ApJ, v. 872, n. 1, p. 39, Feb. 2019.

Liu, X. W.; Luo, S. G.; Barlow, M. J.; Danziger, I. J.; Storey, P. J. Chemical abundances of planetary nebulae from optical recombination lines - III. The Galactic bulge PN M 1-42 and M 2-36. MNRAS, v. 327, n. 1, p. 141–168, Oct 2001.

Lu, K.-X.; Zhao, Y.; Bai, J.-M.; Fan, X.-L. Reddening of the BLR and NLR in AGNs from a systematic analysis of Balmer decrement. MNRAS, v. 483, n. 2, p. 1722–1730, Feb. 2019.

Lumsden, S. L.; Alexander, D. M.; Hough, J. H. Spectropolarimetry of Compton-thin Seyfert 2 galaxies. MNRAS, v. 348, n. 4, p. 1451–1458, Mar. 2004.

Lutz, D.; Maiolino, R.; Moorwood, A. F. M.; Netzer, H.; Wagner, S. J.; Sturm, E.; Genzel, R. Infrared spectroscopy around 4 mu m of Seyfert 2 galaxies: Obscured broad line regions and coronal lines. A&A, v. 396, p. 439–448, Dec. 2002.

Lutz, D.; Veilleux, S.; Genzel, R. Mid-Infrared and Optical Spectroscopy of Ultraluminous Infrared Galaxies: A Comparison. ApJ, v. 517, n. 1, p. L13–L17, May 1999.

Maiolino, R.; Alonso-Herrero, A.; Anders, S.; Quillen, A.; Rieke, M. J.; Rieke, G. H.; Tacconi-Garman, L. E. Discovery of a Nuclear Gas Bar Feeding the Active Nucleus in Circinus. ApJ, v. 531, n. 1, p. 219–231, Mar. 2000.

Maiolino, R.; Krabbe, A.; Thatte, N.; Genzel, R. Seyfert Activity and Nuclear Star Formation in the Circinus Galaxy. ApJ, v. 493, n. 2, p. 650–665, Jan. 1998.

Maiolino, R.; Rieke, G. H. Low-Luminosity and Obscured Seyfert Nuclei in Nearby Galaxies. ApJ, v. 454, p. 95, Nov 1995.

Maiolino, R.; Salvati, M.; Bassani, L.; Dadina, M.; della Ceca, R.; Matt, G.; Risaliti, G.; Zamorani, G. Heavy obscuration in X-ray weak AGNs. A&A, v. 338, p. 781–794, Oct. 1998.

Malaguti, G.; Bassani, L.; Cappi, M.; Comastri, A.; Di Cocco, G.; Fabian, A. C.; Palumbo, G. G. C.; Maccacaro, T.; Maiolino, R.; Blanco, P.; Dadina, M.; dal Fiume, D.; Frontera, F.; Trifoglio, M. BeppoSAX uncovers the hidden Seyfert 1 nucleus in the Seyfert 2 galaxy NGC 2110. A&A, v. 342, p. L41–L44, Feb. 1999.

Malkan, M. A. The reddening of active galactic nuclei. ApJ, v. 264, p. L1–L6, Jan. 1983.

Malkan, M. A.; Gorjian, V.; Tam, R. A Hubble Space Telescope Imaging Survey of Nearby Active Galactic Nuclei. ApJS, v. 117, n. 1, p. 25–88, Jul. 1998.

Malkan, M. A.; Jensen, L. D.; Rodriguez, D. R.; Spinoglio, L.; Rush, B. Emission Line Properties of Seyfert Galaxies in the 12 μm Sample. ApJ, v. 846, n. 2, p. 102, Sep. 2017.

Marconi, A.; Moorwood, A. F. M.; Origlia, L.; Oliva, E. A prominent ionization cone and starburst ring in the nearby Circinus galaxy. *The Messenger*, v. 78, p. 20–24, Dec. 1994.

Markarian, B. E. Galaxies with Ultraviolet Continuum I. Afz, v. 5, p. 443, Jan 1969a.

_____. The galaxies with ultraviolet continuum. II. Afz, v. 5, p. 206–225, Jan 1969b.

_____. Galaxies with ultraviolet continuum. III. Afz, v. 5, p. 286–301, Jan 1969c.

Markarian, B. E.; Lipovetskii, V. A. Galaxies with ultraviolet continuum. IX. Afz, v. 12, p. 657, Nov 1976b.

Markarian, B. E.; Lipovetskii, V. A.; Stepanian, D. A. Galaxies with ultraviolet continuum. X. Afz, v. 13, p. 225–232, May 1977a.

_____. Galaxies with ultraviolet continuum. XII. Afz, v. 15, p. 201–207, Apr 1979.

_____. Galaxies with ultraviolet continuum. XV. Afz, v. 17, p. 619–627, Oct 1981.

Markarian, B. E.; Lipovetskij, V. A. Galaxies with ultraviolet continuum. V. Afz, v. 8, p. 155–164, Jan 1972.

_____. Galaxies with ultraviolet continuum. VI. Afz, v. 9, p. 487–494, Jan 1973.

_____. Galaxies with ultraviolet continuum. VII. Afz, v. 10, p. 185–194, Jan 1974.

_____. Galaxies with ultraviolet continuum. VIII. Afz, v. 12, p. 241–254, May 1976a.

Markarian, B. E.; Lipovetskij, V. A.; Stepanian, J. A. Galaxies with ultraviolet continuum. XI. Afz, v. 13, p. 215–228, May 1977b.

_____. Seyfert Type Objects from 13TH and 14TH Lists of Galaxies with Ultraviolet Continuum. *Astronomicheskij Tsirkulyar*, v. 1134, p. 6, Jan 1980.

Markarian, B. E.; Lipovetsky, V. A. Galaxies with ultraviolet continuum. IV. Afz, v. 7, p. 511–519, Jan 1971.

Marr, J. M.; Backer, D. C.; Wright, M. C. H.; Readhead, A. C. S.; Moore, R. A Fast-moving Knot of Radio Emission in the Active Galaxy NGC 1275. ApJ, v. 337, p. 671, Feb. 1989.

Mathis, J. S. Nebular dust and extinction in ionized nebulae. I - The Balmer decrement. ApJ, v. 267, p. 119–125, Apr 1983.

Mathur, S.; Grupe, D. Black hole growth by accretion. A&A, v. 432, n. 2, p. 463–466, Mar 2005.

Matt, G.; Bianchi, S.; Guainazzi, M.; Barcons, X.; Panessa, F. The Suzaku X-ray spectrum of NGC 3147. Further insights on the best "true" Seyfert 2 galaxy candidate. A&A, v. 540, p. A111, Apr. 2012.

Matt, G.; Fiore, F.; Perola, G. C.; Piro, L.; Fink, H. H.; Grandi, P.; Matsuoka, M.; Oliva, E.; Salvati, M. A reflection-dominated X-ray spectrum discovered by ASCA in the Circinus galaxy. MNRAS, v. 281, n. 4, p. L69–L73, Aug. 1996.

Mauder, W.; Appenzeller, I.; Hofmann, K. H.; Wagner, S. J.; Weigelt, G.; Zeidler, P. Speckle masking observations of the Seyfert galaxy NGC 1386. A&A, v. 264, p. L9–L12, Oct. 1992.

Mayall, N. U. The Spectrum of the Spiral Nebula NGC 4151. PASP, v. 46, n. 271, p. 134, Jun 1934.

_____. The occurrence of [O II]λ3727 in the spectra of extragalactic nebulae. *Lick Observatory Bulletin*, v. 497, p. 33–39, Jan 1939.

Mazzarella, J. M.; Balzano, V. A. A Catalog of Markarian Galaxies. ApJS, v. 62, p. 751, Dec. 1986.

Mazzarella, J. M.; Gaume, R. A.; Aller, H. D.; Hughes, P. A. Multifrequency Observations of the Double-Nucleus Galaxy Markarian 266: Enhanced Synchrotron Emission Induced by a Merger. ApJ, v. 333, p. 168, Oct. 1988.

Mazzarella, J. M.; Gaume, R. A.; Soifer, B. T.; Graham, J. R.; Neugebauer, G.; Matthews, K. The dust enshrouded quasar in the ultraluminous galaxy Markarian 463: radio, near-infrared, and optical imaging. AJ, v. 102, p. 1241–1252, Oct. 1991.

McCready, L. L.; Pawsey, J. L.; Payne-Scott, R. Solar Radiation at Radio Frequencies and Its Relation to Sunspots. *Proceedings of the Royal Society of London Series A*, v. 190, n. 1022, p. 357–375, Aug 1947.

McLaughlin, B. M.; Bell, K. L. Electron collisional excitation of Ne III: ($1s^2 2s^2 2p^4$ $^3P_{2,1,0}$,$^1D_2$,$^1S_0$) fine-structure transitions. *Journal of Physics B Atomic Molecular Physics*, v. 33, n. 4, p. 597–613, Feb 2000.

Mendoza, C. Recent advances in atomic calculations and experiments of interest in the study of planetary nebulae. In: Aller, L. H. (Ed.). *Planetary Nebulae*. [S.l.: s.n.], 1983. (IAU Symposium, v. 103), p. 143–172.

Meurs, E. J. A.; Wilson, A. S. Markarian Seyfert galaxies : Optical and radio luminosity functions and other statistical studies. A&A, v. 136, p. 206–226, Jul 1984.

Miller, B. P.; Brandt, W. N.; Schneider, D. P.; Gibson, R. R.; Steffen, A. T.; Wu, J. X-ray Emission from Optically Selected Radio-intermediate and Radio-loud Quasars. ApJ, v. 726, n. 1, p. 20, Jan. 2011.

Miller, J. S.; Goodrich, B. F. Type 2 Seyfert Galaxies with Obscured Type 1 Regions. In: BAAS. [S.l.: s.n.], 1987. v. 19, p. 695.

Miller, J. S.; Goodrich, R. W. Spectropolarimetry of High-Polarization Seyfert 2 Galaxies and Unified Seyfert Theories. ApJ, v. 355, p. 456, Jun. 1990.

Miller, J. S.; Mathews, W. G. The Recombination Spectrum of the Planetary Nebula NGC 7027. ApJ, v. 172, p. 593, Mar 1972.

Mirabel, I. F.; Laurent, O.; Sanders, D. B.; Sauvage, M.; Tagger, M.; Charmandaris, V.; Vigroux, L.; Gallais, P.; Cesarsky, C.; Block, D. L. A barred spiral at the centre of the giant elliptical radio galaxy Centaurus A. A&A, v. 341, p. 667–674, Jan. 1999.

Mollá, M.; Díaz, A. I. A grid of chemical evolution models as a tool to interpret spiral and irregular galaxies data. MNRAS, v. 358, n. 2, p. 521–543, Apr 2005.

Moorwood, A. F. M.; Baluteau, J. P.; Anderegg, M.; Coron, N.; Biraud, Y.; Fitton, B. Infrared line emission from H II region. III. Airborne observations of S II (18 μm and 33 μm), O III (52 μm and 88 μm), and N III (57 μm) on M 17. ApJ, v. 238, p. 565–576, Jun. 1980.

Moorwood, A. F. M.; Lutz, D.; Oliva, E.; Marconi, A.; Netzer, H.; Genzel, R.; Sturm, E.; de Graauw, T. 2.5-45μm SWS spectroscopy of the Circinus Galaxy. A&A, v. 315, p. L109–L112, Nov. 1996.

Moorwood, A. F. M.; Oliva, E. Infrared spectroscopy of Fe II, H_2, and H line emission in galactic nuclei. A&A, v. 203, p. 278–288, Sep. 1988.

Moorwood, A. F. M.; Salinari, P.; Furniss, I.; Jennings, R. E.; King, K. J. Infrared spectroscopy with a balloon borne Michelson interferometer. II. Observation of O III, O I, and N III fine structure lines in H II regions. A&A, v. 90, n. 3, p. 304–310, Oct. 1980.

Moran, E. C.; Barth, A. J.; Kay, L. E.; Filippenko, A. V. The Frequency of Polarized Broad Emission Lines in Type 2 Seyfert Galaxies. ApJ, v. 540, n. 2, p. L73–L77, Sep. 2000.

Moran, E. C.; Kay, L. E.; Davis, M.; Filippenko, A. V.; Barth, A. J. A Composite Seyfert 2 X-Ray Spectrum: Implications for the Origin of the Cosmic X-Ray Background. ApJ, v. 556, n. 2, p. L75–L78, Aug. 2001.

Morgan, W. W.; Harris, D. L.; Johnson, H. L. Some Characteristics of Color Systems. ApJ, v. 118, p. 92, Jul 1953.

Morganti, R.; Oosterloo, T.; Tsvetanov, Z. A Radio Study of the Seyfert Galaxy IC 5063: Evidence for Fast Gas Outflow. AJ, v. 115, n. 3, p. 915–927, Mar. 1998.

Morganti, R.; Tsvetanov, Z. I.; Gallimore, J.; Allen, M. G. Radio continuum morphology of southern Seyfert galaxies. A&AS, v. 137, p. 457–471, Jun. 1999.

Morris, S.; Ward, M.; Whittle, M.; Wilson, A. S.; Taylor, K. The velocity fields and radio structures of the active galaxies NGC 5643 and NGC 7582. MNRAS, v. 216, p. 193–217, Sep. 1985.

Mulchaey, J. S.; Regan, M. W.; Kundu, A. The Fueling of Nuclear Activity. I. A Near-Infrared Imaging Survey of Seyfert and Normal Galaxies. ApJS, v. 110, n. 2, p. 299–319, Jun. 1997.

Mulchaey, J. S.; Wilson, A. S.; Bower, G. A.; Heckman, T. M.; Krolik, J. H.; Miley, G. K. Hubble Space Telescope Imaging of the Seyfert 2 Galaxy NGC 2110. ApJ, v. 433, p. 625, Oct. 1994.

Murdin, P. *Encyclopedia of Astronomy and Astrophysics*. [S.l.: s.n.], 2003.

Mushotzky, R. F. The X-ray spectrum and time variability of narrow emission line galaxies. ApJ, v. 256, p. 92–102, May 1982.

Nagar, N. M.; Oliva, E.; Marconi, A.; Maiolino, R. NGC 5506 unmasked as a Narrow Line Seyfert 1:. A direct view of the broad line region using near-IR spectroscopy. A&A, v. 391, n. 2, p. L21–L24, Aug. 2002.

Nagar, N. M.; Wilson, A. S. The Relative Orientation of Nuclear Accretion and Galaxy Stellar Disks in Seyfert Galaxies. ApJ, v. 516, n. 1, p. 97–113, May 1999.

Neff, S. G.; de Bruyn, A. G. The compact radio core of MKN 348 : evidence for directed outflow in a type 2 Seyfert galaxy. A&A, v. 128, p. 318–324, Dec. 1983.

Nesvadba, N. P. H.; Lehnert, M. D.; De Breuck, C.; Gilbert, A. M.; van Breugel, W. Evidence for powerful AGN winds at high redshift: dynamics of galactic outflows in radio galaxies during the "Quasar Era". A&A, v. 491, n. 2, p. 407–424, Nov. 2008.

Neugebauer, G.; Morton, D.; Oke, J. B.; Becklin, E.; Daltabuit, E.; Matthews, K.; Persson, S. E.; Smith, A. M.; Soifer, B. T.; Torres-Peimbert, S.; Wynn-Williams, C. G. Recombination spectrum and reddening in NGC 1068. ApJ, v. 238, p. 502–509, Jun. 1980.

Oliva, E.; Marconi, A.; Cimatti, A.; di Serego Alighieri, S. Spectropolarimetry of the Circinus galaxy. A&A, v. 329, p. L21–L24, Jan. 1998.

Oliva, E.; Marconi, A.; Moorwood, A. F. M. Metal abundances and excitation of extranuclear clouds in the Circinus galaxy. A new method for deriving abundances of AGN narrow line clouds. A&A, v. 342, p. 87–100, Feb. 1999.

Oliva, E.; Moorwood, A. F. M. Detection of SI VI 1.962 Microns and New Observations of Infrared H, Fe II, and H_2 Line Emission in the Seyfert Galaxy NGC 1068. ApJ, v. 348, p. L5, Jan. 1990.

Oliva, E.; Origlia, L.; Kotilainen, J. K.; Moorwood, A. F. M. Red supergiants as starburst tracers in galactic nuclei. A&A, v. 301, p. 55, Sep. 1995.

Oliva, E.; Salvati, M.; Moorwood, A. F. M.; Marconi, A. Size and physical conditions of the coronal line region in a nearby Seyfert 2: the Circinus galaxy. A&A, v. 288, p. 457–465, Aug. 1994.

Onori, F.; La Franca, F.; Ricci, F.; Brusa, M.; Sani, E.; Maiolino, R.; Bianchi, S.; Bongiorno, A.; Fiore, F.; Marconi, A.; Vignali, C. Detection of faint broad emission lines in type 2 AGN - I. Near-infrared observations and spectral fitting. MNRAS, v. 464, n. 2, p. 1783–1832, Jan. 2017.

Osterbrock, D. E. Spectrophotometry of Seyfert 1 galaxies. ApJ, v. 215, p. 733–745, Aug. 1977.

_____. Observational Model of the Ionized Gas in Seyfert and Radio-Galaxy Nuclei. *Proceedings of the National Academy of Science*, v. 75, n. 2, p. 540–544, Feb. 1978.

_____. Seyfert galaxies with weak broad H alpha emission lines. ApJ, v. 249, p. 462–470, Oct. 1981.

_____. Active galactic nuclei. QJRAS, v. 25, p. 1–18, Mar. 1984.

_____. *Astrophysics of gaseous nebulae and active galactic nuclei*. [S.l.: s.n.], 1989.

Osterbrock, D. E.; Dahari, O. Spectra of Seyfert galaxies and Seyfert galaxy candidates. ApJ, v. 273, p. 478–488, Oct. 1983.

Osterbrock, D. E.; Ferland, G. J. *Astrophysics of gaseous nebulae and active galactic nuclei*. [S.l.: s.n.], 2006.

Osterbrock, D. E.; Miller, J. S. The Optical Emission-Line Spectrum of Cygnus a. ApJ, v. 197, p. 535–544, May 1975.

Osterbrock, D. E.; Pogge, R. W. The spectra of narrow-line Seyfert 1 galaxies. ApJ, v. 297, p. 166–176, Oct. 1985.

Osterbrock, D. E.; Shaw, R. A. The Relative Number of Seyfert 2 Galaxies. I. Spectra of Emission-Line Galaxies in the Wasilewski Field. ApJ, v. 327, p. 89, Apr 1988.

Osterbrock, D. E.; Shuder, J. M. Emission-line profiles in Seyfert 1 galaxies. ApJS, v. 49, p. 149–174, May 1982.

Padovani, P. Active Galactic Nuclei at all wavelengths and from all angles. *Frontiers in Astronomy and Space Sciences*, v. 4, p. 35, Nov. 2017.

Pagel, B. E. J.; Simonson, E. A.; Terlevich, R. J.; Edmunds, M. G. The primordial helium abundance from observations of extragalactic HII regions. MNRAS, v. 255, p. 325–345, Mar. 1992.

Panessa, F.; Carrera, F. J.; Bianchi, S.; Corral, A.; Gastaldello, F.; Barcons, X.; Bassani, L.; Matt, G.; Monaco, L. Unabsorbed Seyfert 2 galaxies: the case of 'naked' AGN. MNRAS, v. 398, n. 4, p. 1951–1960, Oct. 2009.

Patriarchi, P.; Morbidelli, L.; Perinotto, M.; Barbaro, G. Determination of R_V towards galactic O stars. A&A, v. 372, p. 644–650, Jun 2001.

Payne, C. H. *Stellar Atmospheres; a Contribution to the Observational Study of High Temperature in the Reversing Layers of Stars.* Thesis (Doctoral) — RADCLIFFE COLLEGE., Jan. 1925a.

Payne, C. H. Astrophysical Data Bearing on the Relative Abundance of the Elements. *Proceedings of the National Academy of Science*, v. 11, n. 3, p. 192–198, Mar. 1925b.

Peña-Guerrero, M. A.; Peimbert, A.; Peimbert, M.; Ruiz, M. T. Analysis of Two Small Magellanic Cloud H II Regions Considering Thermal Inhomogeneities: Implications for the Determinations of Extragalactic Chemical Abundances. ApJ, v. 746, n. 2, p. 115, Feb. 2012.

Pedlar, A.; Booler, R. V.; Davies, R. D. An arcsec radio jet in NGC 1275 (Perseus A). MNRAS, v. 203, p. 667–675, May 1983.

Pedlar, A.; Ghataure, H. S.; Davies, R. D.; Harrison, B. A.; Perley, R.; Crane, P. C.; Unger, S. W. The radio structure of NGC 1275. MNRAS, v. 246, p. 477, Oct. 1990.

Peimbert, A.; Peña-Guerrero, M. A.; Peimbert, M. A Classification of H II Regions Based on Oxygen and Helium Lines: The Cases of TOL 2146-391 and TOL 0357-3915. ApJ, v. 753, n. 1, p. 39, Jul. 2012.

Peimbert, M. Temperature Determinations of H II Regions. ApJ, v. 150, p. 825, Dec. 1967.

Peimbert, M.; Costero, R. Chemical Abundances in Galactic H II Regions. *Boletin de los Observatorios Tonantzintla y Tacubaya*, v. 5, p. 3–22, May 1969.

Peimbert, M.; Peimbert, A.; Delgado-Inglada, G. Nebular Spectroscopy: A Guide on H II Regions and Planetary Nebulae. PASP, v. 129, n. 978, p. 082001, Aug. 2017.

Peimbert, M.; Storey, P. J.; Torres-Peimbert, S. The O^{2+}/H^{+} Abundance Ratio in Gaseous Nebulae Derived from Recombination Lines. ApJ, v. 414, p. 626, Sep. 1993.

Penston, M. V.; Perez, E. An evolutionary link between Seyfert I and II galaxies. MNRAS, v. 211, p. 33P–39, Nov. 1984.

Pequignot, D. Photoionization models of low-ionization active nuclei of galaxies : the case of NGC 1052. A&A, v. 131, p. 159–168, Feb 1984.

Pereira-Santaella, M.; Diamond-Stanic, A. M.; Alonso-Herrero, A.; Rieke, G. H. The Mid-infrared High-ionization Lines from Active Galactic Nuclei and Star-forming Galaxies. ApJ, v. 725, n. 2, p. 2270–2280, Dec. 2010.

Perek, L.; Kohoutek, L. *Catalogue of Galactic Planetary Nebulae*. [S.l.: s.n.], 1967.

Perez Garcia, A. M.; Rodriguez Espinosa, J. M.; Santolaya Rey, A. E. The Mid- and Far-Infrared Spectral Energy Distribution of Seyfert Galaxies. ApJ, v. 500, p. 685, Jun. 1998.

Peterson, B. M. *An Introduction to Active Galactic Nuclei*. [S.l.: s.n.], 1997.

Phillips, M. M. The ionized gas in NGC 5128 - Evidence for a shock-heated component. MNRAS, v. 197, p. 659–677, Nov. 1981.

Phillips, M. M.; Charles, P. A.; Baldwin, J. A. Nearby galaxies with Seyfert-like nuclei. ApJ, v. 266, p. 485–501, Mar 1983.

Phillips, M. M.; Frogel, J. A. Infrared and optical properties of the emission-line galaxies NGC 1386 and NGC 1365. ApJ, v. 235, p. 761–768, Feb. 1980.

Pilbratt, G. L.; Riedinger, J. R.; Passvogel, T.; Crone, G.; Doyle, D.; Gageur, U.; Heras, A. M.; Jewell, C.; Metcalfe, L.; Ott, S.; Schmidt, M. Herschel Space Observatory. An ESA facility for far-infrared and submillimetre astronomy. A&A, v. 518, p. L1, Jul. 2010.

Pilkington, J. D. H.; Scott, J. F. A survey of radio sources between declinations 20° and 40°. MmRAS, v. 69, p. 183, Jan 1965.

Pilyugin, L. S.; Lara-López, M. A.; Grebel, E. K.; Kehrig, C.; Zinchenko, I. A.; López-Sánchez, Á. R.; Vílchez, J. M.; Mattsson, L. The metallicity-redshift relations for emission-line SDSS galaxies: examination of the dependence on the star formation rate. MNRAS, v. 432, n. 2, p. 1217–1230, Jun. 2013.

Pogge, R. W. Extended Ionized Gas in the Seyfert 2 Galaxy NGC 4388. ApJ, v. 332, p. 702, Sep. 1988.

_____. The Circumnuclear Environment of Nearby, Noninteracting Seyfert Galaxies. ApJ, v. 345, p. 730, Oct. 1989.

Pogge, R. W.; De Robertis, M. M. Extended Near-Ultraviolet Continuum Emission and the Nature of the Polarized Broad-Line Seyfert 2 Galaxies. ApJ, v. 404, p. 563, Feb. 1993.

_____. Imaging Spectrophotometry of Markarian 573. ApJ, v. 451, p. 585, Oct 1995.

Predehl, P.; Schmitt, J. H. M. M. X-raying the interstellar medium: ROSAT observations of dust scattering halos. A&A, v. 500, p. 459–475, Jan. 1995.

Privon, G. C.; Baum, S. A.; O'Dea, C. P.; Gallimore, J.; Noel-Storr, J.; Axon, D. J.; Robinson, A. Modeling the Infrared Emission in Cygnus A. ApJ, v. 747, n. 1, p. 46, Mar. 2012.

Pronik, I. I.; Merkulova, N. I.; Metik, L. P. UBVRI Observations of the Nucleus of NGC 1275 from 1989 to 1994: Microvariability. AJ, v. 117, n. 5, p. 2141–2151, May 1999.

Puglisi, A.; Daddi, E.; Renzini, A.; Rodighiero, G.; Silverman, J. D.; Kashino, D.; Rodríguez-Muñoz, L.; Mancini, C.; Mainieri, V.; Man, A.; Franceschini, A.; Valentino, F.; Calabrò, A.; Jin, S.; Darvish, B.; Maier, C.; Kartaltepe, J. S.; Sanders, D. B. The Bright and Dark Sides of High-redshift Starburst Galaxies from Herschel and Subaru Observations. ApJ, v. 838, n. 2, p. L18, Apr. 2017.

Quillen, A. C.; Alonso-Herrero, A.; Rieke, M. J.; Rieke, G. H.; Ruiz, M.; Kulkarni, V. NICMOS Imaging of Molecular Hydrogen Emission in Seyfert Galaxies. ApJ, v. 527, n. 2, p. 696–708, Dec. 1999.

Radovich, M.; Rafanelli, P. Spectroscopy of circumnuclear and extranuclear emission line regions in Seyfert galaxies. I. NGC 1667. A&A, v. 306, p. 97, Feb. 1996.

Rakshit, S.; Stalin, C. S.; Chand, H.; Zhang, X.-G. Properties of Narrow line Seyfert 1 galaxies. *Bulletin de la Societe Royale des Sciences de Liege*, v. 87, p. 379–386, Apr 2018.

Ramos Almeida, C.; Alonso-Herrero, A.; Esquej, P.; González-Martín, O.; Riffel, R. A.; García-Bernete, I.; Rodríguez Espinosa, J. M.; Packham, C.; Levenson, N. A.; Roche, P.; Díaz-Santos, T.; Aretxaga, I.; Álvarez, C. A mid-infrared view of the inner parsecs of the Seyfert galaxy Mrk 1066 using CanariCam/GTC. MNRAS, v. 445, n. 2, p. 1130–1143, Dec. 2014.

Ramos Almeida, C.; Martínez González, M. J.; Asensio Ramos, A.; Acosta-Pulido, J. A.; Hönig, S. F.; Alonso-Herrero, A.; Tadhunter, C. N.; González-Martín, O. Upholding the unified model for active galactic nuclei: VLT/FORS2 spectropolarimetry of Seyfert 2 galaxies. MNRAS, v. 461, n. 2, p. 1387–1403, Sep 2016.

Ramos Almeida, C.; Pérez García, A. M.; Acosta-Pulido, J. A. Near-Infrared Spectroscopy of Seyfert Galaxies. Nuclear Activity and Stellar Population. ApJ, v. 694, n. 2, p. 1379–1394, Apr. 2009.

Ramos Almeida, C.; Pérez García, A. M.; Acosta-Pulido, J. A.; González-Martín, O. Unveiling the Narrow-Line Seyfert 1 Nature of Markarian 573 Using Near-Infrared Spectroscopy. ApJ, v. 680, n. 1, p. L17, Jun. 2008.

Reber, G. Cosmic Static. *Proceedings of the IRE*, v. 28, p. 68–70, Feb 1940a.

_____. Notes: Cosmic Static. ApJ, v. 91, p. 621–624, Jun 1940b.

_____. Cosmic Static. ApJ, v. 100, p. 279, Nov 1944.

Rees, M. J. Black Hole Models for Active Galactic Nuclei. ARA&A, v. 22, p. 471–506, Jan. 1984.

Regan, M. W.; Mulchaey, J. S. Using HUBBLE SPACE TELESCOPE Imaging of Nuclear Dust Morphology to Rule Out Bars Fueling Seyfert Nuclei. AJ, v. 117, n. 6, p. 2676–2694, Jun 1999.

Reunanen, J.; Kotilainen, J. K.; Prieto, M. A. Near-infrared spectroscopy of nearby Seyfert galaxies - I. First results. MNRAS, v. 331, n. 1, p. 154–168, Mar. 2002.

_____. Near-infrared spectroscopy of nearby Seyfert galaxies - II. Molecular content and coronal emission. MNRAS, v. 343, n. 1, p. 192–208, Jul 2003.

Revalski, M.; Crenshaw, D. M.; Kraemer, S. B.; Fischer, T. C.; Schmitt, H. R.; Machuca, C. Quantifying Feedback from Narrow Line Region Outflows in Nearby Active Galaxies. I. Spatially Resolved Mass Outflow Rates for the Seyfert 2 Galaxy Markarian 573. ApJ, v. 856, n. 1, p. 46, Mar. 2018a.

Revalski, M.; Dashtamirova, D.; Crenshaw, D. M.; Kraemer, S. B.; Fischer, T. C.; Schmitt, H. R.; Gnilka, C. L.; Schmidt, J.; Elvis, M.; Fabbiano, G.; Storchi-Bergmann, T.; Maksym, W. P.; Gandhi, P. Quantifying Feedback from Narrow Line Region Outflows in Nearby Active Galaxies. II. Spatially Resolved Mass Outflow Rates for the QSO2 Markarian 34. ApJ, v. 867, n. 2, p. 88, Nov. 2018b.

Riffel, R.; Rodríguez-Ardila, A.; Pastoriza, M. G. A 0.8-2.4 μm spectral atlas of active galactic nuclei. A&A, v. 457, n. 1, p. 61–70, Oct 2006.

Risaliti, G.; Bassani, L.; Comastri, A.; Dadina, M.; Della Ceca, R.; Gilli, R.; Maiolino, R.; Matt, G.; Salvati, M.; Zamorani, G. X-ray observations of Seyfert 2 galaxies: N_H distribution and the X ray background. Mem. Soc. Astron. Italiana, v. 70, p. 73–76, Jan. 1999.

Rix, H.-W.; Carleton, N. P.; Rieke, G.; Rieke, M. Probing Intermediate Seyfert Galaxies by PA beta Spectroscopy. ApJ, v. 363, p. 480, Nov. 1990.

Rodríguez-Ardila, A.; Riffel, R.; Pastoriza, M. G. Molecular hydrogen and [FeII] in active galactic nuclei - II. Results for Seyfert 2 galaxies. MNRAS, v. 364, n. 3, p. 1041–1053, Dec. 2005.

Rotaciuc, V.; Krabbe, A.; Cameron, M.; Drapatz, S.; Genzel, R.; Sternberg, A.; Storey, J. W. V. High-Resolution Imaging of Brackett- gamma and H 2 1–0 S(1) Emission in the Seyfert Galaxy NGC 1068. ApJ, v. 370, p. L23, Mar. 1991.

Rothschild, R. E.; Baity, W. A.; Marscher, A. P.; Wheaton, W. A. Nonthermal hard X-ray emission from the nucleus of NGC 1275. ApJ, v. 243, p. L9–L12, Jan. 1981.

Rowan-Robinson, M. On the unity of activity in galaxies. ApJ, v. 213, p. 635–647, May 1977.

Rubin, R. H.; Simpson, J. P.; Erickson, E. F.; Haas, M. R. Determination of N/O from Far-Infrared Line Observations of Galactic H II Regions. ApJ, v. 327, p. 377, Apr. 1988.

Ruiz, M.; Rieke, G. H.; Schmidt, G. D. New Infrared Observations of Seyfert 2 Galaxies and Unification Theories. ApJ, v. 423, p. 608, Mar. 1994.

Salpeter, E. E. Accretion of Interstellar Matter by Massive Objects. ApJ, v. 140, p. 796–800, Aug 1964.

Sandage, A. The Existence of a Major New Constituent of the Universe: the Quasistellar Galaxies. ApJ, v. 141, p. 1560, May 1965.

Sanders, D. B.; Soifer, B. T.; Elias, J. H.; Madore, B. F.; Matthews, K.; Neugebauer, G.; Scoville, N. Z. Ultraluminous Infrared Galaxies and the Origin of Quasars. ApJ, v. 325, p. 74, Feb. 1988.

Sanders, R. L.; Shapley, A. E.; Kriek, M.; Reddy, N. A.; Freeman, W. R.; Coil, A. L.; Siana, B.; Mobasher, B.; Shivaei, I.; Price, S. H.; de Groot, L. The MOSDEF Survey: Detection of [O III] λ4363 and the Direct-method Oxygen Abundance of a Star-forming Galaxy at z = 3.08. ApJ, v. 825, n. 2, p. L23, Jul. 2016.

Sanders, R. L.; Shapley, A. E.; Reddy, N. A.; Kriek, M.; Siana, B.; Coil, A. L.; Mobasher, B.; Shivaei, I.; Freeman, W. R.; Azadi, M.; Price, S. H.; Leung, G.; Fetherolf, T.; de Groot, L.; Zick, T.; Fornasini, F. M.; Barro, G. The MOSDEF survey: direct-method metallicities and ISM conditions at z $\sim$ 1.5-3.5. MNRAS, v. 491, n. 1, p. 1427–1455, Jan. 2020.

Saraph, H. E.; Tully, J. A. Atomic data from the IRON project. IV. Electron excitation of the $\hat{2}\hat{P}\hat{0}\_^{\wedge}3/2\_$-$\hat{2}\hat{P}\hat{0}\_^{\wedge}1/2\_$ fine structure transition in fluorine-like ions. A&AS, v. 107, p. 29–38, Oct 1994.

Savage, B. D.; Mathis, J. S. Observed properties of interstellar dust. ARA&A, v. 17, p. 73–111, Jan 1979.

Schawinski, K.; Thomas, D.; Sarzi, M.; Maraston, C.; Kaviraj, S.; Joo, S.-J.; Yi, S. K.; Silk, J. Observational evidence for AGN feedback in early-type galaxies. MNRAS, v. 382, n. 4, p. 1415–1431, Dec. 2007.

Schmidt, M. The variation of the total brightness of comets with heliocentric distance. Bull. Astron. Inst. Netherlands, v. 11, p. 253, Jan 1951.

_____. 3C 273 : A Star-Like Object with Large Red-Shift. Nature, v. 197, n. 4872, p. 1040, Mar 1963.

Schmitt, H. R.; Antonucci, R. R. J.; Ulvestad, J. S.; Kinney, A. L.; Clarke, C. J.; Pringle, J. E. Testing the Unified Model with an Infrared-selected Sample of Seyfert Galaxies. ApJ, v. 555, n. 2, p. 663–672, Jul 2001.

Schmitt, H. R.; Donley, J. L.; Antonucci, R. R. J.; Hutchings, J. B.; Kinney, A. L. A Hubble Space Telescope Survey of Extended [O III] λ5007 Emission in a Far-Infrared Selected Sample of Seyfert Galaxies: Observations. ApJS, v. 148, n. 2, p. 327–352, Oct. 2003.

Schmitt, H. R.; Kinney, A. L. A Comparison between the Narrow-Line Regions of Seyfert 1 and Seyfert 2 Galaxies. ApJ, v. 463, p. 498, Jun 1996.

Schmitt, H. R.; Kinney, A. L.; Storchi-Bergmann, T.; Antonucci; Robert. A Comparison of Radio Axis with Host Galaxy Plane Axis in Seyfert Galaxies. ApJ, v. 477, n. 2, p. 623–630, Mar. 1997.

Schmitt, H. R.; Storchi-Bergmann, T.; Baldwin, J. A. Anisotropic High-Excitation Emission and Chemical Abundances in the Seyfert 2 Galaxy NGC 5643. ApJ, v. 423, p. 237, Mar. 1994.

Scoville, N. Z.; Evans, A. S.; Thompson, R.; Rieke, M.; Hines, D. C.; Low, F. J.; Dinshaw, N.; Surace, J. A.; Armus, L. NICMOS Imaging of Infrared-Luminous Galaxies. AJ, v. 119, n. 3, p. 991–1061, Mar. 2000.

Scoville, N. Z.; Matthews, K.; Carico, D. P.; Sand ers, D. B. The Stellar Bar in NGC 1068. ApJ, v. 327, p. L61, Apr. 1988.

Seyfert, C. K. Nuclear Emission in Spiral Nebulae. ApJ, v. 97, p. 28, Jan 1943.

Shaw, R. A.; Dufour, R. J. Software for the Analysis of Emission Line Nebulae. PASP, v. 107, p. 896, Sep. 1995.

Shi, Y.; Rieke, G. H.; Smith, P.; Rigby, J.; Hines, D.; Donley, J.; Schmidt, G.; Diamond-Stanic, A. M. Unobscured Type 2 Active Galactic Nuclei. ApJ, v. 714, n. 1, p. 115–129, May 2010.

Shields, G. A.; Oke, J. B. The emission-line spectrum of NGC 1068. ApJ, v. 197, p. 5–16, Apr 1975.

_____. The spectral energy distribution of NGC 1275. PASP, v. 87, p. 879–883, Dec. 1975.

Shields, J. C.; Filippenko, A. V. Extended Broad-Line Emission in the Obscured Seyfert 1 Nucleus of NGC 4388. ApJ, v. 332, p. L55, Sep. 1988.

_____. Emission-Line Properties of the Composite Seyfert/Starburst Galaxy IC 5135. AJ, v. 100, p. 1034, Oct. 1990.

Shu, X. W.; Wang, J. X.; Jiang, P.; Fan, L. L.; Wang, T. G. Investigating the Nuclear Obscuration in Two Types of Seyfert 2 Galaxies. ApJ, v. 657, n. 1, p. 167–176, Mar. 2007.

Shuder, J. M. The optical spectra of narrow-line X-ray galaxies. ApJ, v. 240, p. 32–40, Aug. 1980.

Shuder, J. M.; Osterbrock, D. E. Empirical results from a study of active galactic nuclei. ApJ, v. 250, p. 55–65, Nov. 1981.

Simkin, S. M.; van Gorkom, J.; Hibbard, J.; Su, H.-J. Markarian 348: A Tidally Disturbed Seyfert Galaxy. *Science*, v. 235, n. 4794, p. 1367–1370, Mar. 1987.

Simpson, J. P. Infrared forbidden lines in H II regions and planetary nebulae. A&A, v. 39, p. 43–60, Feb 1975.

Singh, V.; Shastri, P.; Risaliti, G. Measuring the level of nuclear activity in Seyfert galaxies and the unification scheme. A&A, v. 533, p. A128, Sep. 2011.

Slipher, V. M. The spectrum and velocity of the nebula N.G.C. 1068 (M 77). *Lowell Observatory Bulletin*, v. 3, p. 59–62, Jan 1917.

Sosa-Brito, R. M.; Tacconi-Garman, L. E.; Lehnert, M. D.; Gallimore, J. F. Integral Field Near-Infrared Spectroscopy of a Sample of Seyfert and LINER Galaxies. I. The Data. ApJS, v. 136, n. 1, p. 61–98, Sep. 2001.

Sparks, W. B.; Hough, J. H.; Axon, D. J.; Bailey, J. Infrared photometry of the nuclei of early-type radio galaxies. MNRAS, v. 218, p. 429–444, Feb. 1986.

Spinoglio, L.; Fernández-Ontiveros, J. A. AGN types and unification model. *arXiv e-prints*, p. arXiv:1911.12176, Nov. 2019.

Stasińska, G. The Electron Temperature in Ionized Nebulae. In: Henney, W. J.; Franco, J.; Martos, M. (Ed.). Rev. Mexicana Astron. Astrofis.. [S.l.: s.n.], 2002. (Revista Mexicana de Astronomia y Astrofisica Conference Series, v. 12), p. 62–69.

_____. Abundance determinations in H II regions and planetary nebulae. In: Esteban, C.; García López, R.; Herrero, A.; Sánchez, F. (Ed.). *Cosmochemistry. The melting pot of the elements*. [S.l.: s.n.], 2004. p. 115–170.

Stasińska, G.; Tylenda, R.; Acker, A.; Stenholm, B. Comparison of two methods for determining the interstellar extinction of planetary nebulae. A&A, v. 266, p. 486–500, Dec 1992.

Stockton, A.; Ridgway, S. E.; Lilly, S. J. Continuum and Line Emission in Cygnus A. AJ, v. 108, p. 414, Aug. 1994.

Storchi-Bergmann, T.; Bonatto, C. J. Detection of an [O III] λ5007 radiation in the nuclei of NGC 1365. MNRAS, v. 250, p. 138, May 1991.

Storchi-Bergmann, T.; Schmitt, H. R.; Calzetti, D.; Kinney, A. L. Chemical Abundance Calibrations for the Narrow-Line Region of Active Galaxies. AJ, v. 115, n. 3, p. 909–914, Mar 1998.

Storchi-Bergmann, T.; Wilson, A. S.; Baldwin, J. A. The Ionization Cone, Obscured Nucleus, and Gaseous Outflow in NGC 3281: A Prototypical Seyfert 2 Galaxy? ApJ, v. 396, p. 45, Sep. 1992.

Storchi-Bergmann, T.; Winge, C.; Ward, M. J.; Wilson, A. S. Extended gas in Seyfert galaxies: near-infrared observations of NGC 2110 and Circinus. MNRAS, v. 304, n. 1, p. 35–46, Mar. 1999.

Storey, P. J.; Zeippen, C. J. Theoretical values for the [O III] 5007/4959 line-intensity ratio and homologous cases. MNRAS, v. 312, n. 4, p. 813–816, Mar. 2000.

Sturm, E.; Lutz, D.; Verma, A.; Netzer, H.; Sternberg, A.; Moorwood, A. F. M.; Oliva, E.; Genzel, R. Mid-Infrared line diagnostics of active galaxies. A spectroscopic AGN survey with ISO-SWS. A&A, v. 393, p. 821–841, Oct. 2002.

Tadhunter, C. An introduction to active galactic nuclei: Classification and unification. New A Rev., v. 52, n. 6, p. 227–239, Aug 2008.

Tajer, M.; Trinchieri, G.; Wolter, A.; Campana, S.; Moretti, A.; Tagliaferri, G. A sample of X-ray emitting normal galaxies from the BMW-HRI Catalogue. A&A, v. 435, n. 3, p. 799–810, Jun. 2005.

TASOFF, H. *An Identity Problem*. 2019. Available at: <https://www.news.ucsb.edu-/2019/019572/identity-problem>.

Thatte, N.; Quirrenbach, A.; Genzel, R.; Maiolino, R.; Tecza, M. The Nuclear Stellar Core, the Hot Dust Source, and the Location of the Nucleus of NGC 1068. ApJ, v. 490, n. 1, p. 238–246, Nov. 1997.

Thomas, A. D.; Dopita, M. A.; Shastri, P.; Davies, R.; Hampton, E.; Kewley, L.; Banfield, J.; Groves, B.; James, B. L.; Jin, C.; Juneau, S.; Kharb, P.; Sairam, L.; Scharwächter, J.; Shalima, P.; Sundar, M. N.; Sutherland, R.; Zaw, I. Probing the Physics of Narrow-line Regions in Active Galaxies. IV. Full Data Release of the Siding Spring Southern Seyfert Spectroscopic Snapshot Survey (S7). ApJS, v. 232, n. 1, p. 11, Sep. 2017.

Thuan, T. X. Ultraviolet observations of starburst and mini-Seyfert galactic nuclei. ApJ, v. 281, p. 126–134, Jun. 1984.

Tommasin, S.; Spinoglio, L.; Malkan, M. A.; Fazio, G. Spitzer-IRS High-Resolution Spectroscopy of the 12 μm Seyfert Galaxies. II. Results for the Complete Data Set. ApJ, v. 709, n. 2, p. 1257–1283, Feb. 2010.

Toribio San Cipriano, L.; Domínguez-Guzmán, G.; Esteban, C.; García-Rojas, J.; Mesa-Delgado, A.; Bresolin, F.; Rodríguez, M.; Simón-Díaz, S. Carbon and oxygen in H II regions of the Magellanic Clouds: abundance discrepancy and chemical evolution. MNRAS, v. 467, n. 3, p. 3759–3774, May 2017.

Tran, H. D. The Nature of Seyfert 2 Galaxies with Obscured Broad-Line Regions. I. Observations. ApJ, v. 440, p. 565, Feb 1995.

_____. The Nature of Seyfert 2 Galaxies with Obscured Broad-Line Regions. I. Observations. ApJ, v. 440, p. 565, Feb. 1995.

_____. Hidden Broad-Line Seyfert 2 Galaxies in the CFA and 12 μM Samples. ApJ, v. 554, n. 1, p. L19–L23, Jun. 2001.

_____. The Unified Model and Evolution of Active Galaxies: Implications from a Spectropolarimetric Study. ApJ, v. 583, n. 2, p. 632–648, Feb. 2003.

Tran, H. D.; Lyke, J. E.; Mader, J. A. Indecent Exposure in Seyfert 2 Galaxies: A Close Look. ApJ, v. 726, n. 2, p. L21, Jan. 2011.

Tran, H. D.; Osterbrock, D. E.; Martel, A. Extreme Spectral Variations of the Seyfert Galaxy Markarian 993. AJ, v. 104, p. 2072, Dec. 1992.

Tremonti, C. A.; Uomoto, A.; Antonucci, R. R. J.; Tsvetanov, Z. I.; Ford, H. C.; Kriss, G. A. Discovery of the Hidden Seyfert 1 Nucleus in Markarian 463. In: *American Astronomical Society Meeting Abstracts*. [S.l.: s.n.], 1996. (American Astronomical Society Meeting Abstracts, v. 189), p. 11.05.

Trippe, M.; Crenshaw, D.; Kraemer, S.; Turner, T. The Distribution of X-ray Column Densities in Seyfert 1.8 and 1.9 Galaxies. In: *AAS/High Energy Astrophysics Division #11*. [S.l.: s.n.], 2010. (AAS/High Energy Astrophysics Division), p. 8.06.

Tsamis, Y. G.; Barlow, M. J.; Liu, X. W.; Danziger, I. J.; Storey, P. J. Heavy elements in Galactic and Magellanic Cloud H II regions: recombination-line versus forbidden-line abundances. MNRAS, v. 338, n. 3, p. 687–710, Jan. 2003.

Turner, T. J.; Perola, G. C.; Fiore, F.; Matt, G.; George, I. M.; Piro, L.; Bassani, L. BeppoSAX Observation of NGC 7582: Constraints on the X-Ray Absorber. ApJ, v. 531, n. 1, p. 245–256, Mar. 2000.

U, V.; Medling, A.; Sanders, D.; Max, C.; Armus, L.; Iwasawa, K.; Evans, A.; Kewley, L.; Fazio, G. The Inner Kiloparsec of Mrk 273 with Keck Adaptive Optics. ApJ, v. 775, n. 2, p. 115, Oct. 2013.

Ulvestad, J. S.; Wilson, A. S. The nuclear radio source of the X-ray galaxy NGC 2110. ApJ, v. 264, p. L7–L11, Jan. 1983.

_____. Radio structures of Seyfert galaxies. V. A flux-limited sample of Markarian galaxies. ApJ, v. 278, p. 544–557, Mar. 1984.

_____. Radio structures of Seyfert galaxies. VI. VLA observations of a nearby sample. ApJ, v. 285, p. 439–452, Oct. 1984.

Uomoto, A.; Caganoff, S.; Ford, H. C.; Rosenblatt, E. I.; Antonucci, R. R. J.; Evans, I. N.; Cohen, R. D. The Optical Jet in Markarian 463. AJ, v. 105, p. 1308, Apr. 1993.

Urry, C. M.; Padovani, P. Unified Schemes for Radio-Loud Active Galactic Nuclei. PASP, v. 107, n. 715, p. 803, Sep. 1995.

_____. The Unification of Radio-Loud AGN. In: Ekers, R. D.; Fanti, C.; Padrielli, L. (Ed.). *Extragalactic Radio Sources*. [S.l.: s.n.], 1996. (IAU Symposium, v. 175), p. 379.

Vaceli, M. S.; Viegas, S. M.; Gruenwald, R.; de Souza, R. E. Spectroscopy of Seyfert 2 Galaxies, Liners, and H(II) Galaxies. AJ, v. 114, p. 1345, Oct. 1997.

van der Laan, T. P. R.; Schinnerer, E.; Böker, T.; Armus, L. Near-infrared long-slit spectra of Seyfert galaxies: gas excitation across the central kiloparsec. A&A, v. 560, p. A99, Dec. 2013.

Veilleux, S.; Goodrich, R. W.; Hill, G. J. Infrared Spectroscopy of Seyfert 2 Galaxies: A Look through the Obscuring Torus? II. ApJ, v. 477, n. 2, p. 631–660, Mar 1997.

Veilleux, S.; Osterbrock, D. E. Spectral Classification of Emission-Line Galaxies. ApJS, v. 63, p. 295, Feb. 1987.

Veilleux, S.; Sanders, D. B.; Kim, D. C. New Results from a Near-Infrared Search for Hidden Broad-Line Regions in Ultraluminous Infrared Galaxies. ApJ, v. 522, n. 1, p. 139–156, Sep. 1999.

Vermeij, R.; van der Hulst, J. M. The physical structure of Magellanic Cloud H II regions. II. Elemental abundances. A&A, v. 391, p. 1081–1095, Sep. 2002.

Vermeulen, R. C.; Readhead, A. C. S.; Backer, D. C. Discovery of a Nuclear Counterjet in NGC 1275: A New Way to Probe the Parsec-Scale Environment. ApJ, v. 430, p. L41, Jul. 1994.

Véron-Cetty, M. P.; Véron, P. A catalogue of quasars and active nuclei: 13th edition. A&A, v. 518, p. A10, Jul 2010.

Véron-Cetty, M. P.; Véron, P.; Gonçalves, A. C. A spectrophotometric atlas of Narrow-Line Seyfert 1 galaxies. A&A, v. 372, n. 3, p. 730–754, Jun. 2001.

Veron, P.; Lindblad, P. O.; Zuiderwijk, E. J.; Veron, M. P.; Adam, G. On the nature of the so-called narrow-line X-ray galaxies. A&A, v. 87, n. 1-2, p. 245–249, Jul. 1980.

Visnovsky, K. L.; Impey, C. D.; Foltz, C. B.; Hewett, P. C.; Weymann, R. J.; Morris, S. L. Radio Properties of Optically Selected Quasars. ApJ, v. 391, p. 560, Jun 1992.

Vrtilek, J. M.; Carleton, N. P. Seyfert galaxy narrow-line regions. I. Observations of O III lambda 5007. ApJ, v. 294, p. 106–120, Jul. 1985.

Wampler, E. J. Photoelectric Spectrophotometry of Seyfert Galaxies. ApJ, v. 164, p. 1, Feb 1971.

Wamsteker, W.; Rodriguez-Pascual, P.; Wills, B. J.; Netzer, H.; Wills, D.; Gilmozzi, R.; Barylak, M.; Talavera, A.; Maoz, D.; Barr, P.; Heck, A. Ultraviolet and Optical Variations in Active Galactic Nuclei: The Seyfert 1 Galaxy NGC 5548. ApJ, v. 354, p. 446, May 1990.

Wang, J.; Mao, Y. F.; Wei, J. Y. Evolution of [O III] λ5007 Emission-line Profiles in Narrow Emission-line Galaxies. ApJ, v. 741, n. 1, p. 50, Nov. 2011.

Ward, M.; Penston, M. V.; Blades, J. C.; Turtle, A. J. New optical and radio observations of the X-ray galaxies NGC 7582 andNGC 2992. MNRAS, v. 193, p. 563–582, Nov. 1980.

Ward, M. J.; Blanco, P. R.; Wilson, A. S.; Nishida, M. Infrared Spectroscopy of Cygnus A: Implications for the Obscured Active Nucleus. ApJ, v. 382, p. 115, Nov. 1991.

Ward, M. J.; Geballe, T.; Smith, M.; Wade, R.; Williams, P. Near-Infrared Spectra of Seyfert Nuclei. I. The Reddening Problem. ApJ, v. 316, p. 138, May 1987.

Weaver, K. A.; Meléndez, M.; Mushotzky, R. F.; Kraemer, S.; Engle, K.; Malumuth, E.; Tueller, J.; Markwardt, C.; Berghea, C. T.; Dudik, R. P.; Winter, L. M.; Armus, L. Mid-infrared Properties of the Swift Burst Alert Telescope Active Galactic Nuclei Sample of the Local Universe. I. Emission-line Diagnostics. ApJ, v. 716, n. 2, p. 1151–1165, Jun. 2010.

Weaver, K. A.; Wilson, A. S.; Baldwin, J. A. Kinematics and Ionization of Extended Gas in Active Galaxies. VI. The Seyfert 2 Galaxy NGC 1386. ApJ, v. 366, p. 50, Jan. 1991.

Weedman, D. W. Invited Paper - Active Galactic Nuclei. In: BAAS. [S.l.: s.n.], 1974. v. 6, p. 441.

Weedman, D. W.; Hao, L.; Higdon, S. J. U.; Devost, D.; Wu, Y.; Charmandaris, V.; Brandl, B.; Bass, E.; Houck, J. R. Mid-Infrared Spectra of Classical AGNs Observed with the Spitzer Space Telescope. ApJ, v. 633, n. 2, p. 706–716, Nov. 2005.

Wehinger, P. A.; Wyckoff, S. Seyfert galaxies with large Z - an electronographic survey. MNRAS, v. 181, p. 211–231, Oct. 1977.

Wehrle, A. E.; Morris, M. Radio and Hα Images of the "Figure-8" Radio Nucleus of the Interacting Seyfert Galaxy NGC 2992. AJ, v. 95, p. 1689, Jun. 1988.

Werner, M. W.; Roellig, T. L.; Low, F. J.; Rieke, G. H.; Rieke, M.; Hoffmann, W. F.; Young, E.; Houck, J. R.; Brandl, B.; Fazio, G. G.; Hora, J. L.; Gehrz, R. D.; Helou, G.; Soifer, B. T.; Stauffer, J.; Keene, J.; Eisenhardt, P.; Gallagher, D.; Gautier, T. N.; Irace, W.; Lawrence, C. R.; Simmons, L.; Van Cleve, J. E.; Jura, M.; Wright, E. L.; Cruikshank, D. P. The Spitzer Space Telescope Mission. ApJS, v. 154, n. 1, p. 1–9, Sep. 2004.

Whitford, A. E. The law of interstellar reddening. AJ, v. 63, p. 201–207, May 1958.

Wills, B. J.; Netzer, H.; Brotherton, M. S.; Han, M.; Wills, D.; Baldwin, J. A.; Ferland , G. J.; Browne, I. W. A. The Narrow-Line Region of High-Luminosity Active Galactic Nuclei. ApJ, v. 410, p. 534, Jun. 1993.

Wilson, A. S.; Baldwin, J. A.; Ulvestad, J. S. Kinematics and ionization of extended ionized gas in active galaxies.I. The X-ray luminous galaxies NGC 2110, NGC 5506, and MCG -5-23-16. ApJ, v. 291, p. 627–654, Apr. 1985.

Wilson, A. S.; Braatz, J. A.; Heckman, T. M.; Krolik, J. H.; Miley, G. K. The Ionization Cones in the Seyfert Galaxy NGC 5728. ApJ, v. 419, p. L61, Dec 1993.

Wilson, A. S.; Ulvestad, J. S. Radio jets and high velocity gas in the Seyfert galaxy NGC 1068. ApJ, v. 275, p. 8–14, Dec. 1983.

Wilson, A. S.; Ward, M. J.; Haniff, C. A. High-Resolution Emission-Line Imaging of Seyfert Galaxies. II. Evidence for Anisotropic Ionizing Radiation. ApJ, v. 334, p. 121, Nov. 1988.

Winge, C.; Storchi-Bergmann, T.; Ward, M. J.; Wilson, A. S. Extended gas in Seyfert galaxies: near-infrared observations of 15 active nuclei. MNRAS, v. 316, n. 1, p. 1–18, Jul. 2000.

Winkler, H. Variability studies of Seyfert galaxies - II. Spectroscopy. MNRAS, v. 257, p. 677–688, Aug. 1992.

Woltjer, L. Emission Nuclei in Galaxies. ApJ, v. 130, p. 38, Jul 1959.

Wu, Y.-Z.; Zhao, Y.-H.; Meng, X.-M. The Diagnostics and Possible Evolution in Active Galactic Nuclei Associated with Starburst Galaxies. ApJS, v. 195, n. 2, p. 17, Aug. 2011.

Zajaček, M.; Busch, G.; Valencia-S., M.; Eckart, A.; Britzen, S.; Fuhrmann, L.; Schneeloch, J.; Fazeli, N.; Harrington, K. C.; Zensus, J. A. Radio spectral index distribution of SDSS-FIRST sources across optical diagnostic diagrams. A&A, v. 630, p. A83, Oct. 2019.

Zaritsky, D.; Kennicutt ROBERT C., J.; Huchra, J. P. H II Regions and the Abundance Properties of Spiral Galaxies. ApJ, v. 420, p. 87, Jan 1994.

Zel'dovich, Y. B.; Novikov, I. D. The Radiation of Gravity Waves by Bodies Moving in the Field of a Collapsing Star. *Soviet Physics Doklady*, v. 9, p. 246, Oct 1964.

Zwicky, F. Compact Galaxies and Compact Parts of Galaxies. II. ApJ, v. 143, p. 192, Jan 1966.

Zwicky, I. F. Compact Galaxies and Compact Parts of Galaxies. ApJ, v. 140, p. 1467, Nov 1964.